Stefano Gialanella
Alessio Malandruccolo

Aerospace Alloys

Springer

Topics in Mining, Metallurgy and Materials Engineering

Series editor

Carlos P. Bergmann, Federal University of Rio Grande do Sul, Porto Alegre, Rio Grande do Sul, Brazil

"Topics in Mining, Metallurgy and Materials Engineering" welcomes manuscripts in these three main focus areas: Extractive Metallurgy/Mineral Technology; Manufacturing Processes, and Materials Science and Technology. Manuscripts should present scientific solutions for technological problems. The three focus areas have a vertically lined multidisciplinarity, starting from mineral assets, their extraction and processing, their transformation into materials useful for the society, and their interaction with the environment.

More information about this series at http://www.springer.com/series/11054

Stefano Gialanella • Alessio Malandruccolo

Aerospace Alloys

🐎 Springer

Stefano Gialanella
Industrial Engineering Department
University of Trento
Trento, Italy

Alessio Malandruccolo
Metallurgy Industrial Consultant
Bolzano, Italy

To my son Giulio Carlo
(SG)
To my friends and to all those who supported
me
(AM)

Preface

The aerospace field is traditionally strategic for the development of novel materials needed for the specific requirements of aircraft structures and propulsion systems. A large number of advanced materials and relevant processing routes have been implemented first for aerospace needs. On many occasions, aerospace materials and technologies have subsequently been transferred successfully to a wider range of applications, like chemical industry, energy production, nuclear plants, terrestrial and marine transportation, and many more.

The aim of this book is to present an overview of the main classes of metallic materials, like light alloys (Al-, Mg-, and Ti-based, including Ti-aluminides), steels, superalloys, refractory alloys, oxide dispersion strengthened alloys, ordered intermetallics, shape memory alloys, and related systems, e.g., laminate composites and coatings.

The basic concepts concerning the structure of aircrafts and the working principles of gas turbine engines are recalled to provide the reader with indications on the specific needs and possible issues in this field, so that the adoption of given materials systems and relevant processing routes are better understood.

The content of the book is organized according to the main classes of materials that are of actual and potential interest for aerospace applications. In each chapter, materials properties and relevant technological aspects, particularly as concerns processing, are presented.

The motivations that have guided the research efforts for the development of new materials systems have changed over the comparatively short life of aeronautics. Nowadays, energy-saving and environmental issues are paramount: these stand points and their role in materials development are also highlighted.

A deliberate attempt, pursued in writing *Aerospace Alloys*, has been to include an updated bibliography and indication of further readings, both important in a continuously evolving field. A list of general references concerning materials science and engineering and physical metallurgy is included among the "Further Readings" lists at the end of each chapter. In this way, the fundamental aspects of these disciplines,

which may contribute to a better understanding of the book content, can easily be recovered.

We believe the book can be used in advanced undergraduate courses in materials and mechanical engineering, considering that the starting point for writing this book has been a collection of lecture notes of courses that SG ran over several years at the University of Trento and the University of Florence in Italy. However, we would expect that the subject and relevant materials information may also be of interest to researchers working in R&D industrial laboratories, considering that in this perspective, we have included compositional tables, some in the appendices, so that the textbook turns out be reasonably self-consistent. We believe that the mixed academic (SG's) and industrial (AM's) background may provide original and complementary stand points on the different subjects, attracting the interest of researchers and professionals working in the different but still strongly interacting development laboratories in the academia and industry.

We conclude this *preface* with the acknowledgments. In the first place, we wish to thank all the students (AM has been one of them at some stage!), who during the lecture classes placed questions and contributed to a stimulating discussion, promoting in this way the improvement and correction of the lecture notes. We also thank our colleagues for stimulating discussions and suggestions on several subject dealt in the book.

Trento, Italy   Stefano Gialanella
Bolzano, Italy   Alessio Malandruccolo

Contents

Abbreviations

ACARE	Advisory Council for Aviation Research and Innovation in Europe
AISI	American Iron and Steel Institute
ALPS	Advanced low-pressure systems
AOD	Argon oxygen decarburization
APB	Antiphase boundary
APS	Air plasma spraying
ASM	American Society of Materials
ASTM	American Society for Testing and Materials
ATC	Atmosphere and temperature controlled plasma spraying
AUW	All-up weight
BC	Before Christ
bcc	Body centered cubic
bct	Body-centered tetragonal
BVI	Blade-vortex interaction
CBN	Cubic boron nitride
CCT	Continuous cooling transformation
CEVAM	Consumable electrode arc melting
CEVAR	Consumable electrode vacuum arc remelting
CF	Casting factor
CFRP	Carbon fiber reinforced polymer
CGDS	Columnar-grained directionally solidified
CHM	Cold heart melting
CMAS	Calcium-magnesium-aluminosilicate
CP	Commercially pure
CROR	Counter-rotating open rotor
CTE	Coefficient of thermal expansion
CTOL	Conventional take-off and landing
CV	Carrier variant
CVD	Chemical vapor deposition
DAS	Dendrite arm spacing
DB	Diffusion bonding

DBT	Ductile to brittle transition
DBTT	Ductile to brittle transition temperature
DC	Direct current
D-Gun	Detonation gun
DIN	Deutsche Institut für Normung
DMHT	Dual microstructure heat treatment
DOS	Density of states
DRX	Direct recrystallization
DS	Directionally solidified or directional solidification
EAF	Electric arc furnace
EB	Electron beam
EBCHR	Electron beam cold heart remelting
EBM	Electron beam melting
EB-PVD	Electron beam physical vapor deposition
EDXS	Energy-dispersive X-ray spectroscopy
EFTA	European Free Trade Association
ELI	Extra low interstitial
EN	European Norms (Euronorm)
ESR	Electroslag remelting
ESRR	Electroslag rapid remelting
ETEM	Environmental transmission electron microscopy
F/M	Ferritic martensitic
F1	Formula 1
fcc	Face-centered cubic
FML	Fiber-metal laminate
GAR	Grain aspect ratio
GB	Grain boundary
GE	General Electric
GFRP	Glass fiber reinforced polymer
GPZ	Guinier-Preston zone
GT	Gas turbine
GTE	Gas turbine engine
GTEs	Gas turbine engines
HAZ	Heat-altered zone or heat-affected zone
hBN	Hexagonal boron nitride
hcp	Hexagonal close packed
HCP	High-pressure compressor
HDI	High density inclusion
HE	Hydrogen embrittlement
HEAC	Hydrogen environmental assisted cracking
HEDE	Hydrogen-enhanced decohesion
HELP	Hydrogen-enhanced localized plasticity
HID	Hard interstitial defects
HIP	Hot isostatic pressing

HSLA	High-strength low-alloy steels
HTHC	High-temperature hot corrosion
HTLA	High-temperature low activity
HVOF	High-velocity oxy-fuel flame spraying
IADS	International Alloy Designation System
IHAC	Internal hydrogen-assisted cracking
IUPAC	International Union of Pure and Applied Chemistry
LBW	Laser beam welding
LCF	Low-cycle fatigue
LDI	Low-density inclusions
LPPS	Low-pressure plasma spraying
LPSO	Long-period stacking ordered
LPT	Low-pressure turbine
LTHA	Low-temperature high activity
LTHC	Low-temperature hot corrosion
MA	Mechanical alloying
MISS-NC	Mechanically induced surface self-nanocrystallization
M_s	Martensite start
NDT	Nondestructive testing
NEO	Near Earth objects
NEP	Nuclear electric propulsion
NS	Nanostructured
NTP	Nuclear thermal propulsion
ODS	Oxide dispersion strengthened
OEW	Operating empty weight
OPR	Overall pressure ratio
OTB	Oxygen top and bottom blowing
OWSME	One-way shape memory effect
PAM	Plasma arc melting
PCA	Process control agent
PFZ	Precipitation-free zone or precipitate-free zone
PGM	Platinum group metal
PH	Precipitation hardening or precipitation hardenable
PHSS	Precipitation hardening stainless steels or precipitation hardenable stainless steels
PM	Powder metallurgy
PS	Plasma spraying
PSZ	Partially stabilized zirconia
PTC	Plasma transferred arc
PVD	Physical vapor deposition
R&D	Research and development
RA	Reduced activation
RRB	Reconfigurable rotor blade

RS	Rapid solidification
SAE	Society of Automotive Engineers
SAP	Sinter-aluminum pulver
SC	Single crystal
SCC	Stress corrosion cracking
SE	Superelasticity
SEM	Scanning electron microscopy
SFC	Specific fuel consumption
SFE	Stacking fault energy
SFH	Simulated flying hours
SHE	Standard hydrogen electrode
SIM	Stress-induced martensite
SMA	Shape memory alloy
SMAT	Surface mechanical attrition treatment
SME	Shape memory effect
SNC	Surface nanocrystallization
SPF	Superplastic forming
SRZ	Secondary reaction zone
SSCP	Stress-strain calculation program
STOVL	Short take-off and vertical landing
TBC	Thermal barrier coating
TBCs	Thermal barrier coatings
TBO	Time between overhaul
TCP	Tetragonally close packed
TD	Thoriated
TEM	Transmission electron microscopy
TET	Turbine entry temperature
TGO	Thermally grown oxide
TISS-NC	Thermally induced surface self-nanocrystallization
TPS	Thermal protection system
TTT	Time-temperature-transformation
TWSME	Two-way shape memory effect
UNFCCC	United Nations Framework Convention on Climate Change
UNS	Unified Numbering System
USD	US dollar
UT	Ultrasonic testing
VAFN	Variable area fan nozzle
VAR	Vacuum arc remelting
VARTM	Vacuum assisted resin transfer molding
VARTMFML	Vacuum-assisted resin transfer molding fiber-metal laminate
VARTMPCL	Vacuum-assisted resin transfer molding-infused plasma coated laminates
VGC	Variable geometry chevron

VIM	Vacuum induction melting
VOCD	Vacuum oxygen converter decarburization
VOD	Vacuum oxygen decarburization
VPS	Vacuum plasma spraying
VSTOL	Vertical and/or short take-off and landing
XRD	X-ray diffraction
YSZ	Yttria-stabilized zirconia

About the Author

Stefano Gialanella is an Associate Professor in materials science and technology at the Department of Industrial Engineering, University of Trento, Italy. He is responsible for delivering courses to undergraduate students in industrial engineering, Master's students in materials engineering and cultural heritage, and PhD students in materials, mechatronics, and system engineering. In addition, he has given lectures and courses in materials science at the University of Florence, University of Pisa, Politecnico di Milano, and Universitat Autonoma de Barcelona (Spain). Dr. Gialanella's research interests include intermetallics, oxidation of structural alloys, nondestructive testing of power plant components, shape-memory alloys, tribology with particular reference to automotive brake systems, and environmental monitoring of cultural heritage with particular reference to phase transformations and relevant structural and microstructural aspects. Based on this activity, he has coauthored more than 130 scientific papers in international refereed journals. He is also a member of the editorial boards of *Materials Science Foundations* and *Journal of Metallurgy*.

Alessio Malandruccolo is a plant metallurgist at an Italian steel and nickel alloy company, a position held since the time he received his Master degree in Materials Science and Engineering at the University of Trento. He is currently involved in R&D, quality control and improvement, failure analysis, and revamping and design of new installations for production of new alloys. He has also worked as a teaching assistant in Materials Technology and Applied Chemistry in the Master course in Architecture and Building Engineering at the University of Trento (Italy), collaborating also with the Faculty of Science and Technology of the University of Bolzano (Italy), with lectures and seminars regarding his professional sector. He developed part of his research experience and skills at the European Synchrotron Radiation Facility – ESRF (Grenoble, F) – and at the Diamond Light Source (Didcot, UK), focusing mainly on X-ray diffraction applied to inorganic materials characterization. He cultivates a personal interest in product design and perception, user-oriented design, and cognitive sciences.

Chapter 1
A Brief Introduction to Aerospace Applications

1.1 Historical Background

Aerospace applications represent an extremely challenging field, for the development of new materials, and for the improvement of the existing ones, with the important additional requirement of complying with highest safety standards, particularly as concerns civil and commercial aviation. A successful design and manufacturing of components, relevant performances, certification, maintenance, and safe operation are all directly influenced by the properties of materials used for engines and airframe structures. Therefore, mechanical strength, creep, corrosion, and oxidation resistance must be optimized for any specific application in this field (Mouritz 2012). Process technologies for materials and production of components are also subjected to a continuous evolution, with important reciprocal interaction.

Aerospace materials technology proceed very rapidly, in order to keep up with the momentum of changes in the air transportation that over the years have been driven by different forces. Nowadays, compositional refining and novel processing routes attain better properties in already existing material systems so that more demanding servicing conditions and higher safety standards can be met. The development of new materials and processing technologies, needed for the new engines, airframes, and control systems, not only resulted in improved aircraft performances but was also transferred and applied in other technological fields (King et al. 2009), as recalled in the next chapters.

The first engine-operated aircraft was the Flyer I (1903, Fig. 1.1), built by Wilbur and Orville Wright. In order to achieve an adequate rigidity, the wing structure was realized using a triangulated frame (see Fig. 1.2).

The triangulated structure of the wing provides several advantages, in addition to rigidity, especially interesting for the aircraft:

- High maneuverability.
- Low weight as compared to bulk structures.
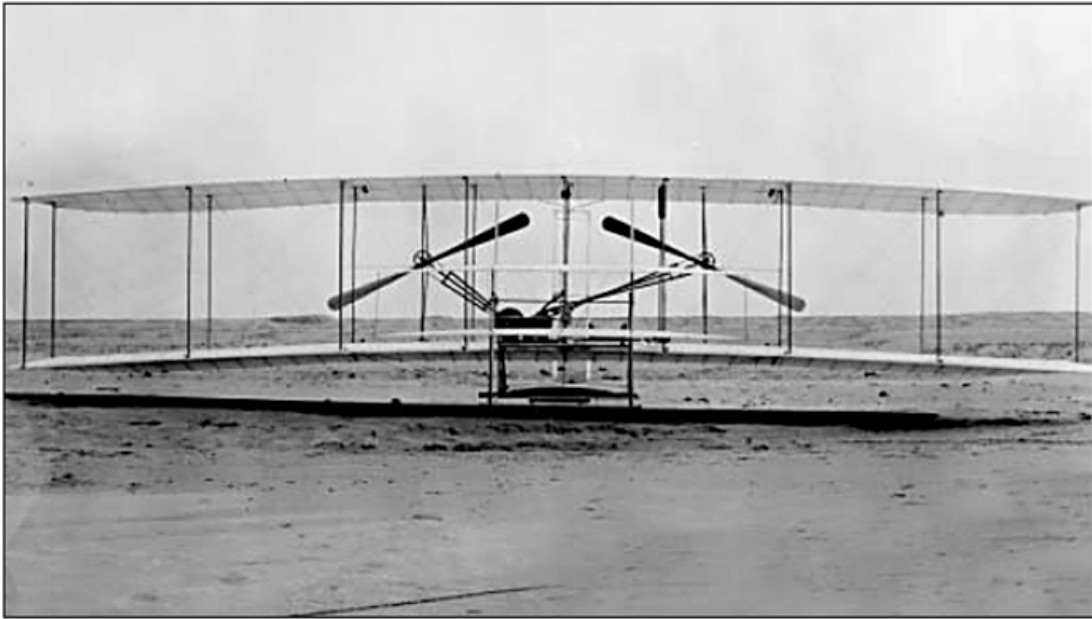
Fig. 1.1 The Flyer I airplane of the Wright brothers (NASA 2003)
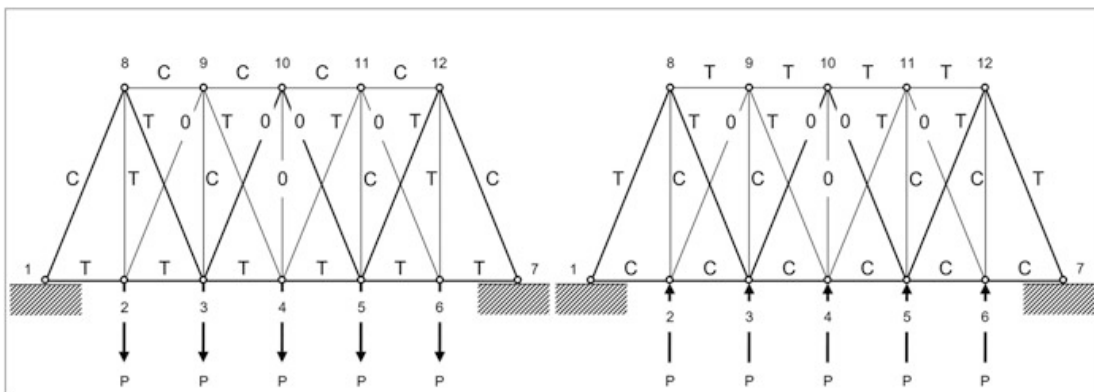
Fig. 1.2 Schematic of triangulated structures under two different loading regimes. The letter C indicates compressive load, the letter T indicates tensile load, the number 0 indicates the load-free condition, and P is the overall load acting on the structure. (Redrawn from Curtis 1997)

- Possibility to swap from tension to compression of the bracing wires to sustain the spars in all operational conditions.

At the time the Flyer I was built, no specific materials were available for the construction of an aircraft, mostly due to the absence of an industrial field dedicated to these applications. The materials used for the fabrication of the Flyer I were:

- Aluminum. An aspect not always mentioned is that the engine of the Flyer I airplane, to meet the weight reduction requirements, was made of cast aluminum.
- Cotton fabric used as coating for the wing surface.
- Steel used for the critical structural parts, like the bracing wires (i.e., tension-compression wires) and the wing struts.
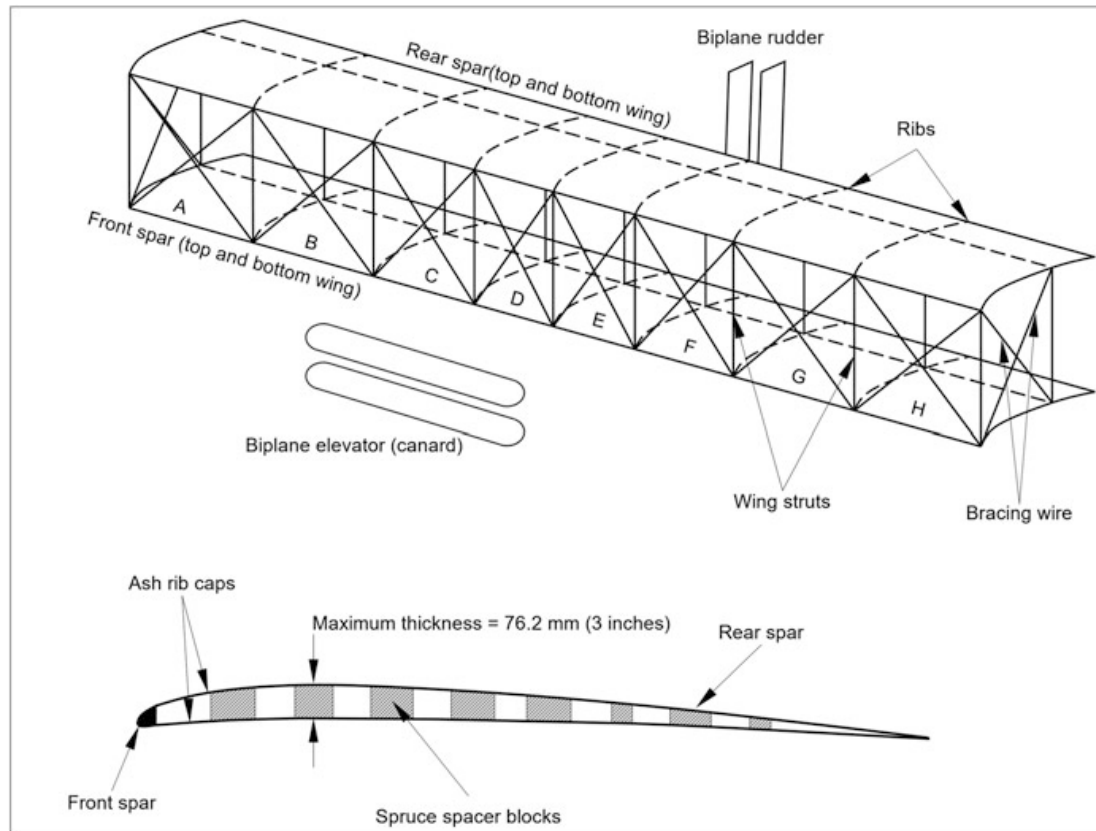
Fig. 1.3 Schematic of the overall structure of the Flyer I wing and detail of the wing rib. (Redrawn from Curtis 1997)

- Wood for the fabrication of the ash (inner part the wing), the ribs, the spars, and the propeller.

The maximum speed of the Flyer I was 56 km/h, due to the limitations caused by the aerodynamic drag associated with the shape of the aircraft, in particular with the structure of the double-wing with bracing wires (see Fig. 1.3). To overcome the drag effect of the double-wing surface and relevant wiring, needed to achieve a suitable rigidity of the structure, as a possible approach to reduce this effect, a cantilever wing was developed.

A sort of intermediate step toward this innovative structure can be found in the Blériot monoplane (1909). The Blériot monoplane had a single wing, although not fully self-sustaining, so that steel wires were needed to ensure the rigidity of the structure (see Fig. 1.4). This airplane was the first to feature a particularly rigid fuselage structure, a choice made to improve further its stability and maneuverability. The airframe was made of tension and compression wires (see Fig. 1.5) with a similar geometry to the wings of the Flyer I (see Fig. 1.3). The maximum speed of this aircraft was still below 100 km/h, due to the poor aerodynamics of the whole structure.

The situation was improved with the introduction of real cantilever wing structures. The main difference with respect to past geometries was that this new design
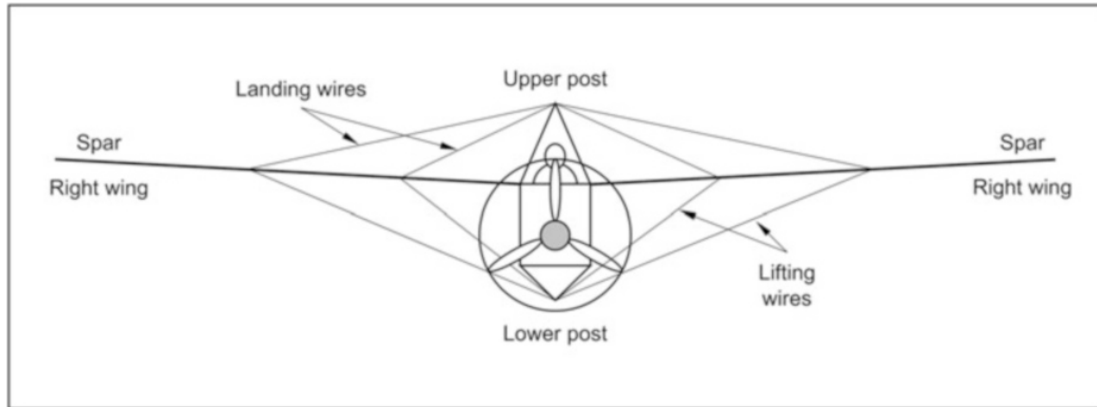
Fig. 1.4 1909 Blériot monoplane and overall schematic of the structure. (Redrawn from Curtis 1997)
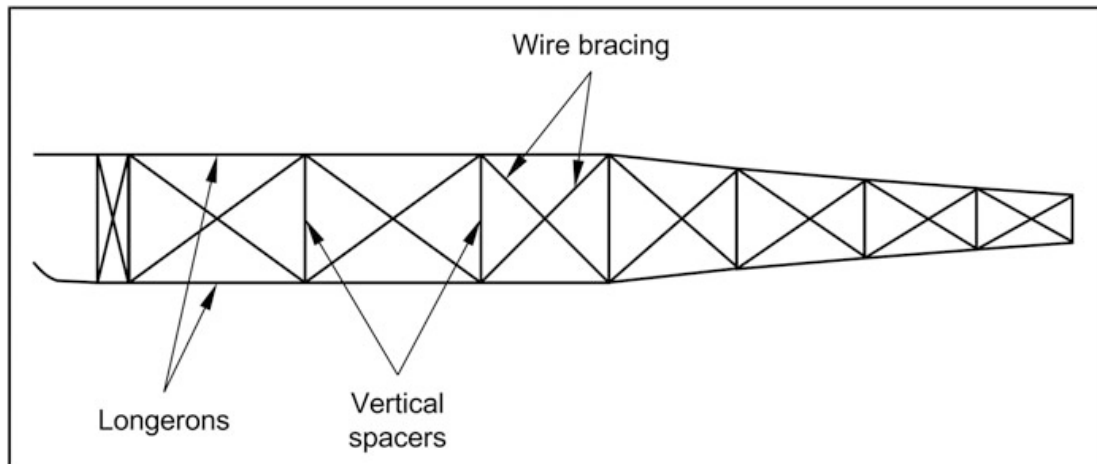
Fig. 1.5 Schematic of the Blériot's fuselage. (Redrawn from Curtis 1997)

was based on a self-standing structure, not requiring bracing wires and parts other than the wing itself, to guarantee an adequate rigidity. An example, probably the first, certainly the most popular, of the application of cantilever wings was the Fokker DR 1 (1917) (Fig. 1.6). The main feature of this kind of wing is its thickness that is the key factor as concerns its strength and rigidity. The internal structure of the wing, characterized by composite ribs, is sufficient to avoid any additional external structure (e.g., bracing wires). Thanks to the cantilever wing, the maximum speed increased up to 160 km/h, still maintaining substantially the same materials as the Flyer I. The situation evolved with the availability of more performing piston engines and, subsequently, toward the end of World War II, with the development of gas turbine engines, affording even higher speed and in principle capable to overcome the speed of sound.

This evolution required, in the first place, new wing geometries and, consequently, the selection of new materials.

The higher velocity had another important consequence: the overheating of the aircraft skin, particularly at the wing leading edge and other frontal parts of the
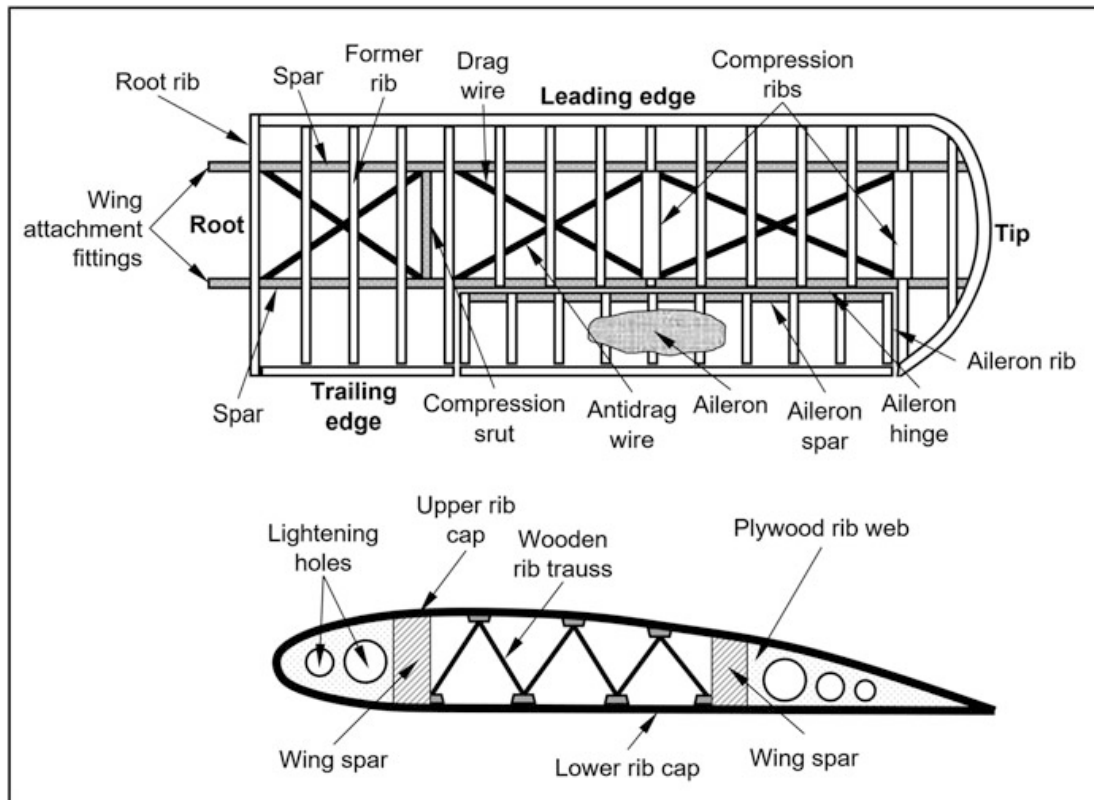
Fig. 1.6 The cantilever wing of the Fokker DR 1 (Redrawn from Curtis 1997)

aircraft in direct contact with the static air film that forms along the splitting line of the air flux. Therefore, the materials traditionally used for aircraft skin, especially fabric and wood, turned out to be absolutely inadequate to face the temperature reached under the new operational conditions.

The search for new materials was also encouraged by the contemporary shortage of wood, a factor that turned to be critical, particularly in the late years of World War II, so that alternative structural materials were increasingly needed. The solution to these two problems was the production of metallic aircrafts, like the Junkers J-1 (1915). This airplane was fully built using steel: quite an important demonstration of what might have been achieved with metal in aircraft structures. On the other hand, the exceedingly high density of the ferrous alloy, notwithstanding the adopted design solutions, rendered the airplane not very practical and flexible in operational maneuvering. Therefore, few years later (1917), the availability of a novel aluminum alloy was very much welcome, and a full-aluminum airplane was produced: the Junkers J-4. No pure aluminum but an Al-Cu alloy was used (see Sect. 3.2). The alloy had been developed a few years earlier by the German metallurgist Alfred Wilm, who could only confirm empirically the hardening effect of thermal treatments, without having the possibility of a direct observation of the precipitates responsible for this improvement in the mechanical properties (see Sect. 3.2.3.3). It can be noted that this was quite a fast technological transfer, from materials research to product development, of particular specific interest, considering the

importance that Al-alloys were bound to have in the aerospace field, still lasting until the present times. These two cases are particularly important, since they have demonstrated for the first time the possibilities of metallic materials in the fabrication of aircrafts: airframe, fuselage, and engines. This was certainly an enabling factor for the development of commercial aviation that in fact, in between World War I and World War II, started its history. In this regard, a year that is worth mentioning is 1933. In February the first Boeing 247, a full-metal airliner, capable to carry ten passengers, took off for the first time, being regarded as the first modern transport airliner. Although on board comfort was very much limited by structural restrictions, the orders started to arrive soon, so numerous that the company was not able to keep up with the pace. The situation was better exploited by Douglas Aircraft, which launched in the second half of the same year 1933 the 12-passenger DC-1 airliner, more spacious and comfortable than the Boeing 247. Other DCs (DC stays for Douglas Commercial) were delivered in the following years: DC-2 (1934, 14 passengers) and DC-3 (1935, 21 passengers). The DC-3, thanks to its flight performances and payload capabilities, gained enormous success among the starting up airline companies that also thanks to this airplane, realized the possibility of making profit out of air transportation.

Although, particularly in the war years, the technological advancements in the military field were transferred to civilian air transportation, in some cases, the needs were rather divergent. This is the case of the maximum operational speed that with the advent of gas turbine engines disclosed the possibility to overcome the intrinsic limit for a propeller aircraft, i.e., the speed of sound. The supersonic flight implies a change both in the profile and in the dimension of the wings, in order to reduce air drag, being the lift anyway guaranteed by the higher accessible speed. A good example of this new philosophy was the Lockheed F-104 "Starfighter" (see Fig. 1.7) capable to reach a maximum speed of Mach 2.2. Shorter and thinner wings require a change not only in their design but also in the selected materials. Titanium alloys for the fabrication of structural components became an obvious choice. The development of aircraft structures, considering the interplay with the development of new materials, is actually quite a complex process, since a great number of variables must be considered. When increasing the maximum speed, the skin temperature becomes an issue. In this regard, the application of titanium alloys reached a particularly impressive level in the Lockheed YF 12 A and its successor, the Lockheed SR-71 "Blackbird" (see Fig. 1.8), in which not only structural parts but also the skin and control surfaces were made of newly developed β-Ti-alloys (see Chap. 4 and Sect. 4.3.1.4).

The adoption of titanium alloys also for the fabrication of the skin of the SR-71 was a necessary choice to stand the peak temperatures at its highest speed of Mach 3.35. It is worthwhile to note that conventional aluminum alloys would not have had a sufficient strength to resist above Mach 2.0 and steel would be too heavy. On this occasion too, the experience and knowledge developed for a military aircraft were important also for the design and its implementation in supersonic civil aircrafts. The Concorde structure and skin were made of aluminum alloys (see Chap. 3), suitable for a peak speed not exceeding Mach 2.
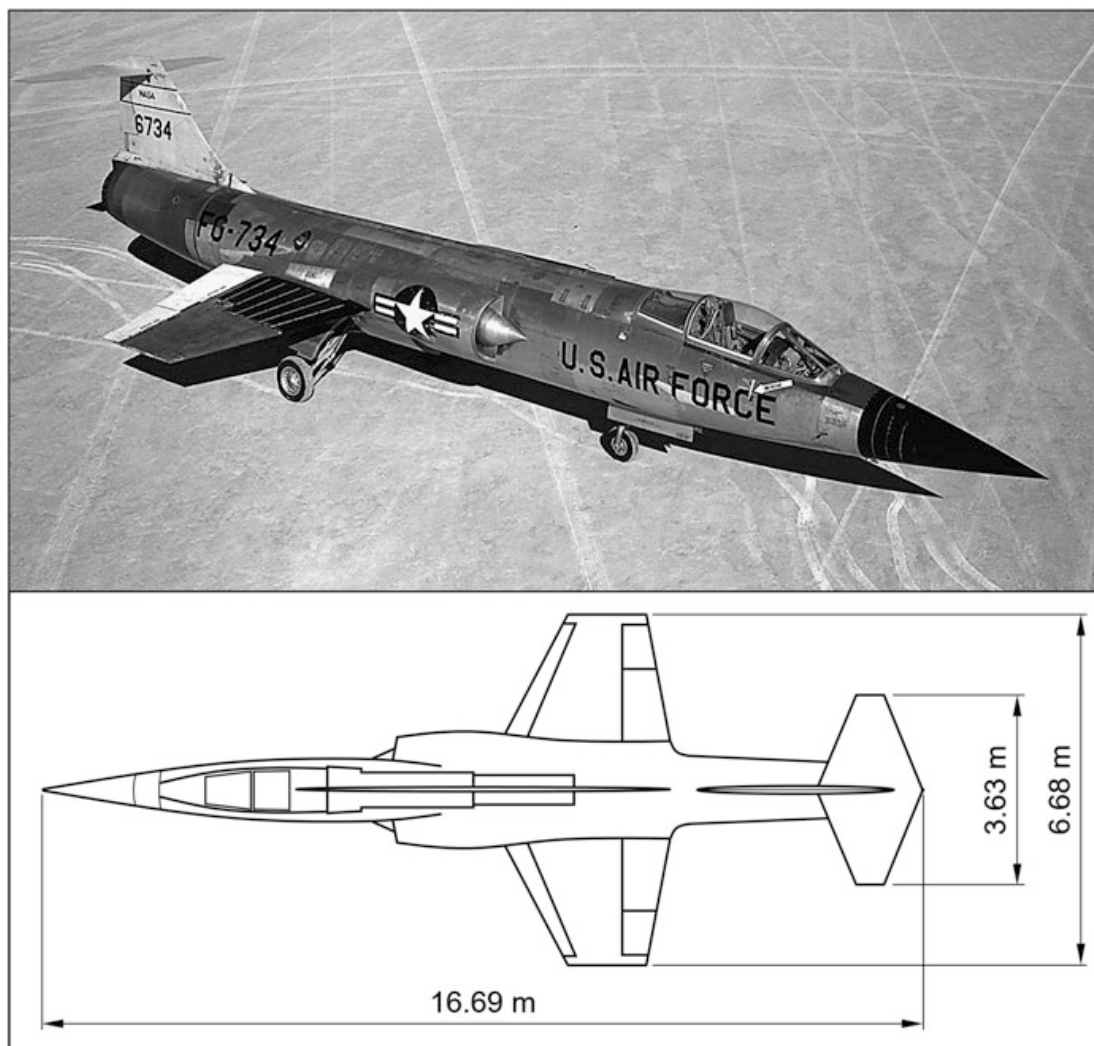
Fig. 1.7 Lockheed F-104 Starfighter. (Friend and Sefic 1972, NASA 2017, reproduced with permission of the Publisher)
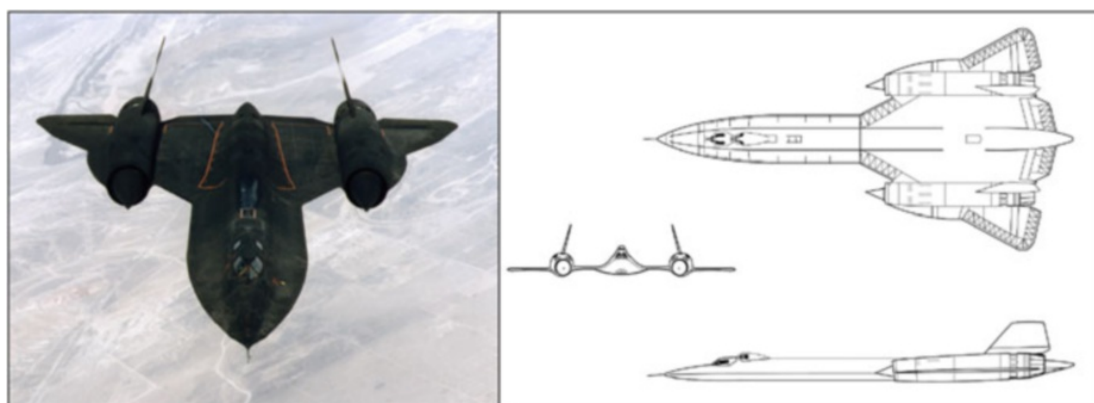
Fig. 1.8 Lockheed SR-71 "Blackbird." (NASA 2008, reproduced with permission of the Publisher)

If higher temperatures of the aircraft skin are to be stood, considering, for instance, the conditions faced in atmosphere reentry after orbital flight, like in case of the Space Shuttle, a composite, reusable, ceramic-based protection system is needed, made of tiles of zirconia-glassy silica felt and, for the hottest parts, carbon-carbon composites. Thanks to this protective shield, surface temperatures in excess of 1300 °C do not provoke any harm to the underlying Al-alloy frame, unless faults in the protection system would intervene, as occurred in case of a tragic accident (Savino et al. 2005). The engine temperature is another parameter that has been sensitively influenced by the selected materials properties. The trend in the operational temperatures and capabilities of aircraft engines has always been increasing, starting from the in-line piston engines of the early propeller-operated aircrafts, reaching material temperature in the 200 °C range, going through the radial high-efficiency engines, with peak temperatures of 500 °C, arriving to the extreme thermal challenge of the newly developed gas turbine engines. The hottest structural parts, i.e., the high-pressure stage turbine blades, nowadays made of nickel-based superalloys (see Sect. 6.4), are operated at gas temperatures above the material capability, i.e., its incipient melting point. It is only thanks to the specific microstructure of the components, i.e., single crystal, and optimized cooling design, i.e., hollow blades, that these conditions can be safely sustained.

1.2 Novel Design Criteria

In recent years, the development of aircraft structures has become increasingly complex in terms of metrics and design drives, with respect to the early times, when technical performances were by far the dominant aspects. Nonetheless, as in the past, contemporary materials are still a decisive enabling factor, since only suitable materials properties will render new design requirements feasible. A remarkable evolution has occurred in the selection criteria that, depending on the specific aircraft structure, will anyway be a trade-off choice.

The improvements achieved in aircraft structures have been continuously accompanied by a growing concern for safety. This aspect becomes increasingly important with the development of civil aviation, where the protection of passengers' lives is not only an ethical issue but also an economic parameter, considering the impact of insurance costs on the business plan budget of any company, not to mention the indirect costs that air accidents may provoke. This aspect appeared soon dramatically evident, for the accidents occurred at two de Havilland Comet aircrafts during take-off at the airport of Ciampino in Rome (Italy) in 1954. The de Havilland Comet (1952, see Fig. 1.9) was a commercial plane derived from a military cargo that originally had no windows in the fuselage that were present instead in the case of the commercial version.

The reason for the failure, occurring under the effect of pressurization-depressurization cycles, was an inappropriate design of the window frames, whose corners acted as initiation spots for the fracture, propagating to the rest of the
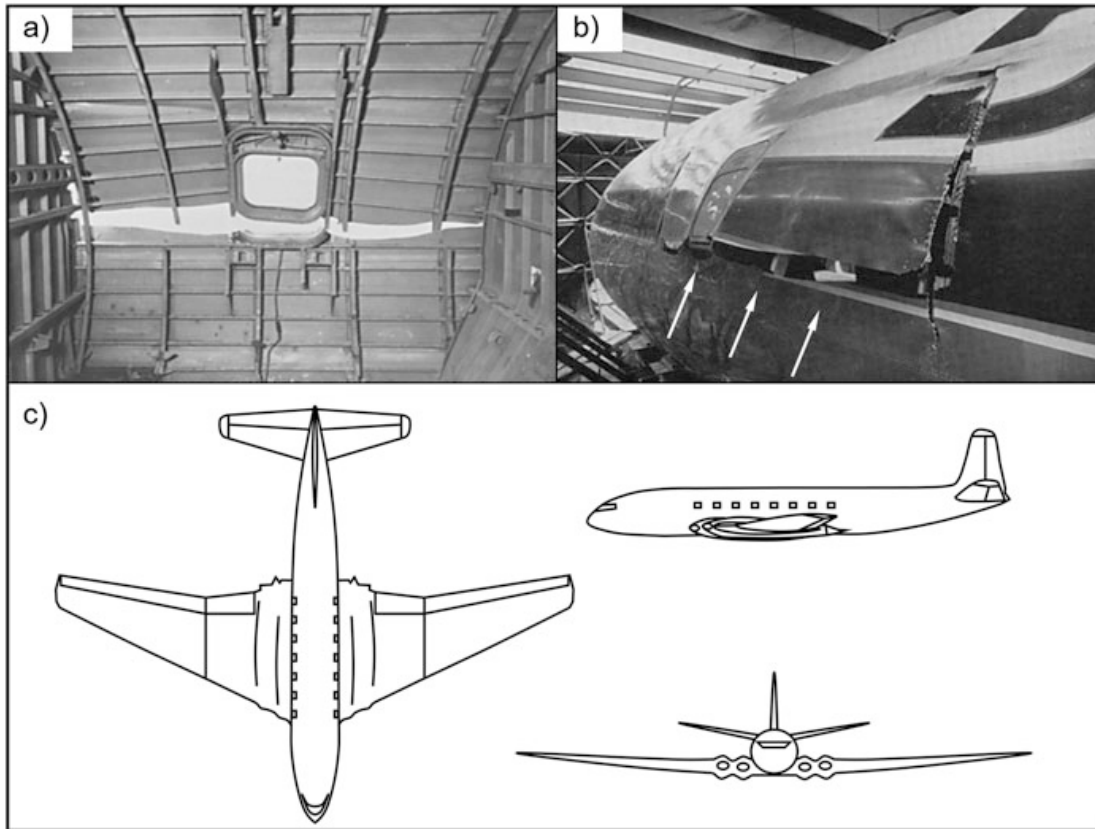
Fig. 1.9 RCAF de Havilland Comet. (**a**) Internal view of the aircraft showing the rupture around the window; (**b**) external view showing the same rupture in the skin of the fuselage (see arrows for the indication of the position of the window and the crack nearby); (**c**) schematic of the airplane (Darling 2001; The National Archives 2019)

fuselage. This failure could not occur in the original military model since no windows were there in the fuselage. The disasters blocked the fast expansion of British Airways that at the time was gaining a leading position in civil aero-transportation. Important consequence of this sort of structural failures was the adoption of two general design criteria for aircraft structures: *safe life* and *fail safe*, which can be regarded as the main guidelines for the development of passenger airliners and in general of all aircrafts for commercial transportation. *Safe life* criterion means the possibility to predict the useful lifetime of structures, components, and systems of an aircraft, in order to schedule maintenance, to proceed with limited repairs, and to replace heavily damaged parts. As to the *fail safe* criterion, it is paramount in aircraft structures since it should allow the airplane to retain sufficient operational capabilities, notwithstanding any possible failure, allowing, for instance, emergency landing procedures.

Looking at the present and past use of aluminum alloys in aircraft structures, it sounds strange that after the Comet disasters, Al-Zn alloys (see Fig. 1.10 and also Chap. 3) were banned, since they were considered the main responsible for the structural failure. Once the real reasons for the accidents were made clear, the use and consequent development of these alloys was resumed and is continuing until
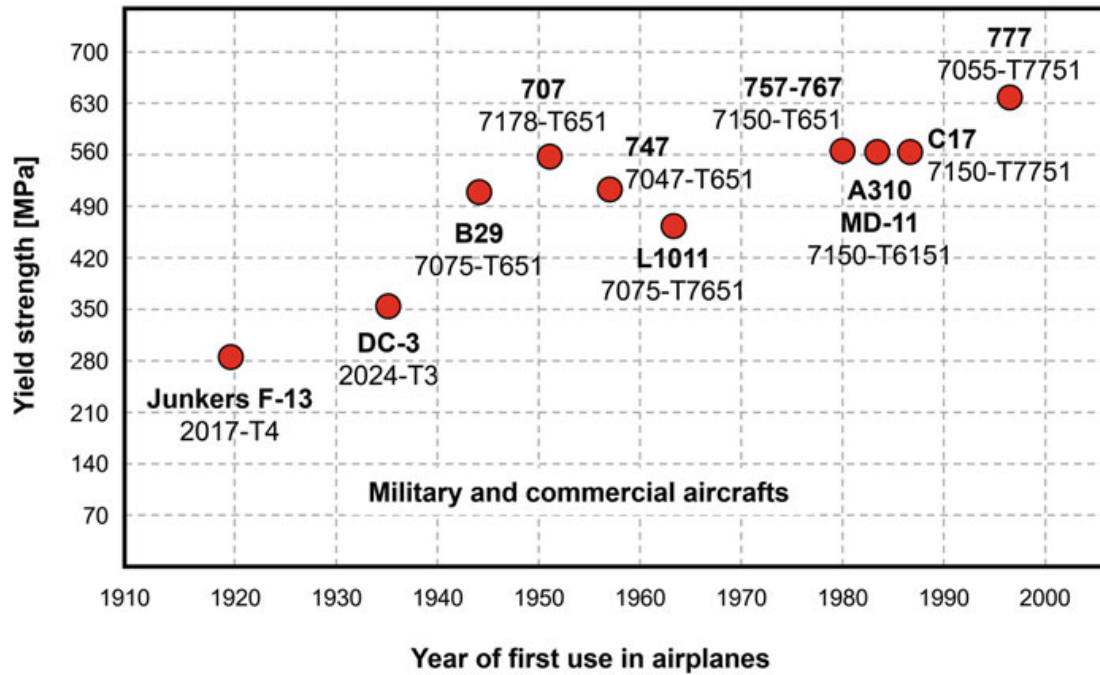
Fig. 1.10 Evolution of the yield strength of various Al-alloys as a function of the 1st year they were used in relevant commercial aircrafts. (Redrawn from Starke and Staley 1996)

present, involving also other systems like: Al-Li and Al-Sc alloys, the latest families of Al-alloys to be developed.

The success of aluminum in aerospace applications is due to the excellent specific material properties, considering its comparatively low density, also as concerns its alloys. For this same reason, magnesium alloys are attracting renovated interest, after having had an important role particularly in military aircraft soon after the end of World War II and a decline afterward, for their limitations (see Sect. 3.3) but also for the strong competition by Al-alloys. The absolute leading role of Al-alloys in aircraft industry has been "spoiled" by a real breakthrough brought about by the latest Boeing airliner: the 787 Dreamliner (see Fig. 1.11). The whole project has been developed on the basis of completely new approaches, redesigning all parts and systems, according to new standards. One of the most innovative and revolutionary aspects regards the massive use of structural composites, adopted also for the fabrication of large single-piece components, like the wing box and the forward fuselage piece including the cockpit, and the barrel section. These are polymer matrix composites with reinforcing carbon fiber felts, manufactured directly with the component shape, thus requiring particularly large infrastructures.

Interestingly the extended use of structural composites in the Dreamliner, summing up to 50% of the operating empty weight (OEW, see Fig. 1.11), has occurred in association with a further increase in the percentage of titanium alloys. These materials had already been extensively used in the previous Boeing airliner, the B777 for structural components and other parts, previously largely made of steel (see Table 1.1).

Fig. 1.11 Materials used in Boeing 787 Dreamliner. (Redrawn from Boeing 2013)

Table 1.1 Titanium alloys used on the Boeing 777

Alloy	Condition	UTS [MPa]	Forms
Commercially pure	Annealed	345–550	Bar, plate, sheet
Ti-3Al-2.5 V	Cold worked and stress relieved	860	Hydraulic tubing
	Annealed	690	Honeycomb core
Ti-6Al-4 V	Annealed	895	All forms
	β-annealed	895	Forgings
	Solution treated and annealed	1100	Fasteners
Ti-10V-2Fe-3Al	Solution treated and annealed	1190	Forgings
Ti-15V-3Cr-3Al-3Sn	Solution treated and annealed	1035	Sheet
	Solution treated and annealed	1140	Castings
Ti-3Al-8V-6Cr-4Mo-4Zr	Cold drawn and aged	1240–1450	Springs
Beta-21S	Solution treated and annealed	≥860	Nacelle area

This choice is coherent with the deliberate strategy, which drove the design of these more recent airliners, for an extreme weight reduction. This is of course generally important for aircraft structures. As concerns composites, also in the past, their early use in aeronautics turned out to be decisive on some notorious occasions. The vertical takeoff option of the Sea Harrier could only be implemented once some structural parts were made using polymer matrix composites, as illustrated in Fig. 1.12, with a consequent decisive weight reduction. However, the choice of lighter materials is nowadays driven also by the need to reduce fuel consumption, with relevant benefits not only on budget savings but also environmental sustainability. For a large airliner, a weight reduction of 1000 kg reduces the fuel consumption by 1.1–1.5% (King et al. 2009). This can be achieved by an intelligent combination of the different classes of available materials, as shown by the data in Table 1.2 pertaining to popular aircrafts.
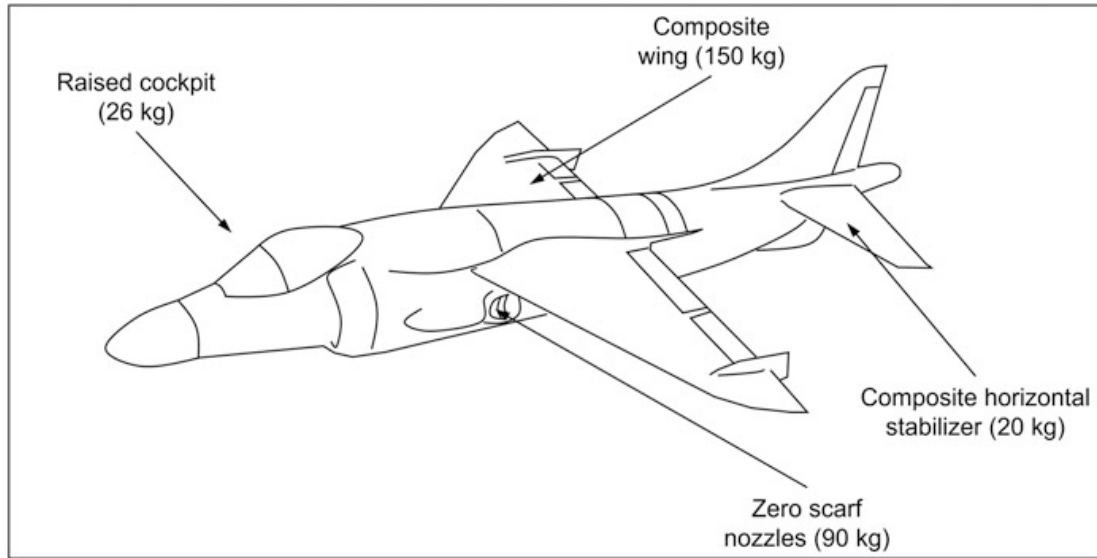
Fig. 1.12 Sea Harrier and some parts replaced by structural composites to achieve an adequate weight reduction. Values among brackets refer to the weight saving obtained by means of composite materials. (Redrawn from Calvert 1990)

Table 1.2 Weight percentages of structural materials used in the airframes of civilian and military aircrafts (Mouritz 2012)

Aircraft	Aluminum alloys	Composites	Steel	Titanium	Other materials
Boeing 737	81%	3%	6%	3%	7%
Airbus A330-340	68%	17%	9%	4%	2%
Airbus A380	61%	25%	10%		4%
McDonnell Douglas F-18 Hornet	51%	9%	16%	13%	11%
Lockheed F-22 Raptor	11%	35%	5%	33%	16%

As it is for other transportation fields, also aviation companies have to consider their own economical sustainability and competitiveness. A successful aerospace product should be valuable for the customers, with a low environmental impact, and still retain elevated safety standards. The cost for the end user, the passenger in case of civil aviation, results from a number of parameters, including initial cost and cost of ownership. The total cost of ownership includes several terms, according to the scheme in Fig. 1.13. It is worth saying that a more efficient management affords not only money savings to the companies but also a reduction of the impact of aviation on the environment and, thereby, on human health. Better designed and lighter aircraft structures will have better aerodynamic performances, lower exhaust, and noise emissions. Of course, for these latter aspects, an improved efficiency of the engines is paramount. This is the reason why also for the engines, a continuous search for new materials and part design have been pursued, as reflected by the evolution over the years of the turbine inlet temperature, even named turbine entry temperature (TET).
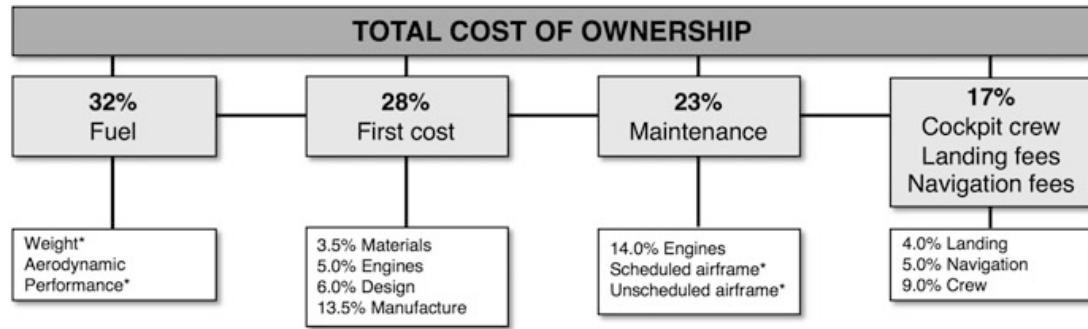
Fig. 1.13 Total cost of ownership and its split in the main components. ∗ refers to parameters that are influenced by custom features such as aircraft type, age of the aircraft, operating conditions, and owner (Cantor et al. 2001)
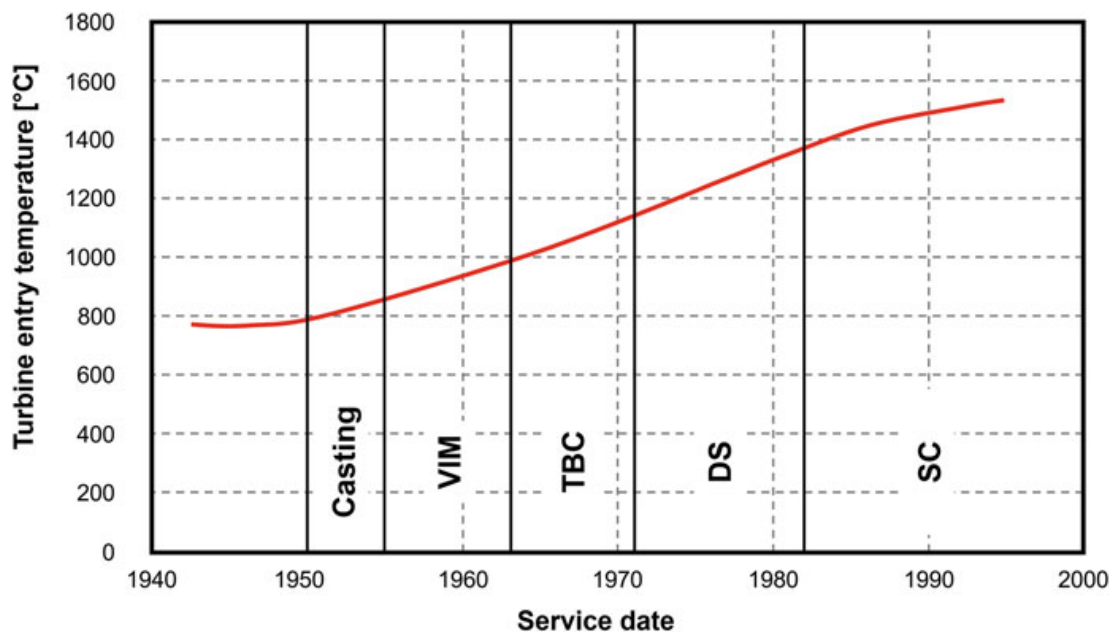
Fig. 1.14 Evolution of the turbine inlet temperature as a function of the in-service date. See main text for the legend of the processing techniques recalled in the graph. (Redrawn from King et al. 2009)

As it will be illustrated in Chap. 2, the turbine inlet temperature is also a very important parameter to assess the efficiency of a GT engine. An increase by 50 °C of the turbine inlet temperature can increase by 1% the engine efficiency, with a consequently lower fuel consumption and reduced exhaust emission. Considering that fuel costs are the most important expenses for airline companies (see Fig. 1.13), the interest in better performing engines becomes evident and may explain the remarkable development of the processing routes for the manufacturing of turbine blades. This is shown in Fig. 1.14, in which the main enabling process technologies used for the production of high-pressure blades, regarded as the most critical parts of a gas turbine engine, are associated with the relevant achieved TETs. Casting and vacuum induction melting (VIM, see Sect. 5.3.2) were used to produce

polycrystalline equiaxed blades, in general solid or with cooling channels drilled after solidification. These components suffered from creep-limited performances, since the elevated concentration of grain boundaries determined comparatively high deformation rate, mainly due to diffusive creep (see Sect. 6.5.1). A possible approach to improve creep life was through the reduction of the metal temperature, attained with the deposition of a thermal barrier coating (TBC, see Sect. 7.3.2).

A lower blade temperature would display a lower creep deformation rate. This was actually the case, although the durability of TBC systems and the prediction of their useful lifetime were soon regarded as critical parameters for key components, as high-pressure turbine blades are. The creep problem was therefore tackled acting directly on the structural reason for its occurrence in turbine blades, i.e., the presence of grain boundaries, particularly those oriented normally to the maximum stress, applied along the blade main axis. Therefore, using directional solidification (DS) and, subsequently, single-crystal (SC) solidification (see Sect. 6.5), blades with grain boundaries aligned along the main axis of the blade, or missing at all, were obtained. These components, since the 1980s, are the standard for commercial aircrafts and are being adopted also for land-based gas turbines, again for enhancing their performances at the acceptable costs afforded by the now mature technology of the directional solidification and single-crystal processes.

1.3   Aerospace-Related Fields

The mentioned land-based gas turbine engines are just one of the many technologies and materials developed for the aerospace field and then transferred to terrestrial applications. The situation is actually not always so clear-cut: in fact, gas turbine engines exploit some of the working principles of turbo-charged piston engines, originally developed for automotive applications. It is therefore advisable thinking in terms of two-way exchange between aerospace and other technological fields.

It is certainly true that the aerospace field has always had a particular focus on the development of materials and systems complying with strict limitations, as concerns safety and reliability. These standards require important systemic research efforts to study problems in depth and to find optimal solutions. Therefore, materials and systems developed and/or optimized for the aerospace fields are most interesting candidates for applications also in other fields. In the present book, only some of those more directly involved with the use of aerospace alloys will be considered.

The field of energy production is certainly benefitting from the processing technologies for the production of components made of superalloys (see Chap. 6) and special steels (see Chap. 5), used in land-based gas turbines, vapor turbines, and other systems working at comparatively high temperatures, although generally lower than the aerospace counterpart, but still demanding for the alloy materials. This is so even because the environmental conditions that are faced by components of terrestrial plants may be more demanding in terms of corrosion resistance, considering that

the quality of the fuels used in this field is definitely worse than the extremely refined aerospace ones.

Light alloys, in particular aluminum and magnesium (see Chap. 3), are being employed to increasing extent in the automotive field, for the same reason just discussed for aerospace applications, to reduce the weight of the vehicle in order to reduce fuel consumption and consequently the environmental pollution associated with the production of particulate matter and gaseous emissions.

Titanium alloys (see Chap. 4) are very important for biomedical applications, as concerns particularly their biocompatibility. Shape-memory alloys (see Sect. 9.5), which have been applied for the first time as cryo-fit joints in a military aircraft, are now having an important set of applications in the aerospace field, in some case really strategic, like the deployment system Frangibolt (see Sect. 9.5.2). At the same time, still remaining in the field of products with high added value, numerous biomedical applications are now available, like stents, orthodontic wires, surgery tools, and many more.

Structural polymer matrix composites are now finding their way in aerospace, already widely employed for terrestrial application, and are gaining more interest.

The aircraft brake systems, based on carbon-carbon composites, have provided fundamental knowledge and performance data for the application of similar principles and technical design to brakes of top and high-performance cars, like the F1 racing.

References

Boeing (2013) 787 Aircraft Rescue & Firefighting Composite Structure. Available via DIALOG. http://www.boeing.com/assets/pdf/commercial/airports/faqs/787_composite_arff_data.pdf. Accessed 18 Aug 2017

Calvert D J (1990) Harrier. Ian Allan Publishing Ltd

Cantor B, Assender H, Grant P (2001) Aerospace Materials. Institute of Physics Publishing

Curtis H D (1997) Fundamentals of aircraft structural analysis. Irwin Publ., Chicago

Darling K (2001) Airliner Tech Volume 7 – De Havilland Comet. Specialty Press Publishers and Wholesalers

Friend E L, Sefic W J (1972) Flight Measurements of Buffet Characteristics of the F-104 Airplane for Selected Wing-Flap Deflections. Nasa Technical Note D-6943. Available via DIALOG. https://www.nasa.gov/centers/dryden/pdf/87804main_H-666.pdf. Accessed 05 May 2019

King D et al (2009) Advanced Aerospace Materials: Past, Present and Future. Aviation and the Environment 3(9): 22–27

Krishnan K S (2006) Materials and the Aerospace Industry. In: Enhancing Innovation and Competitiveness Through Investments in Fundamental Research, Westin Hotel, Arlington, VA, 3–5 December 2006

Mouritz A P (2012) Introduction to Aerospace Materials. Woodhead Publishing Ltd

NASA (2003) Learning to Fly: The Wright Brothers' Adventure – A Guide for Educators and Students With Activities in Aeronautics. NASA Educational Division. Available via DIALOG. https://www.nasa.gov/audience/foreducators/topnav/materials/listbytype/Learning.to.FlyThe. Wright.Brothers.Adventure.html. Accessed 09 Jun 2017

NASA (2008) SR-71 Blackbird. NASA Facts. Available via DIALOG. https://www.nasa.gov/centers/dryden/pdf/495839main_FS-030_SR-71.pdf. Accessed 10 Jun 2017

NASA (2018) F-104 Starfighter Image Gallery. https://www.nasa.gov/centers/armstrong/multimedia/imagegallery/F-104/index.html. Accessed 05 May 2019

Savino R et al (2005) Aerothermodynamic Study of UHTC-based Thermal Protection Systems. Aerospace Science and Technology 9 (2): 151–160

Starke E A, Staley J T (1996) Application of Modern Aluminum Alloys to Aircraft. Progr Aerospace Sci 32:131–172

The National Archives (2019) Public Information Films | 1945 to 1951. Available via DIALOG. http://www.nationalarchives.gov.uk/search/results?_q=de+havilland+comet. Accessed 05 May 2019

Torenbeek E (2013) Advanced Aircraft Design. John Wiley & Sons Ltd

Further Reading

Bowman M W, Vogelsang M (2000) Lockheed F-104 Starfighter. The Crowood Press Ltd, Ramsbury

Cutler J (2005) Understanding Aircraft Structures. Blackwell Science

Federal Aviation Administration (2012) Aviation Maintenance Technician Handbook – Airframe Vol. 1. Federal Aviation Administration

Federal Aviation Administration (2012) Aviation Maintenance Technician Handbook – Airframe Vol. 2. Federal Aviation Administration

Federal Aviation Administration (2012) Aviation Maintenance Technician Handbook – Powerplant Vol. 1. Federal Aviation Administration

Federal Aviation Administration (2012) Aviation Maintenance Technician Handbook – Powerplant Vol. 2. Federal Aviation Administration

Gates D (2004) Sky Wars: A History of Military Aerospace Power. Reaktion Books Ltd

Megson T (2013) Aircraft Structures for Engineering Students. Elsevier

Withey P (2019) The Real Story of the Comet Disaster: De Havilland Comet – Structural Fatigue. In: Hamburg Aerospace Lecture Series. Available via DIALOG. https://zenodo.org/record/2551089#.XNHwSI5LiUl. Accessed 05 May 2019

Wixey K E (1987) Lockheed Constellation. Ian Allan Ltd

Chapter 2
Gas Turbine Aero-Engines

2.1 Introduction

Gas turbine engines are mechanical systems able to provide an extremely efficient conversion of the energy, produced by internal combustion, into mechanical work, to power an electric generator or to provide thrust for an aircraft to fly. Several features of gas turbine engines have been especially developed for aircraft propulsion, since the pioneering studies by René Lorin in 1913 (Rolls-Royce 1996), followed by Frank Whittle in the UK and Hans von Ohain in Germany, in the years preceding the burst of the World War II (Gunston 1995). A jet propulsion engine is a particular type of reaction engine, in which a fast-moving airflow (jet) generates a thrust, according to Newton's third law of motion. Several different types of jet engines do exist, named according to the relevant working principles. Strictly speaking, a pure jet propulsion occurs in turbojets, ramjets, pulse jets, and rockets too. In turbo-propeller and turbofan engines, the thrust is completely or largely produced by the compression waves generated by the propeller or ducted fan, respectively. Gas turbines have moving parts, which pose important challenges to materials owing to the combined effects of mechanical stresses, corrosive atmosphere, and high temperatures. In these air-breathing systems, a rotary compressor, powered by the turbine, provides high-pressure air to the combustor. Here, air is mixed up with the fuel and spark ignited to produce the flame and enthalpy output that through the gas is transferred to the turbine rotor. Although, working under continuous gas flux, the efficiency of these thermal machines can be evaluated referring to a closed Brayton cycle, thermal efficiency is not the only parameter that qualifies different classes of jet aero-engines. In fact, specific fuel consumption; specific thrust, particularly during takeoff; noise; and other issues pertaining to the environmental impact are all other important parameters to be considered.

2.2   Types of Aircraft Engines

The development of gas turbine engines stems from the need to overcome the intrinsic limits of piston engines, used since the early flight of the Wright brothers (see Chap. 1) to operate a standard wooden propeller. The two main drawbacks that have emerged in applying these engines to aircraft propulsion are efficiency reduction for speeds in excess of about 600 km/h and reduction in the propulsion efficiency determined by the so-called air starvation at high altitude flights. The first limit is due to the fact that the propeller cannot reach, and overtake, the speed of the pressure waves it produces. Therefore, the propulsion efficiency of the engine would progressively decrease as the speed of sound is approached. The second phenomenon is caused by the reduction of air density in the upper layers of the Earth's atmosphere, with a consequent effect on the compression ratio that can be reached inside the piston chamber.

   The first patent for a jet propulsion system was issued by René Lorin (1913, see Fig. 2.1), although the early application of this new technology appeared more than 20 years later, due to the limitations in technological processes and materials properties. The main idea behind the development of jet propulsion engines can be retrieved in the working principle of a turbocharger engine (see Fig. 2.2).

Fig. 2.1 Scheme of the first jet propulsion system developed by René Lorin, 1913. (Redrawn from Rolls-Royce 1996)
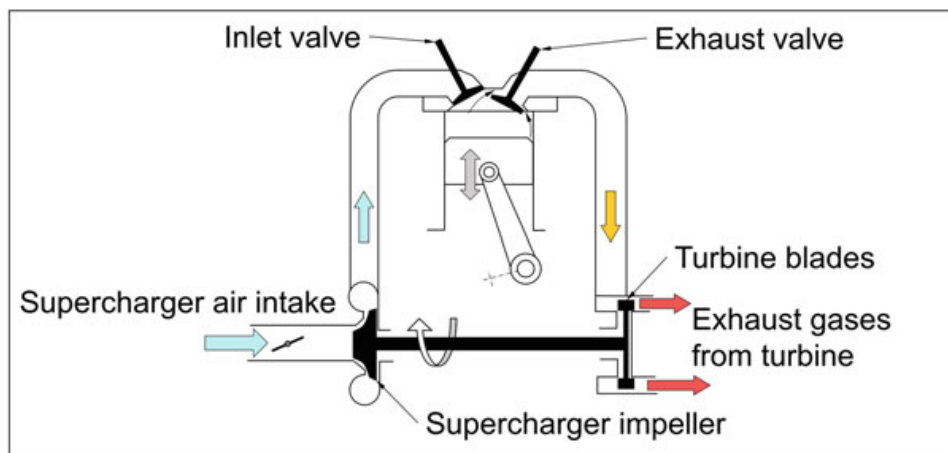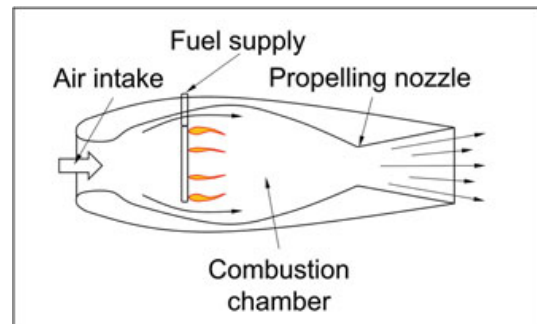
Fig. 2.2 Turbocharger engine with centrifugal compressor. (Redrawn from Meetham 1981)
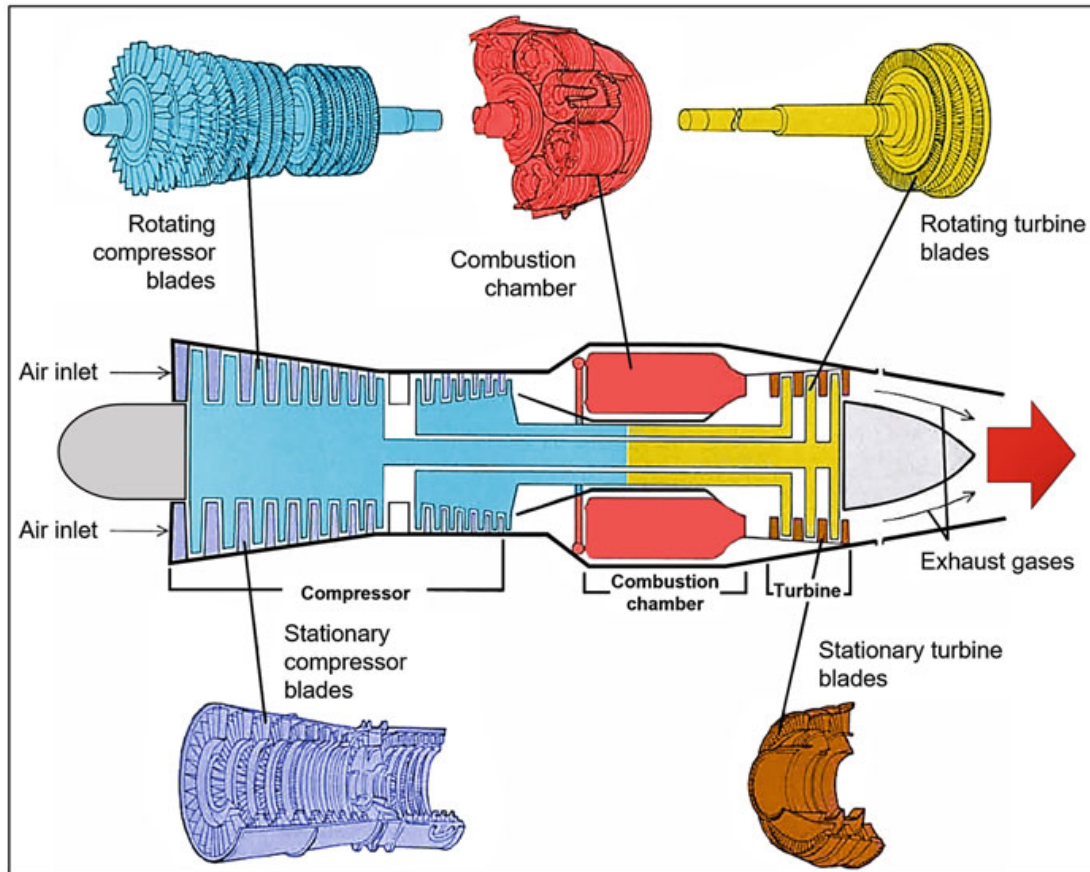
Fig. 2.3   Structure of a two-stage gas turbine jet engine

The pressure of the air entering the piston chamber is raised by a centrifugal compressor connected to the turbine. The turbine is operated by the exhaust emission ejected from the combustion chamber, so that further energy can be recovered from the gas before it is emitted from the engine. Similarly, in gas turbine engines, a compressor is meant to increase the pressure of the air entering the combustors to optimize the combustion under all operational conditions. Part of the energy carried by the gas flux is transferred back to the compressor by the turbine stages through coaxial multiple shafts. The rest of the combustion energy output is used to generate thrust or other forms of energy in case of non-aero applications, e.g., marine and terrestrial engines. The main operation stages of a gas turbine (GT, Fig. 2.3) can be summarized as follows:

- Air inlet into the compressor
- Air compression
- Compressed air inlet into the combustion chamber
- Fuel addition
- Ignition
- Entrance of the exhaust gas into the turbine
- Generation of thrust work
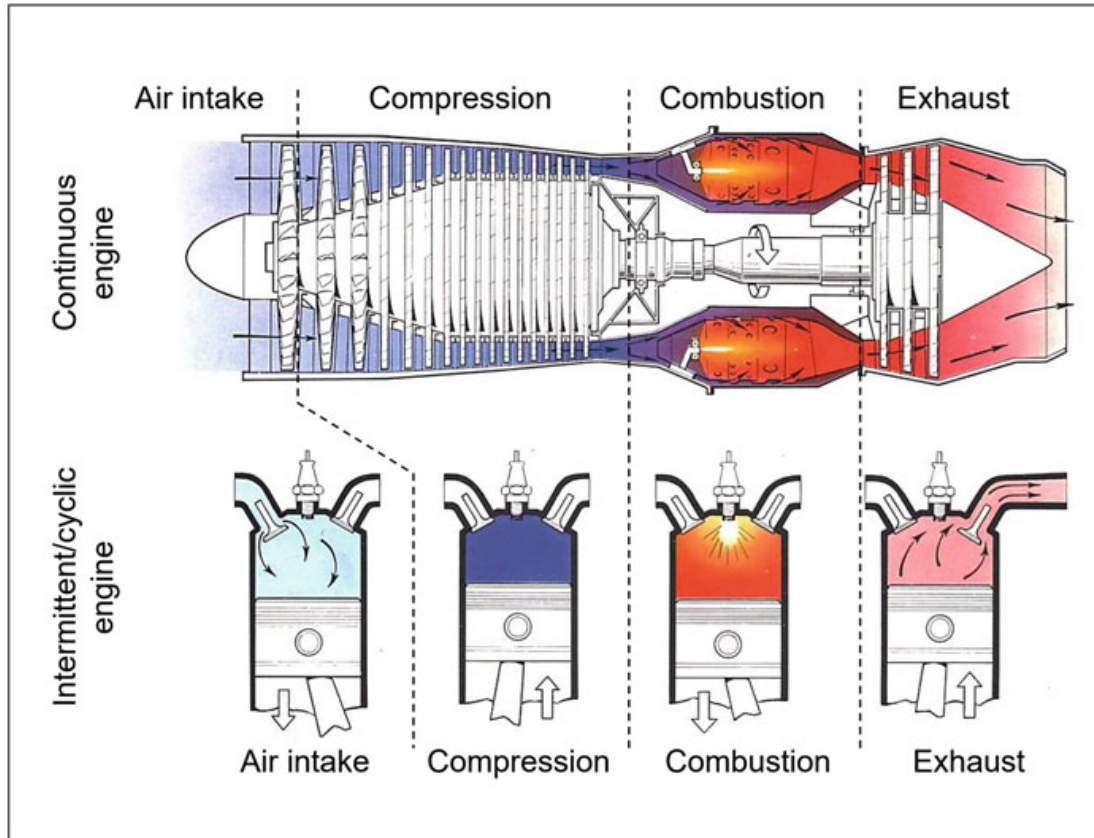
Fig. 2.4 Comparison between a gas turbine jet engine and a four-stroke piston engine. (Rolls-Royce 1996, images courtesy of Rolls-Royce plc)

GT engines may reach extremely high efficiencies, close to 100%. They operate according to a continuous process with a free expansion in the combustion area.

Piston engines are characterized by a lower efficiency, if compared with GTs, since just one out of the four strokes is active (see Fig. 2.4). Furthermore, they must be more massive in order to withstand an instantaneous increase in pressure associated with the constrained, fixed combustion volume.

These two features contribute to make these engines a non-ideal choice for aerospace applications. Notwithstanding the "open" character of a GT engine, it is common practice to analyze its working principles referring to a basic thermodynamic approach, using an equivalent thermodynamic cycle to estimate its efficiency and to evaluate the associated work output from the relevant cycle area, as depicted by the general Carnot cycle in Fig. 2.5.

As anticipated in the introductory paragraph of this chapter, the GT engine working principles can be described according to the Brayton cycle. It is evident that the thermodynamic cycle is different if compared to the piston engine, considering that this latter is better represented by the Otto cycle (Fig. 2.6).

One of the most important parameters to take into account while analyzing GT engine thermodynamic cycles is the turbine entry, or inlet, temperature (TET). This

Fig. 2.5 P-V diagram of the
Carnot cycle
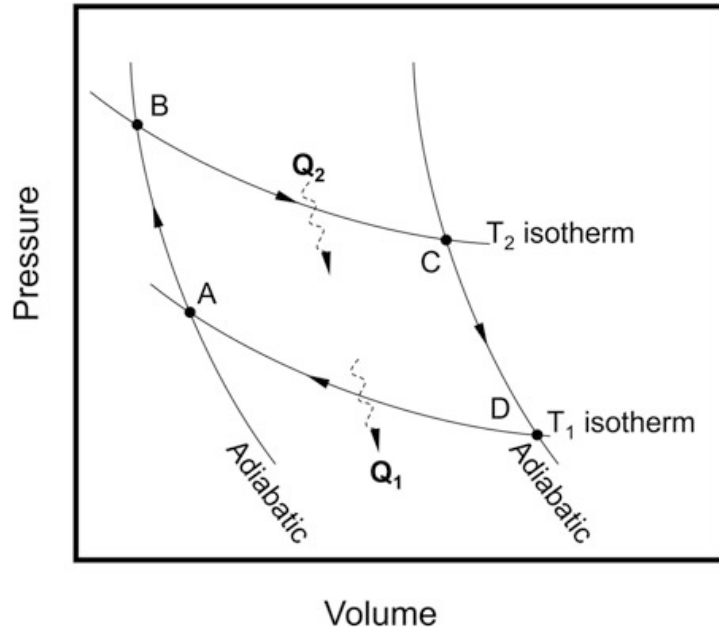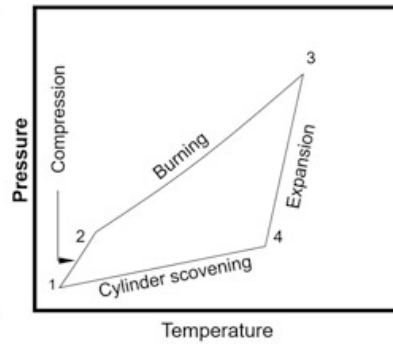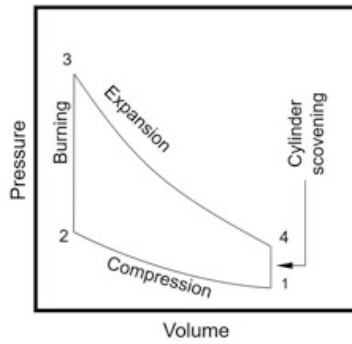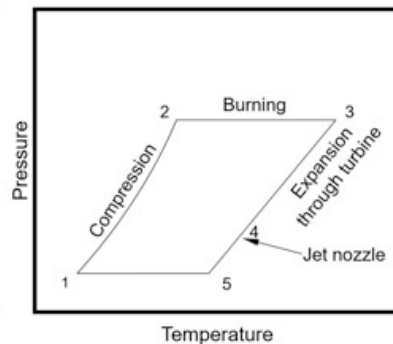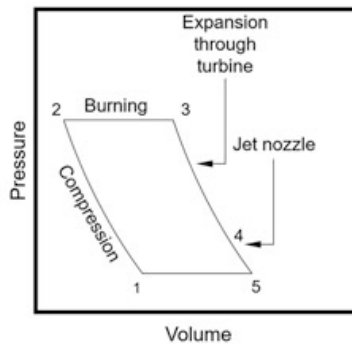
Fig. 2.6 Comparison between Otto and Brayton cycles using P-V and P-T diagrams

is a very important parameter for evaluating the efficiency of the propulsion system.
The most severe operating conditions inside the jet engine are those corresponding to
point 3 in Figs. 2.6 and 2.7. In fact, this point of the cycle features the highest
temperature of the hot gases, impinging directly on the vanes and blades of the
turbine.
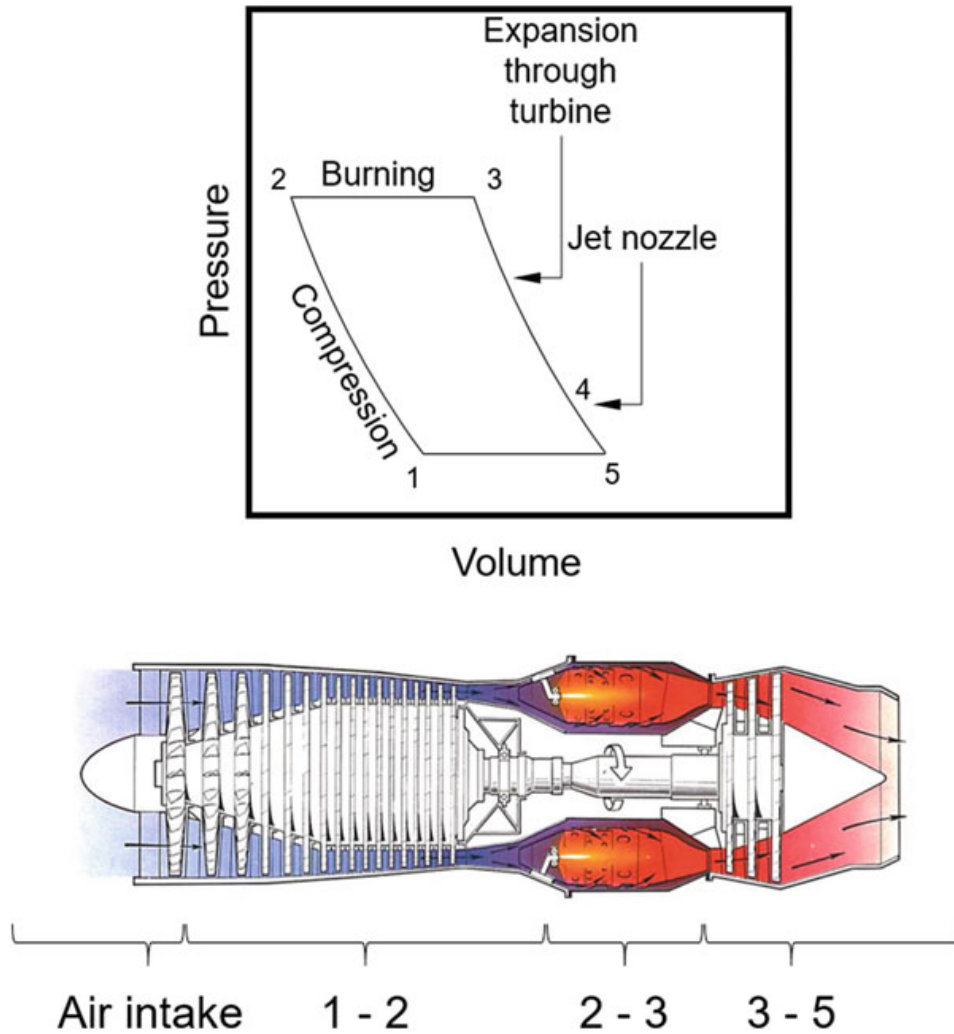
Fig. 2.7 Brayton cycle and correspondence with different GT operational stages. (Rolls-Royce 1996, images courtesy of Rolls-Royce plc)

In addition to the combustion gases and relevant thermomechanical stresses, blades are also under the effect of the centrifugal force generated by the disc and blade high-speed rotation.

The efficiency of the propulsion system is improved by increasing the difference in temperature between points 1 and 3 (see Fig. 2.6, Brayton cycle). Inlet air temperature is a parameter that cannot be changed straightaway, depending on the atmospheric conditions. Conversely, T_3, i.e., the turbine entry temperature, can be modified and, in particular, increased with an appropriate design of the engine and selection of suitable materials. However, the improvement in thermodynamic efficiency is accompanied by an unwanted increase in the specific fuel consumption (SFC). SFC can be regarded as a fuel-related efficiency parameter of the engine, and it is given by the amount of fuel consumed per unit thrust. This increase in SFC can be compensated for by a corresponding increase in the overall pressure ratio (OPR), i.e., the ultimate air pressure value that can be achieved in the latest stage of the compressor, before air injection into the combustion chamber. The situation is
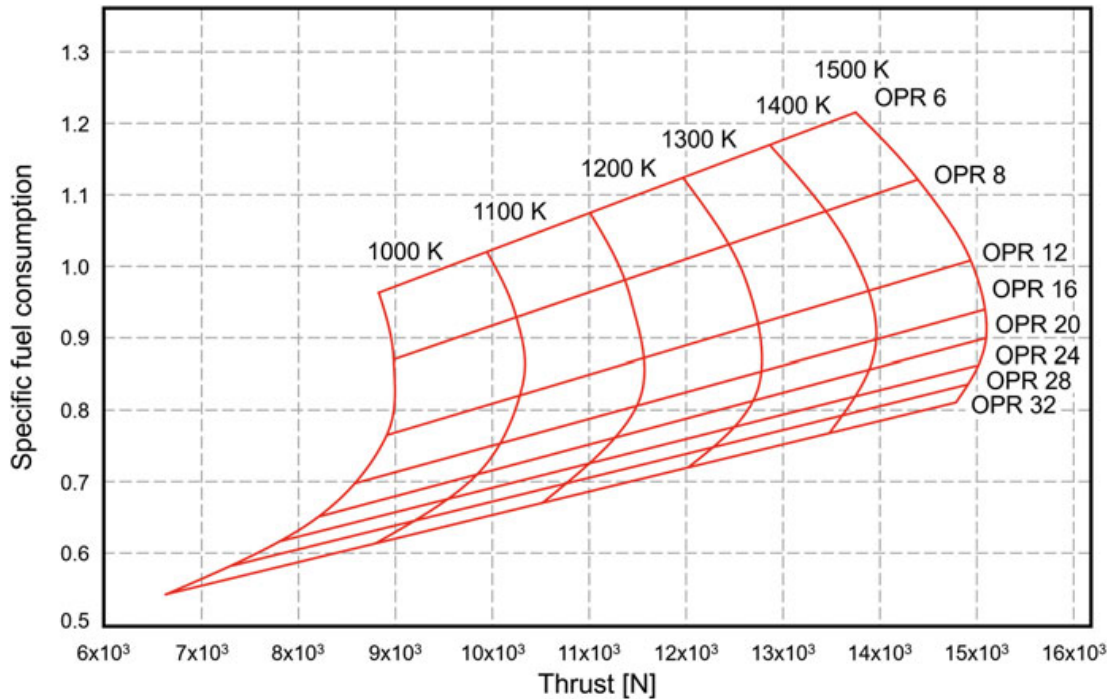
Fig. 2.8 Dependence of the specific fuel consumption and engine thrust as a function of the turbine entry temperature (TET) and overall pressure ratio (OPR). (Redrawn from Reed 2006)
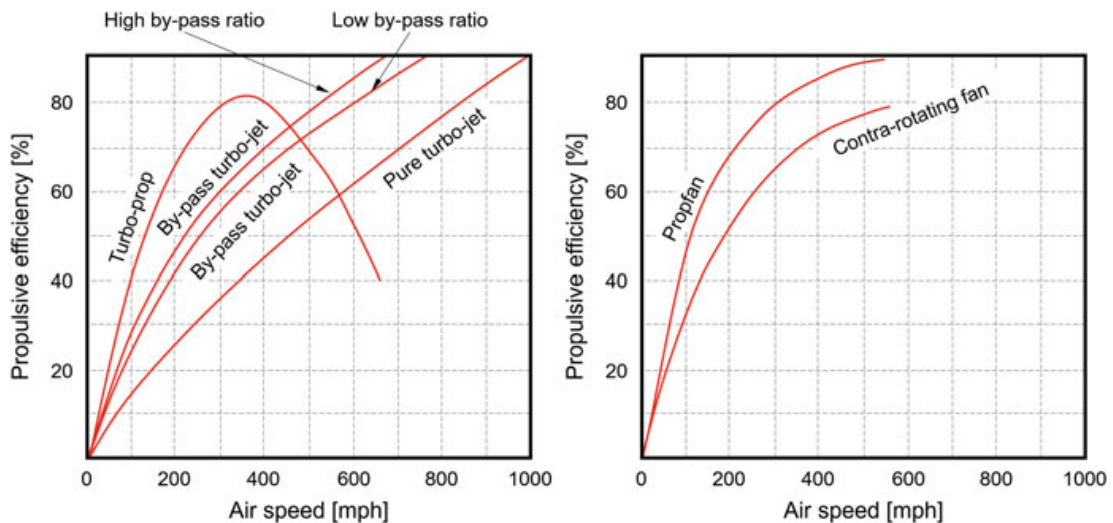
Fig. 2.9 Propulsive efficiency vs aircraft speed for different engines (1 mph = 1.609 km/h). (Redrawn from Rolls-Royce 1996)

depicted by the graph in Fig. 2.8, displaying the combined effect of TET and OPR on the engine performances. In state-of-the-art gas turbine engines, e.g., Rolls-Royce Trent XWB, the OPR has reached values of 50 or so. Concerning the efficiency of the propulsion system, turbojets show an increase in their efficiency with the aircraft speed, since this reduces the dissipation of the energy of the outlet gas flux against the surrounding static air (see Fig. 2.9). The peak followed by a decreasing trend at
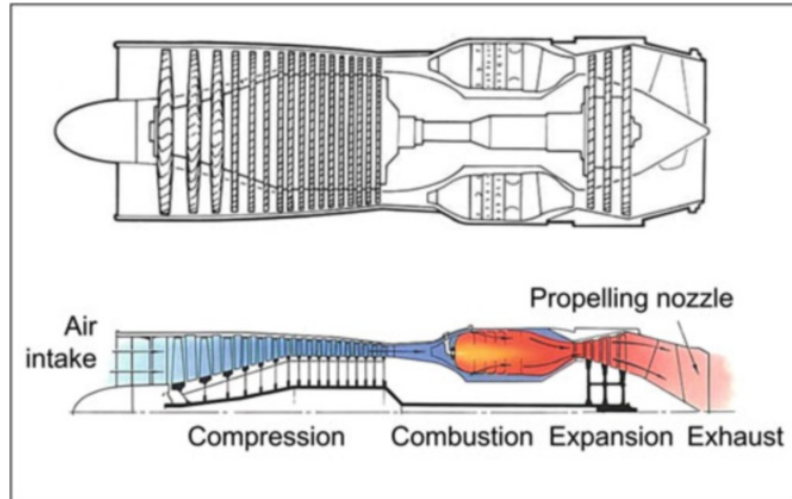
Fig. 2.10 Rolls-Royce Avon single-shaft engine. (Rolls-Royce 1996, images courtesy of Rolls-Royce plc)

higher speeds observed in the efficiency curve of the propeller-operated aircrafts is dependent instead on the reduction in efficiency that occurs once the advancement speed of the propeller in air is approaching the speed of sound.

Differences in gas turbine engines for aircraft applications can be found in the architecture and in the range of performances. Turbojet engines use the combustion gases directly for the propulsive thrust. In turbofans, the propulsion is provided by the fan and to minor extent only by the jet of the exhaust gas. This is the basis for the by-pass principle, which implies a split in the airflow. The whole air intake is given an initial low compression, and a large fraction is then ducted to the bypass, the rest being delivered to the combustion chamber (Fig. 2.11). The idea behind the development of by-pass engines is related to the following specific aspects: better fuel consumption, higher thrust (even at low-speed regimes), noise reduction, and reduced relative weight of the engine. These aspects have been achieved thanks to the evolution of the engine design, starting from a comparatively simple single-shaft turbojet, as shown by the schematic of the Avon engine (see Fig. 2.10), to reach the complexity of the multiple-shaft engines in Fig. 2.11, featuring also higher by-pass ratios.

The by-pass ratio, i.e., the ratio between cool air by-passed through the outer duct and the air flowing through the high-pressure inner part of the engine, is an important feature of these engines. With low bypass ratios (e.g., 1:1), the two air streams are generally mixed before being emitted through the exhaust duct of the engine. In turbofan engines requirements for higher bypass ratios, up to 5:1, are met by large front fans and multiple-stage compressor, using a twin- or triple-shaft configuration (see Fig. 2.11). In this case the front fan acts also as a low-pressure compressor stage. Bypass ratios in the order of 15:1 are achieved using prop-fans (Rolls-Royce 1996). Custom design has been developed for complying with the specific requirements of the different aircrafts and relevant operational conditions. Correspondingly, different pressure and temperature profiles are present along the engine like those shown in
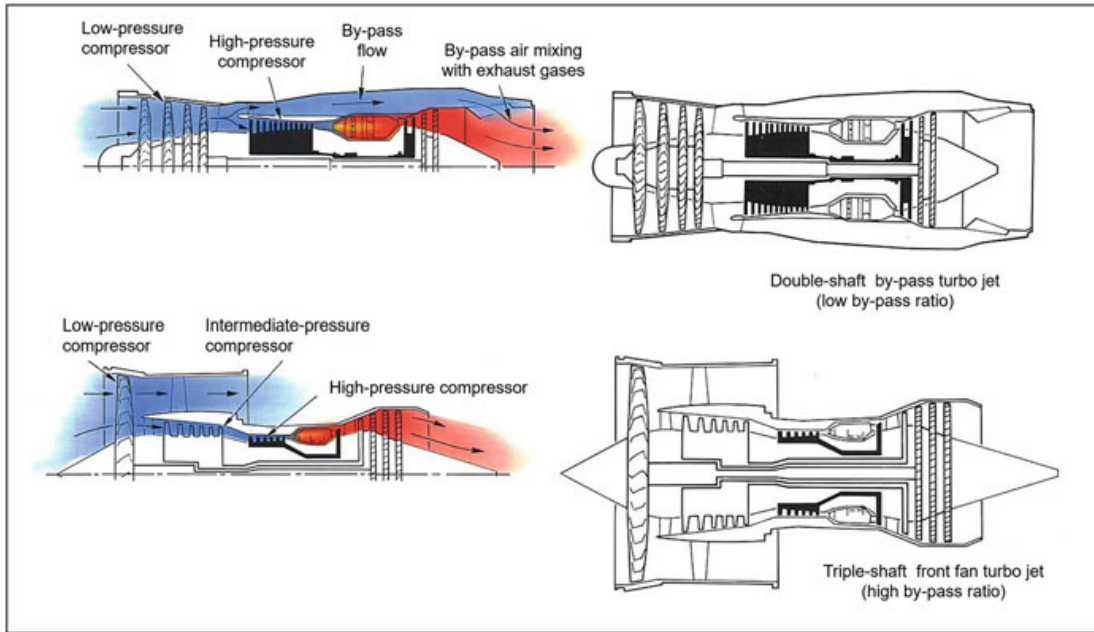
Fig. 2.11 Rolls-Royce engines with a multiple-shaft design. (Rolls-Royce 1996, images courtesy of Rolls-Royce plc)
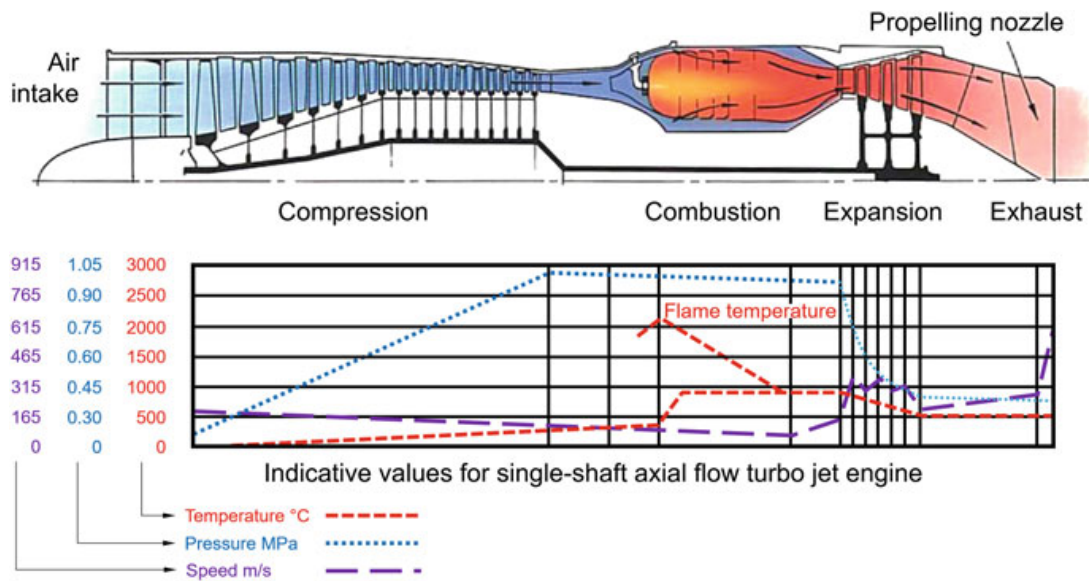
Fig. 2.12 Air speed, pressure, and temperature profiles in a turbojet engine. (Rolls-Royce 1996, image courtesy of Rolls-Royce plc)

Fig. 2.12 for a turbojet engine. These fundamental changes in the structure of the aircraft engines have been possible thanks to the availability not only of better performing materials but also of new technical choices in the design of the engine components. These aspects are considered in the following sections.

2.3   Compressors

In a gas turbine engine, the compressor converts the power from the turbine into kinetic energy of the airflow, by increasing its pressure. An upstream rotating compressor is coupled to a downstream turbine. The combustion chamber is placed in between these two components. Energy is added to the gas flow through the ignition of the fuel-air mixture that forms inside the combustor by spraying fuel into the compressed air. The resulting enthalpy output raises the gas temperature, the *flame temperature*, which in the most severe operating conditions can even reach values of 3000 °C.

The work output of the combustion is used to drive, through coaxial components of the shaft, the different stages of the turbine and the corresponding stages in the compressor. All energy that is not used for the shaft operation leaves the engine as an exhaust gas flux and contributes to the thrust of the aircraft.

Actually, a multi-stage compressor is rather common in case of axial geometry, but not so much in centrifugal compressors, the earliest to be used in aerospace gas turbines. In this regard, compare typical schemes for centrifugal (Fig. 2.13) and axial (Fig. 2.14) compressors, respectively. The complex trajectories of the air flux inside centrifugal compressors (see Figs. 2.13 and 2.15) lead to instabilities that can be regarded among the main reasons for their decline. In jet engines equipped with axial compressors, the pressure raise is due to the progressive reduction of the volume available to the fluid as it proceeds inside the engine (see Fig. 2.15). Axial compression produces a nearly linear velocity profile of the gas, and it is definitely more stable than in centrifugal compression. One important parameter is the compressor exit temperature, increasing over the years (see Fig. 2.16), following the trend of the OPR, also quoted in the same graph for different engines. The related increasing trend of the pressure ratio for both aerospace and industrial applications is also displayed (Fig. 2.16).

The two main components of the compressor rotor are the discs and the blades. Disc materials should exhibit adequate values of the following properties:

- Resistance to high-frequency fatigue
- Resistance to low-frequency fatigue (engine start and shutdown phases)
- Tensile strength, toughness, and creep resistance

Single-entry two-stage
centrifugal turbo propeller

Double-entry two-stage
centrifugal turbo jet
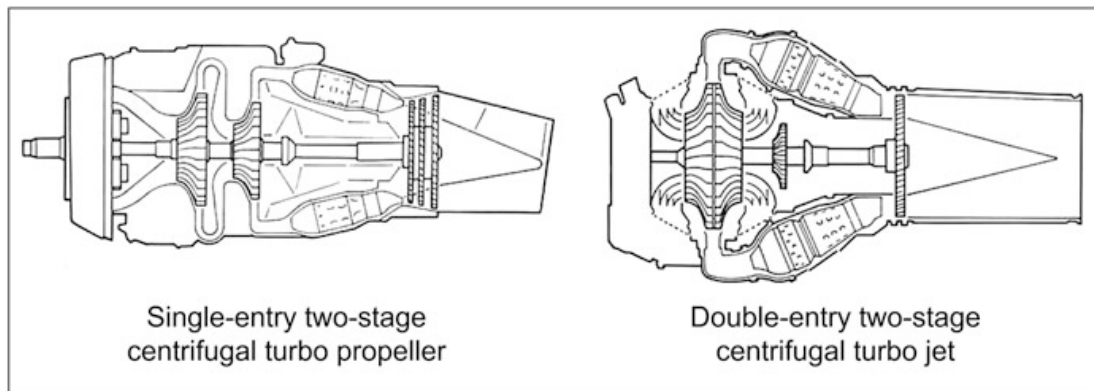
Fig. 2.13   Two examples of centrifugal compressors used in early aero gas turbine engines. (Rolls-Royce 1996, images courtesy of Rolls-Royce plc)
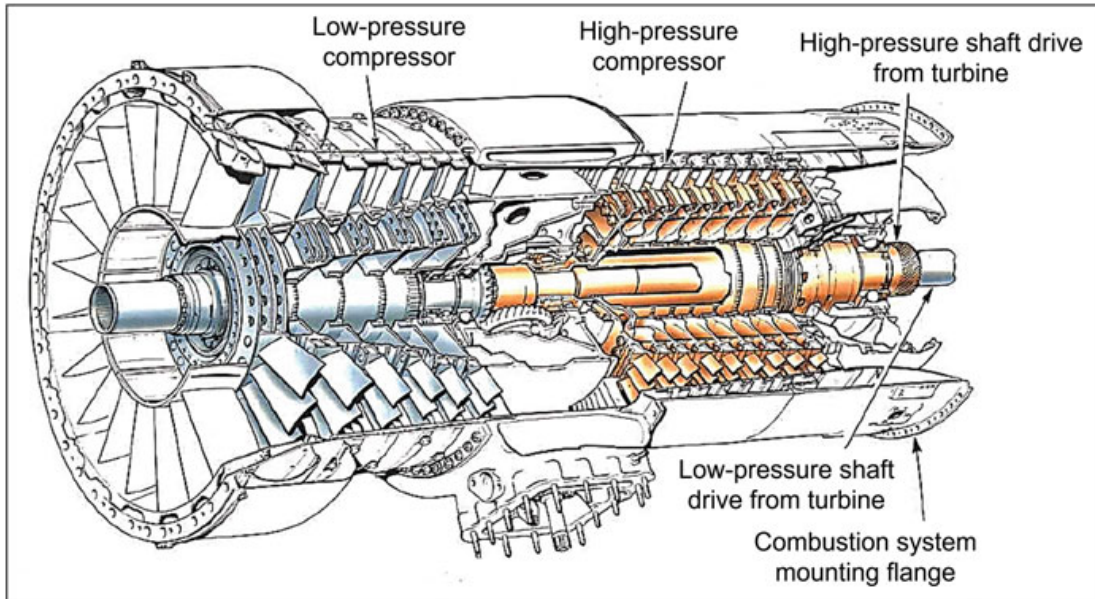
Fig. 2.14 Twin-shaft compressor. (Rolls-Royce 1996, image courtesy of Rolls-Royce plc)
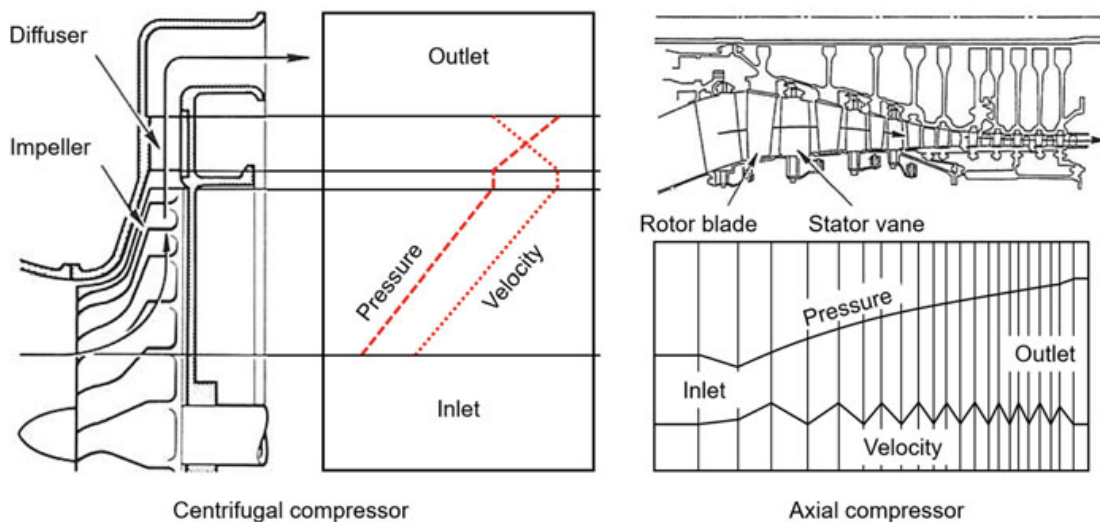
Fig. 2.15 Air velocity and pressure for centrifugal and axial compression systems. (Rolls-Royce 1996, images courtesy of Rolls-Royce plc)

Compressor blades have some specific requirement too. In particular, they must be characterized by good values of:

- Erosion resistance
- Resistance to high-frequency fatigue
- Tensile strength
- Fracture toughness

Erosion resistance can be improved using protective composite coatings; Co-WC-based coatings show excellent erosion resistance and tribological properties
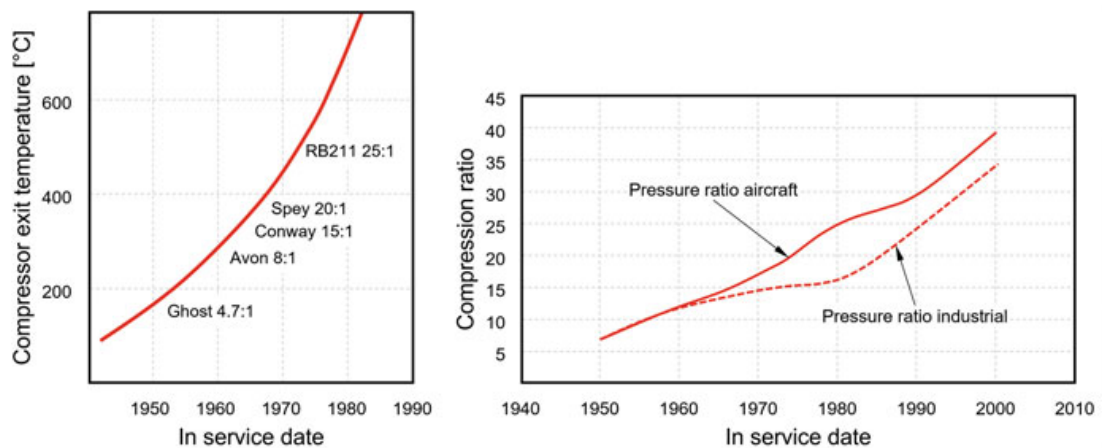
Fig. 2.16 Compressor exit temperature vs in-service date for several GT engine models (for each one of them, the OPR value is also indicated) and compression ratio vs in-service date for aircraft and industrial applications. (Redrawn from Boyce 2012; Meetham 1981)

(see Sect. 7.3.5). In Table 2.1 a list of materials used for the fabrication of compressor rotor parts of a commercial GT engine is presented.

Titanium alloys (see Chap. 4) are used for the first outer stages, both discs and blades, since they provide a good compromise of high specific mechanical strength, creep, and oxidation resistance. Where higher temperatures are achieved and render diffusion-assisted phenomena more important, nickel- and iron-based superalloys, like Inconel 718 (see Sect. 6.3), and precipitation hardened austenitic stainless steels (PHSS), like A286 (see Sect. 5.4.3.3), are preferably used. These materials indeed provide adequate mechanical stability even against creep deformation, and the definitely higher densities, as compared to Ti-alloys, are not resulting in too large inertial momenta, due to high-speed rotation, for the comparatively smaller dimensions of these parts. The intrinsically good oxidation resistance can be improved further with suitable coating systems, like Ni-aluminides diffusion coatings or MCrAlY overlay coatings (see Sect. 7.3.1).

2.4   Combustors

The combustor is the part of the GT engine in which the conversion of the chemical energy content of the fuel is turned into the thermal energy of the gas flow. This is achieved through the combustion of the air-fuel mixture with the as higher as possible efficiency, also to keep the emission of undesired pollutants at the lowest levels. To meet this target, a highly turbulent gas flow is very much welcome (Cumpsty 2003). In early GT engines, the combustor was made of separated chambers, with several inlet hole access for the compressed air, in order to improve the homogeneity of the composition of the combustion mixture (see Fig. 2.17).

Table 2.1 Compressor rotor materials, coating systems, and part finish

Part name	Material	Finishing	Part name	Material	Finishing
Blades, stage 1	Ti-6Al-4V	WC	Blades, stages 4–5	Ti-6Al-4V	Colloidal graphite
Adapter retainer	AMS 5754	None	Blades, stages 6–9	Ti-6Al-2Sn-4Zr-2Mo	Colloidal graphite
Air duct	A286	Cu-Ni-In	Bumper bearing	AMS 5612	Ni graphite
		Ag plate	Disc, stage 1	Ti-6Al-4V	Ni-aluminide
Assembly, air seal	Inconel 718	Ni-aluminide			Molydisulfide
		Aluminum oxide	Disc, stage 2	Ti-6Al-4V	Molydisulfide
Blades, stage 1	Ti-6Al-4V	Cu-Ni-In	Discs, stages 10 and 14	Inconel 718	None
		Molydisulfide	Hub tie clamps	Inconel 718	Ni-aluminide
Blades, stage 2	Ti-6Al-4V	Cu-Ni-In			Cu-Ni-In
	Ti-6Al-2Sn-4Zr-2Mo	Molydisulfide	Hub tie supports	Inconel 718	None
Blades, stage 3	Ti-6Al-2Sn-4Zr-2Mo	Colloidal graphite	Rear shaft	Inconel 718	Cr plate
		Cu-Ni-In			Ni-aluminide
		Molydisulfide	Spline adapter	AMS 6381	None
Blades, stages 10–12	A286	Colloidal graphite	Spools, stages 3–9	Ti-6Al-2Sn-4Zr-2Mo	Ni-aluminide
Blades, stages 13–14	A286 / Inconel 718	Colloidal graphite	Spools, stages 11–13	Inconel 718	Ni-aluminide

Nowadays, annular combustors have been developed (see Fig. 2.18), although a multiple-chamber design afforded higher safety standards, since the failure or the malfunctioning of one component element is not necessarily jeopardizing the whole combustor. Air enters into the chamber at different places along the combustor, thanks to the presence of calibrated gaps left among the metal sheets of the annular chamber walls. A double-wall architecture is mandatory for this part of the engine where the peak temperatures of the whole thermodynamic cycle are achieved and an effective cooling is thus paramount, and in fact a fraction of the air flux from the compressor is used to cool down the combustor walls. Different operating regimes such as take-off, cruise, and landing would feature specific ranges for the actual air mass flow and of the air/fuel ratio. Requirements for combustor materials are:

- Oxidation/corrosion resistance. In the steady cruise regime, gas phase corrosion, i.e., oxidation and vanadation, may occur. During the engine shutdown and start-up phases, deposition of sodium sulfate may occur, introducing an additional surface instability process, i.e., hot corrosion (see Sect. 8.2.5).
- Thermal fatigue resistance.
- Thermal stability.
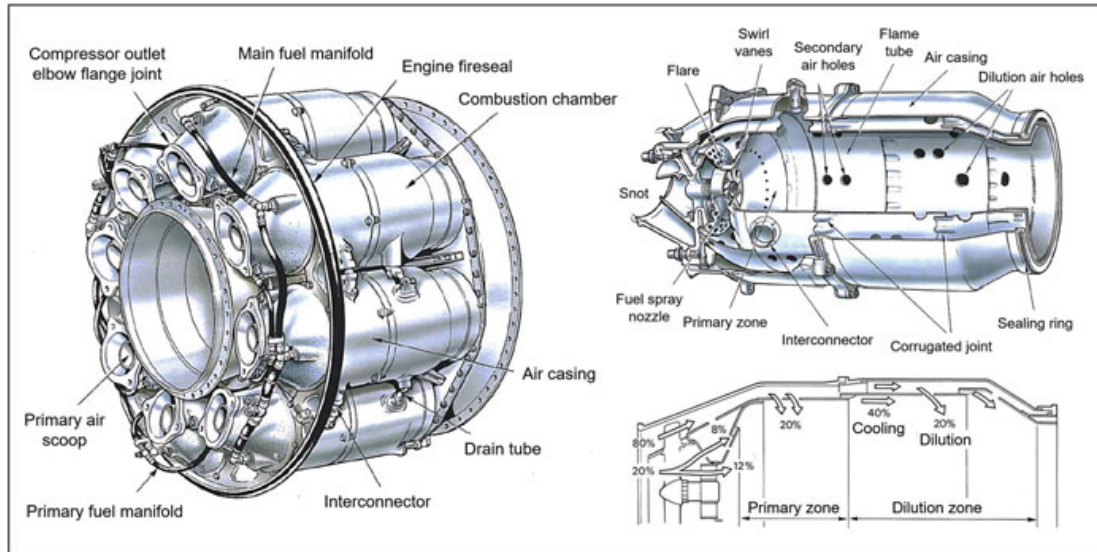
Fig. 2.17 Scheme of an early multiple-chamber system with detail regarding the single combustion chamber component and indication of the main functions of the inlet airflow coming from the compressor. (Rolls-Royce 1996, images courtesy of Rolls-Royce plc)
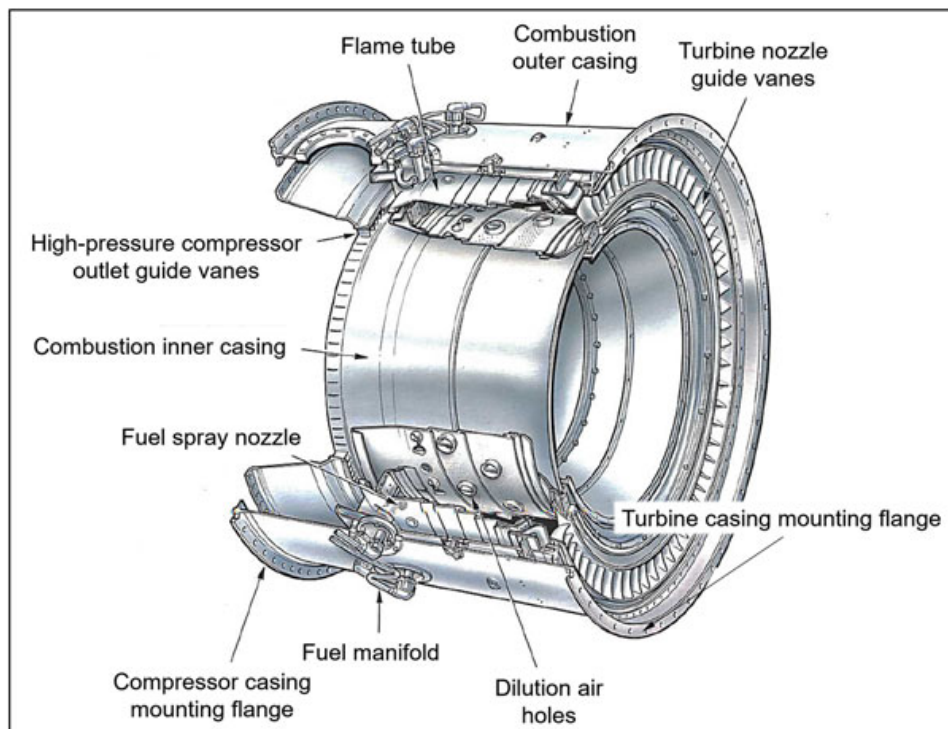
Fig. 2.18 Scheme of an annular combustion chamber. (Rolls-Royce 1996, image courtesy of Rolls-Royce plc)

According to these requirements, it is possible to identify some solutions that are highly reliable and, thereby, recommended for the fabrication of combustion chambers.

- Co-based superalloys (see Sect. 6.2). They usually display a lower strength than the companion materials, Ni-based superalloys (see Sect. 6.4). However, their strengthening mechanisms, mostly based on carbide precipitation, together with a comparatively lower coefficient of thermal expansion, render these materials preferable for the combustion chambers.
- Ceramic-based thermal barrier coatings (see Sect. 7.3.2). Coatings made of ZrO_2 with suitable stabilizer additions, like Y_2O_3 and ScO_2, are a standard choice in this respect; thanks to the thermomechanical compatibility with the underlying superalloy, they guarantee for these critical parts.

2.5 Turbines

The turbine converts the kinetic energy of the gases coming from the combustor into mechanical energy used to drive possible appliances and, most importantly, the compressor rotor stages and the fan, if present. In the turbine, a slight reduction, with respect to the combustion chamber, in the gas pressure and temperature takes place. The hot gases are at temperatures above 1500 °C, and the flow rate may exceed 750 m/s. The energy conversion process involves high stresses and high rotational speeds. Altogether, this renders the working conditions in the high-pressure stage of the GT extremely harsh. Vanes (static blades) and turbine blades of the first high-pressure stage are the most critical components of the whole engine, as concerns materials requirements (see Fig. 2.19). In fact, they are directly exposed to the jet of hot gases leaving the combustor, whose temperature (TET, see Fig. 2.20) has continuously increased over the years.

As depicted in Figs. 2.10 and 2.11, different architectures for jet engines are possible, with a different number of shafts and therefore of turbine stages. High bypass ratio fan engines may be equipped with a third intermediate-pressure turbine stage to operate the fan. This further stage is located between the high- and low-pressure turbines (*vide infra*, Fig. 2.22), according to a triple-spoon arrangement (Rolls-Royce 1996).

High peak temperatures and high-temperature gradients are not the only critical conditions for these turbine components, which have to withstand the high level of stresses, related to both the rotational motion and differential heating. Nickel-based superalloys (see Sect. 6.4) are the obvious choice, not only for the blades but also for other critical components of the turbine, requiring excellent strength associated with creep and fatigue resistance. Optimal performances have been achieved thanks to the use of newly developed casting techniques, leading to the manufacturing of directionally solidified and single-crystal components (see Sect. 6.5). It is important to highlight also the role of inner cooling channels. In cooled blades, the energy transferred from the flame to the material is removed so fast and efficiently that the alloy can even stand working temperatures that are important fractions of its incipient melting temperature.
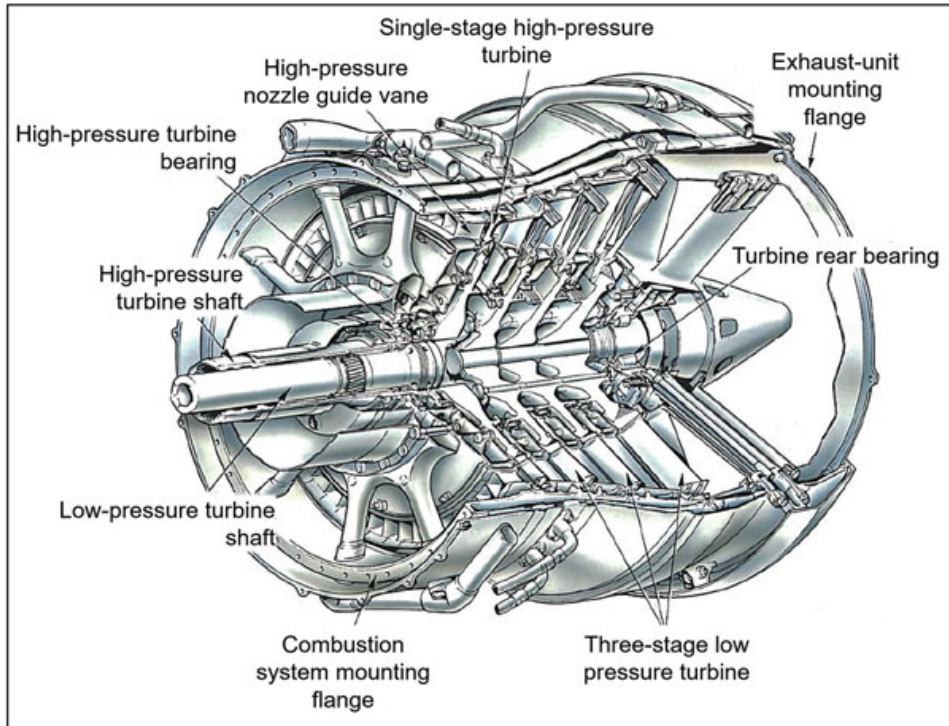
Fig. 2.19 Twin turbine and relevant double-shaft arrangement. (Rolls-Royce 1996, images courtesy of Rolls-Royce plc)
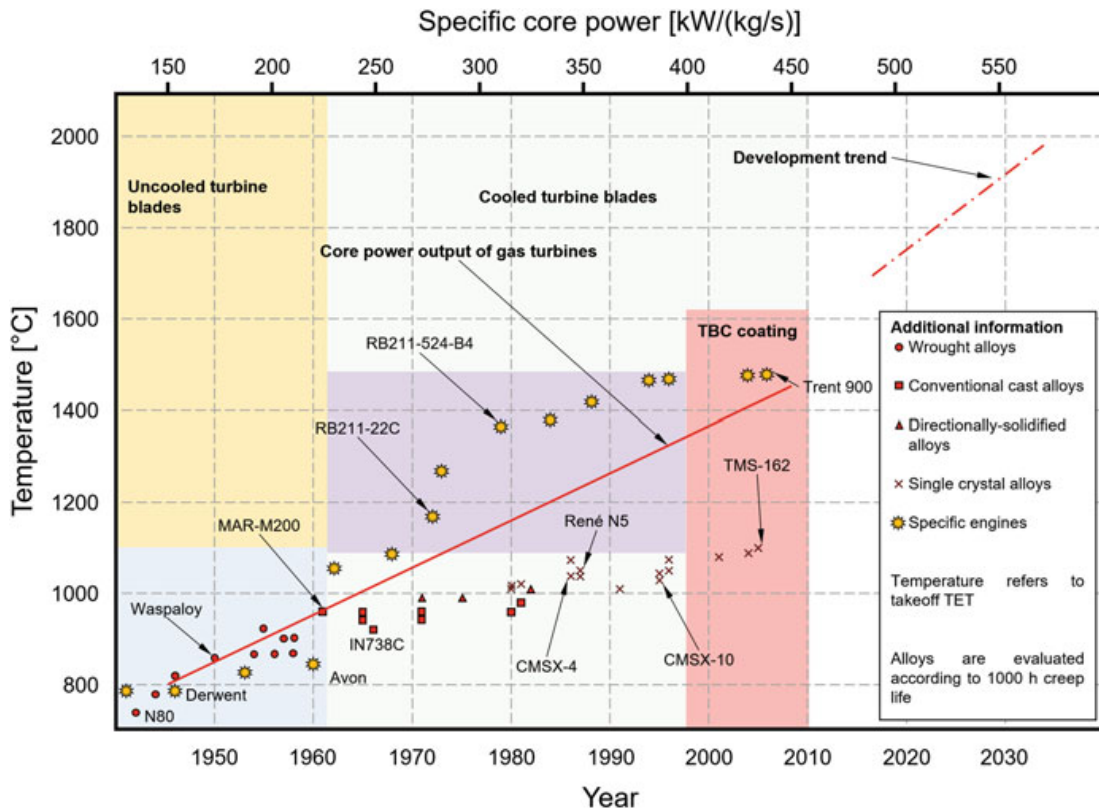
Fig. 2.20 Temperature capability of the blade superalloys and dependence also on the blade design: cooled or solid blades. In the graph the evolution of the take-off TET of civil aero-engines is considered. (Redrawn from Mukherji et al. 2011)

Eventually, surface reactions, induced by the interactions with the aggressive atmosphere, require an intrinsic resistance of the alloy against high-temperature corrosion (see Sect. 8.2). This feature can be improved with suitable coating systems. The already mentioned diffusion coatings, based on nickel aluminides, or the MCrAlY overlay coatings (M being Ni and/or Co and/or Fe) are excellent choices (see Sect. 7.3.1). As concerns coatings, turbine high-pressure blades have been in some engines also protected with thermal barrier coatings, using specific deposition techniques based on electron beam physical vapor deposition (see Sects. 7.2.2 and 7.3.2).

2.6 State of the Art and Future Trends

The aerospace industry has a great impact in terms of employees and output value. As an example, 14.9 billion USD in 2004 were invested in aviation gas turbine engines, and 3.7 billion USD have been used for military aircraft applications, while 11.2 billion USD have been invested in the field of commercial aviation (Giampaolo 2006). Aerospace industry permeates several other industries and is used as a fundamental benchmark for experimenting and testing new materials and technologies. Some of the most important driving forces pushing the efforts for innovation are associated with the improvement of aircraft performances, concerning safety and, in more recent times, pollution reduction. The reduction in emissions has become a major issue, considering that commercial aviation alone is responsible for the release in the atmosphere of 705 million of metric tons of CO_2 per year, corresponding to about 2% of the yearly global carbon emissions. Moreover, there is evidence that the greenhouse gases in jet fuel have greater effects on the atmosphere, since they are released at elevated altitudes (Martin 2016). The typical emission profile of a two-engine aircraft during 1 h flight with 150 passengers is given in Fig. 2.21. Pollutant substances and greenhouse gases in engine exhaust are present: CO_2, CO, H_2O, NO_x, SO_2, various hydrocarbons, and particulate matter, just to mention the main constituents. Some of these substances had attracted already investigation interests and research efforts, mainly in connection with their influence on corrosion (see Sect. 8.2) and erosion (see Sect. 7.3.5) aspects in gas turbine engines.

The European market is one of the largest for commercial aviation. According to the data reported by international agencies, like EU28 and European Free Trade Association (EFTA), and by the United Nations Framework Convention on Climate Change (UNFCCC), CO_2 emissions in the atmosphere have experienced a 77% growth between 1990 and 2005. Starting from the present aviation traffic forecast, notwithstanding the improvement rate of innovative technologies, an unavoidable 44% increase in CO_2 emissions from 2005 to 2035 period (European Commission 2016) is expected. For this reason, several international programs aiming at reducing atmospheric pollution are being conducted. ACARE (Advisory Council for Aviation and Innovation in Europe) Vision 2020 and Flightpath 2050 are two examples of European collaborative programs that set the targets for the future of the air
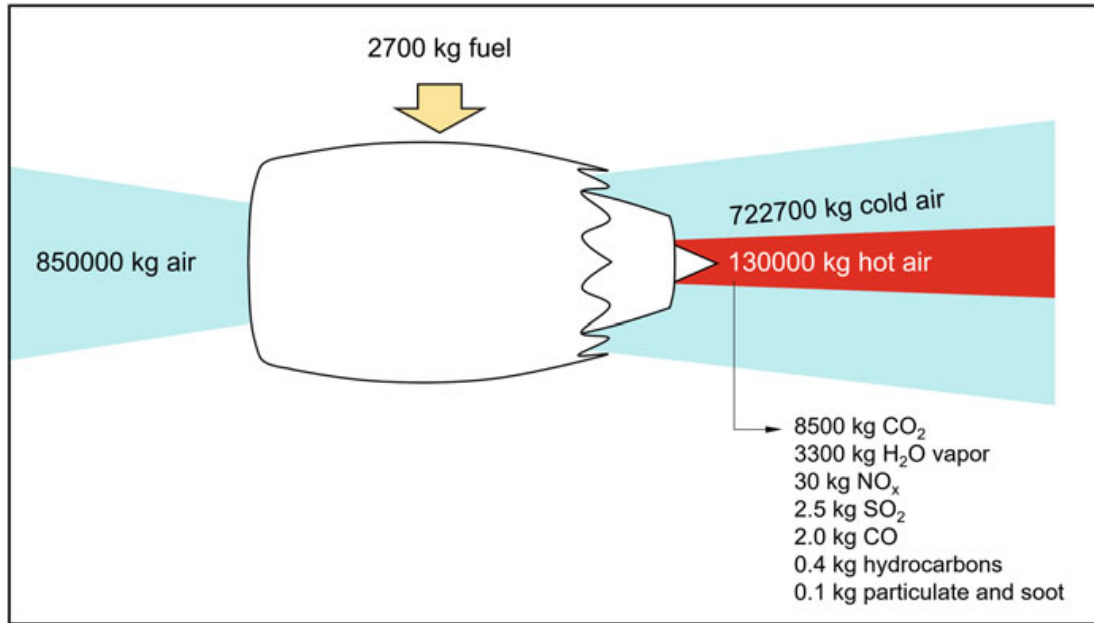
Fig. 2.21 Typical emission profile of a two-engine aircraft during 1 h flight with 150 passengers. (Redrawn from European Commission 2016)

transportation, also as concerns climate change and atmospheric pollution reduction. The two programs will set ambitious goals in terms of emissions cut:

- 90% reduction in NO_x emissions (15% achieved through operational efficiency and 75% from technology improvements)
- 75% reduction in CO_2 emissions per passenger per kilometer
- 25–30% overall CO_2 emissions reduction

For meeting these targets, multidisciplinary approaches are necessary. The main pillars on which research efforts are based can be summarized as follows:

- Average improvement in fuel efficiency, by at least 1.5% per year from 2009 to 2020
- Development of a more efficient air traffic management system
- Improvement in aircraft operational efficiency
- Technology improvement including sustainable low-carbon fuels and biofuels

As concerns low-carbon fuels, in 2009 the incidence of biofuels in the total fuel consumption was 0.05% only. A widespread use of biofuels for aircraft engines is not that easy to achieve, first of all due to the competitive demand by other transportation sectors. Furthermore, the hesitation of the industry concerning investments in dedicated production facilities for biomass to liquid fuels transformation can be justified by the limited foreseen supply of 0.05 million tons by 2020 (European Commission 2016). Therefore, biofuels introduction is still far from its potential target, and the main approach behind the development of more environmental-friendly jet engines is rather through the improvement of their efficiency. This has been highlighted already in the previous sections of this chapter,

with reference to the improvement in the engine performances demonstrated by the evolution of parameters like TET, OPR, SFC, and bypass ratio.

However, increasing TET will result in higher emissions that can be limited by the adoption of catalytic combustors, capable to reduce the NO_x formation in the combustion chamber directly. Furthermore, higher TET would require the development of more resistant thermal barrier coatings and more efficient cooling design for the components, in order to withstand the more demanding operating temperatures. There are several examples of newly developed engines with improved performances. One of these is the Pratt & Whitney F135 engine for the F35 military aircraft. This engine is characterized by an OPR of 28 and is capable of 190 kN of takeoff thrust and, in general, maximum efficiency under different operational conditions: conventional take-off/landing (CTOL), carrier variant (CV), and short take-off/vertical landing (STOVL) (Pratt and Whitney 2012). In commercial aviation the latest Airbus A380 is powered by the General Electric-Pratt & Whitney GP 7000 or by the Rolls-Royce Trent 900 engines (Giampaolo 2006). The GP 7000 has a maximum thrust of 340 kN with an OPR of 43.9 and a bypass ratio of 8.7:1 (MTU Aero Engines 2016). The Trent 900 is a three-shaft turbofan engine capable of a maximum thrust of about 342 kN. Its architecture consists of an eight-stage intermediate-pressure compressor, a six-stage high-pressure compressor, a single-stage high-pressure turbine, a single-stage intermediate-pressure turbine, and a five-stage low-pressure turbine. Its OPR is 39, and the bypass ratio reaches a value of 8.5:1 (Rolls-Royce 2015). A further evolution of this engine, the Rolls-Royce Trent XWB (see Fig. 2.22) is a three-shaft turbofan engine capable of a thrust value between
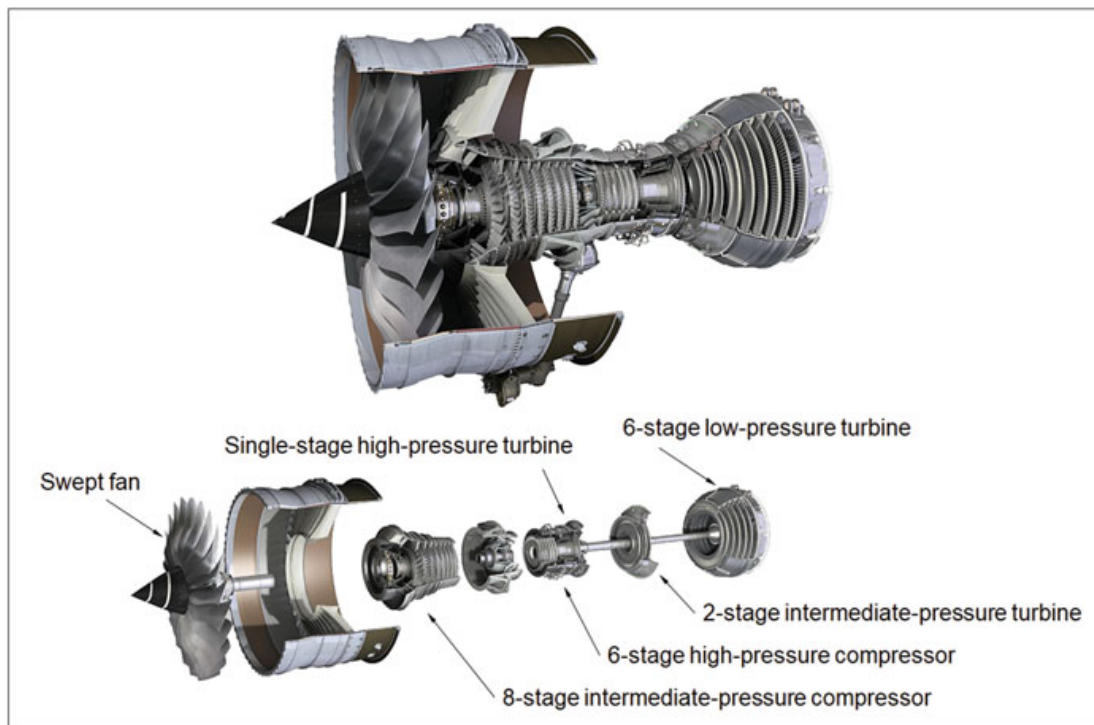
Fig. 2.22   Modern Rolls-Royce Trent XWB. (Rolls-Royce 2016, images courtesy of Rolls-Royce plc)

374 and 432 kN (84,000–97,000 lbf). A large diameter swept fan and an eight-stage intermediate-pressure compressor followed by a six-stage high-pressure compressor characterize the front part of the engine. The combustor has an innovative design, incorporating advanced ceramic coatings that can withstand combustion temperatures exceeding 2700 °C. A six-stage low-pressure turbine follows a single-stage high-pressure turbine. The power generated by the turbine system can reach values as high as 50,000 hp. Its overall pressure ratio (OPR) can climb up to 50, well above those given in Fig. 2.8. The bypass ratio of the engine is 9.6:1. These features allow the Trent XWB to improve several performances, including a fuel consumption reduction by 10% (Rolls-Royce 2016).

Future developments are already on their way, and the engine of the future should be lighter, less noisy, and more energy-efficient than conventional engines used today. Pratt & Whitney developed a new engine that might save up to 20% of fuel, with respect to the present average engine. One of the features that enable to achieve this result is a gearbox that slows down the fan. Meanwhile, CFM International is working on a conventional turbofan architecture engine that will reach similar results but without adding weight and drag through a gearbox. The increase in efficiency is obtained thanks to lightweight composite materials used in several components, such as carbon fiber-based fan blades (Martin 2016). Eventually, Rolls-Royce is developing an innovation plan, based on Advance® and UltraFan® engines (see Fig. 2.23).

Advance® will be ready for the market by 2020 and can be defined as a hybrid engine that will be manufactured with novel materials, like the light ceramic matrix composites (CMCs), 3D-printed components, and the innovative low-pressure system with carbon-titanium (C-Ti) composite fan system, including fan casing and blades. The engine will provide a 20% better efficiency as compared to the early Trent engine, fewer parts, and lower weight. UltraFan® engine will be available starting from 2025. One of the most impressive features of this engine will be its OPR, reaching a value of 70:1. It will be equipped with an innovative gearing system, i.e., *geared* architecture, located between the fan and the intermediate-pressure compressor. This system will be able to ensure that the fan runs at the optimum speed in any condition. Further improvements in the C-Ti composites will allow the removal of the thrust reverser and, thereby, a slim-line nacelle system. When compared with the first Trent engine, the UltraFan® engine will provide a 25% increase in fuel efficiency (Rolls-Royce 2017).

Aircrafts and their components are usually subjected to research and development cycles, whose duration can reach 20 years. For this reason, research efforts are based on a long-term planning approach that provides continuity over several years. The European Union Clean Sky research program comprises several projects aiming to meet both performance increase and environmental challenges. Two examples of R&D projects in this context are:

- Advanced low-pressure systems (ALPS). These engines are intended to demonstrate the feasibility of innovative lightweight materials for the production of engine components such as C-Ti composite fan blades and coatings. The use of these materials will be expected to lead to a weight saving of around 700 kg on a twin-shaft engine.

Fig. 2.23 Future Rolls-Royce engines. (Rolls-Royce 2017, images courtesy of Rolls-Royce plc)

- Counter-rotating open rotor engines (CROR). This aero-engine family should reach a 30% reduction in emissions compared to a year 2000 benchmark engine. The relevant noise level should be comparable to that of a modern turbofan engine. Airbus and Rolls-Royce are currently involved in research programs on this propulsion system (European Commission 2016).

CROR and ALPS are just two of the many research programs currently under development. Engine producers are now facing many other challenging tasks in the search for the "best engine:"

- Advanced cycles.
- Airframe optimization.
- Hybrid systems with separate power and thrust generation. They are turboelectrical hybrid propulsion system with a gas turbine for electricity generation and electrically driven fans coupled to batteries for energy storage.
- Pressure gain combustion.

Considering the above scenario, it is possible to conclude that gas turbine engines will still have a lot of potential in the future of aircraft propulsion. Furthermore, they will generate the power for aircraft propulsion to a great extent, possibly through hybrid systems and electrically driven engines (Wenger 2014).

References

Boyce M P (2012) Gas Turbine Engineering Handbook 4th edn. Elsevier, Oxford

Cumpsty N (2003) Jet Propulsion: A Simple Guide to Aerodynamic and Thermodynamic Design and Performance of Jet Engine 2nd edn. Cambridge University Press

European Commission (2011) Flightpath 2050 Europe's Vision for Aviation. Available via DIALOG. http://ec.europa.eu/transport/modes/air/doc/flightpath2050.pdf. Accessed 17 Aug 2017

European Commission (2016) European Aviation Environmental Report 2016. Available via DIALOG. https://ec.europa.eu/transport/sites/transport/files/european-aviation-environmental-report-2016-72dpi.pdf. Accessed 17 Aug 2017

Giampaolo A (2006) Gas Turbine Handbook Principles and Practices. The Fairmont Press Inc., Lilburn

Gunston B (1995) The Development of Jet and Turbine Aero Engines. Patrick Stephens Ltd Publ

Kear B H (1986) Advanced Metals. Scientific American 220: 130–139

Martin R (2016) The Race for the Ultra-Efficient Jet Engine of the Future. In: Sustainable Energy. MIT Technology Review. https://www.technologyreview.com/s/601008/the-race-for-the-ultra-efficient-jet-engine-of-the-future/. Accessed 15 Aug 2017

Meetham G W (1981) The Development of Gas Turbine Materials. Applied Science Publishers Ltd, London

MTU Aero Engines (2016) GP7000 turbofan engine. Available via Dialog. http://www.mtu.de/fileadmin/EN/7_News_Media/2_Media/Brochures/Engines/GP7000.pdf. Accessed 07 Sept 2017

Mukherji D et al (2011) Beyond Ni-based Superalloys: Development of CoRe-based Alloys for Gas Turbine Applications at Very High Temperatures. International Journal of Materials Research 102(9): 1125–1132

Pratt & Whitney (2012) F135 Specs Charts. Available via DIALOG. http://www.pw.utc.com/F135_Engine. Accessed 06 Sept 2017

Reed R C (2006) The Superalloys-Fundamentals and Applications. Cambridge University Press, New York

Rolls-Royce (1996) The Jet Engine 5th edn. Rolls-Royce plc, Derby

Rolls-Royce (2015) Trent 900. Available via DIALOG. https://www.rolls-royce.com/products-and-services/civil-aerospace/airlines/trent-900.aspx#training. Accessed 07 Sept 2017

Rolls-Royce (2016) Trent XWB. Available via DIALOG. http://www.rolls-royce.com/site-services/images/trent-xwb-infographic.aspx. Accessed 17 Aug 2017

Rolls-Royce (2017) Pioneering intelligent innovation for our customers. https://www.rolls-royce.com/products-and-services/civil-aerospace/future-products.aspx#/. Accessed 23 Aug 2017

The Washington Post (2017) The next generation of eco-friendly airplanes has arrived. . .quietly. http://www.washingtonpost.com/sf/brand-connect/wp/enterprise/the-next-generation-of-eco-friendly-airplanes-has-arrivedquietly/. Accessed 17 Aug 2017

Wenger U (2014) Rolls-Royce Technology for the Future Aircraft Engines. Lecture for RAeS, DGLR, VDI at the Hamburg University of Applied Sciences, Hamburg, 20 March 2014

Further Reading

Connors J (2010) The Engines of Pratt & Whitney. American Institute of Aeronautics and Astronautics, Inc.
Hill P G, Peterson C R (1992) Mechanics and Thermodynamics of Propulsion 2nd edn. Pearson
Kerrebrock J L (1992) Aircraft Engines and Gas Turbines 2nd edn. The MIT Press
Soares C (2015) Gas Turbines: A Handbook of Air, Land and Sea Applications. Elsevier

Chapter 3
Alloys for Aircraft Structures

3.1 Introduction

As seen in Chap. 1, the Flyer I of the Wright brothers was mostly made of wood and fabric. However, in addition to steel, used in the wing struts and the bracing wires, an aluminum alloy was used for the crankcase of the piston engine, in order to reduce its weight. So, aluminum started to fly since the very early beginning of modern aviation. After this start, aluminum attracted further interest and research efforts, since the need for new materials capable to resist the mechanical and thermal stresses associated with the increasing flight performances emerged soon (see Chap. 1). Moreover, the shortage of wood, particularly spruce and willow tree, caused by the massive aircraft production during World War I, created the conditions for the development and use of *light alloys* in aircraft structures. *Light* refers to the comparatively low densities of alloys based on elements like aluminum, magnesium, and titanium. Although definitely higher than the average density of wood, which was the main structural material of the early airplanes, the densities of aluminum alloys are still absolutely acceptable, even considering their effect on the specific structural properties, i.e., properties averaged by the material density. Aluminum alloys were among the first metallic alloys used in aircraft structures, and they still are the most used alloys in this field. Magnesium alloys are other interesting systems, particularly now that compositions displaying acceptable corrosion resistance and interesting mechanical properties have been developed. These alloys are nowadays gaining an increasing importance in the aeronautic field, where actually had already been used in the past. For them, some issues are still standing, like the search for mechanically workable compositions, which are introducing some obstacle to a more rapid widespread use of these materials. Titanium alloys, owing to their specific properties, are used not only for aircraft structures but also for engine parts. Therefore, they will be treated separately in Chap. 4. Laminate composite materials instead are included in this chapter. Many of them are based on aluminum alloys and represent a very important class of aerospace structural materials.
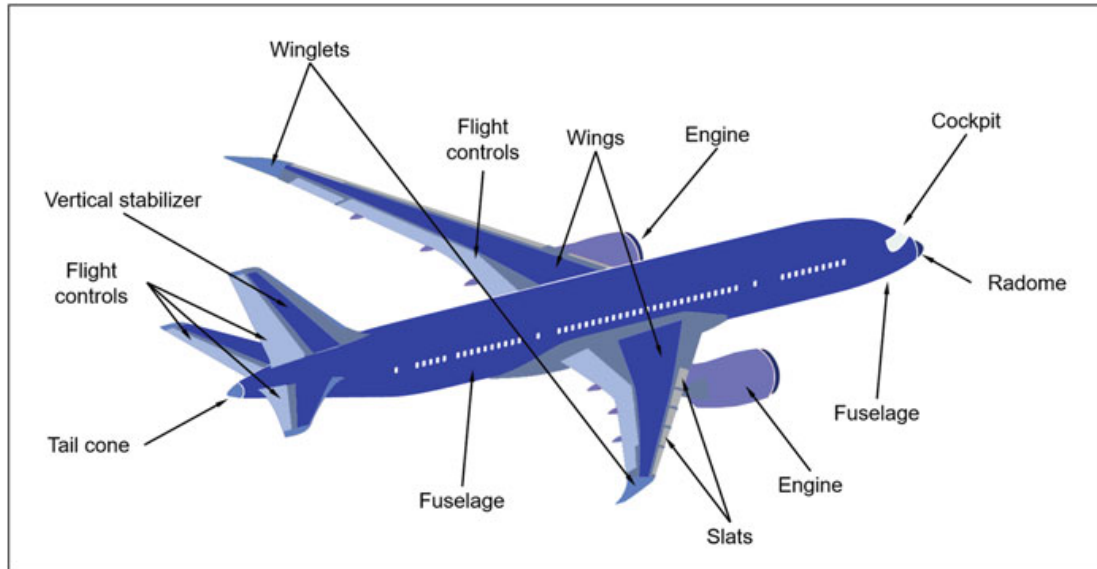
Fig. 3.1 Structure and main components of a commercial aircraft. (Redrawn from Boeing 2008)

The structure of modern aircrafts, although recalling to some extent early airplanes, exhibits obvious aerodynamic optimization. Commercial and military aircrafts share the airframe shape and the denomination of the main components (Fig. 3.1), although major differences in size, geometry, and structural properties are necessary to comply with the specific operational requirements.

The main structural parts of an airframe are the fuselage, the wings, the landing gear, and the flight control surfaces.

The wings are meant to provide the necessary lift but are also subjected to other mechanical stresses, like, for instance, the weight of fuel and engines. Their design and internal structure are therefore conceived to fit the specific needs of any aircraft (Fig. 3.2). Similar principles apply, obviously with different parameters, to fuselage, vertical stabilizers, and all the other parts of an aircraft (Fig. 3.3). In general terms, the components whose failure would endanger the safety of the whole aircraft are called *primary structures*, being *secondary structures* all the other. Fuselage, wings, empennage, and landing gears are typical *primary structures*, and for some of them, aluminum alloys are an excellent choice.

3.2   Aluminum Alloys

3.2.1   Introduction

Aluminum is a post-transition metal with atomic number 13 (13th group, 3rd period) of the periodic table. It is characterized by a face-centered cubic (*fcc*) crystal lattice, a density of 2.70 g/cm^3, and a Young's modulus of 70 GPa. The name aluminum derives from the term *alum*, used by Greeks and, afterward, by the Romans with
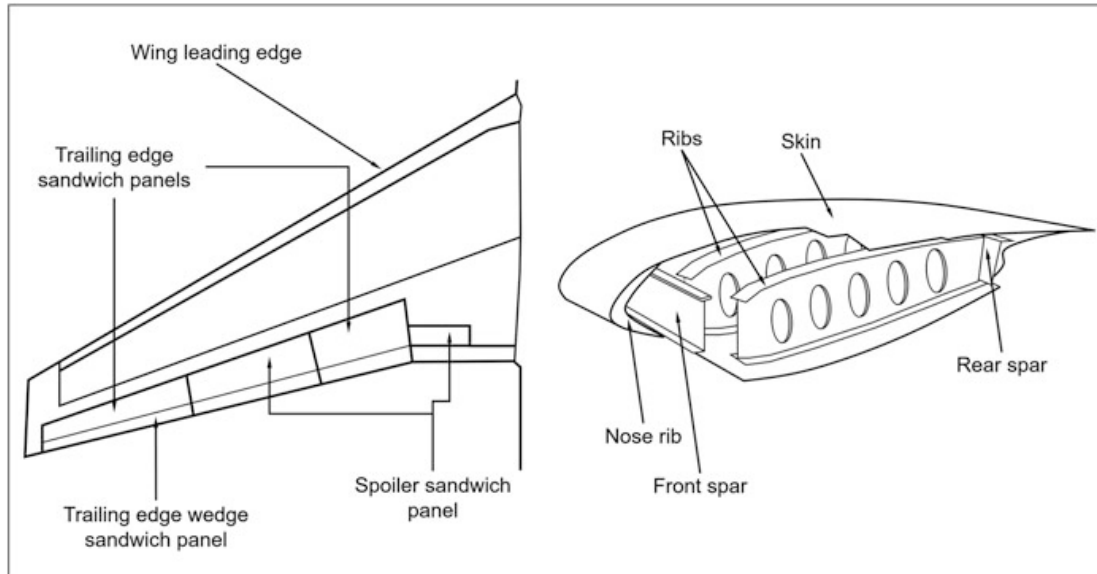
Fig. 3.2 Wing components and structure. (Redrawn from Federal Aviation Administration 2012)
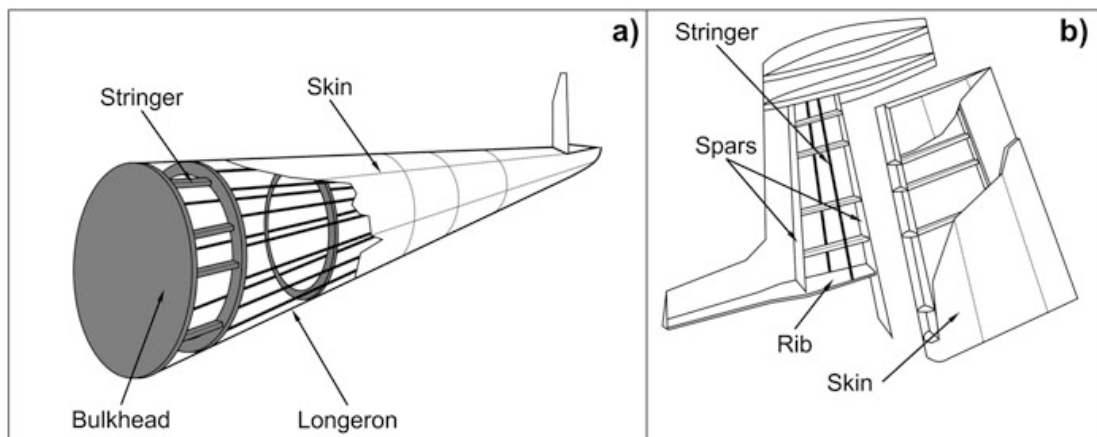
Fig. 3.3 (**a**) Semimonocoque tail part of the fuselage; (**b**) structure of the vertical stabilizer. (Redrawn from Federal Aviation Administration 2012)

reference to a bitter salt, based on aluminum double sulfate hydrated (e.g., KAl $(SO_4)_2$ H_2O), used in medicine as an astringent but also for skin tanning and glass production. The first who actually identified the presence of aluminum in alum salt was Sir Humphry Davy at the beginning of 1800, although he was not able to isolate it. In 1807, he proposed the name *aluminium* for the metal. Shortly after, the name aluminium was adopted by the IUPAC. However, in 1925 the American Chemical Society introduced the name *aluminum*, still used in the American English literature (Totten et al. 2003). The driving force for the development of Al-alloys for aerospace structures has been the improvement in static strength, as well as fracture toughness and resistance to crack growth, particularly in fatigue regimes, damage tolerance, and stress corrosion. As shown next, an incremental progress and an alloy-targeted design have been particularly successful so that Al-alloys are still strategic materials
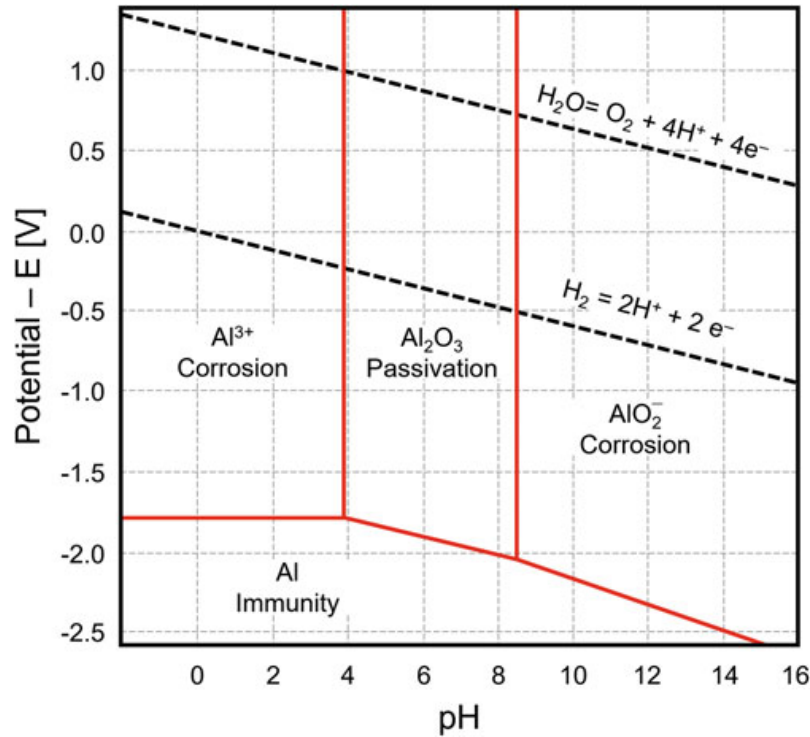
Fig. 3.4 Pourbaix diagram of pure aluminum. (Redrawn from McCafferty 2010)

for aerospace industry. This is also due to common features of these alloys, which can be largely ascribed, and to some extent retrieved, in pure aluminum, by far their majority component:

- Acceptable corrosion resistance.
- Good fatigue resistance, due to the high intrinsic ductility of the *fcc* structure given by the high number of slip systems.
- Good oxidation resistance.
- Good specific mechanical resistance.
- High specific stiffness ($E = 70$ GPa, average density of the alloys $= 2.768$ g/cm^3).

In standard conditions, the presence of a self-passivating and self-healing Al$_2$O$_3$ surface layer is the main reason for the fairly good surface stability of aluminum alloys, resulting in their good resistance to dry oxidation.

For similar reasons, it is possible to see from the Pourbaix diagram in Fig. 3.4 that Al-alloys still provide a positive response in not too aggressive corrosive environments, like aqueous solutions with a pH in the 3.9–8.6 range that do not determine localized corrosion phenomena, like pitting and crevice corrosion, discussed in Chap. 8 (ASM International 2003). As concerns fatigue resistance, Al-alloys are extremely sensitive to the presence of hard inclusions, which may act as stress concentrators. An intrinsic beneficial factor, as concerns fatigue resistance, is the face-centered cubic structure of aluminum and relevant large number of slip systems that help in accommodating local stresses by plastically straining, thus keeping their level relatively low.

The availability of aluminum and its alloys has remarkably influenced the aerospace industry since the beginning. Aluminum alloys were used during the World War I for the production of structural parts of the Zeppelin dirigibles and during the World War II for military and civil aircrafts. In these early applications, the hardenable Al-3.5Cu-0.5Mg-0.5 Mn alloy, named Duralumin, developed in the 1906 by the German chemist Alfred Wilm, was used. Hardening of Duralumin was attained thanks to a precipitation treatment, which induced in the alloy properties interesting not only for aerospace but also automotive applications (Lumely 2011). Notwithstanding the intrinsic corrosion resistance, a critical aspect of this alloy, that emerged soon in outdoor applications, was its tendency to exfoliation corrosion (see Sect. 8.1.4), which of course would not be acceptable for any application involving a long-term exposure to external atmosphere and meteorological events.

The problem was successfully solved with two alternative approaches, developed in the late 1920s: cladding the aluminum alloy with pure aluminum sheets and alloy protection through the formation of a surface film made of reaction products, using an anodizing process. Concerning this latter process, by means of appropriate bath composition and deposition parameters, it is possible to produce protective surface layers thicker than those forming spontaneously by the self-passivation tendency of the alloy. Moreover, by tuning the composition of the bath, it is possible to obtain deposits containing chemical agents, actively enhancing the corrosion resistance (Thompson et al. 1999). Thanks to these fundamental improvements, aluminum alloys rapidly became, and still are, the most used materials for aircraft structures, as outlined in the following.

Concerning the production of Al-alloys, raw materials usually are oxide-based ores with various grades of purity and levels of hydration. Bauxite, from the French village Les Baux, where alumina was first discovered, is the most important example. It is a sedimentary formation containing different aluminum hydroxides, like $AlO(OH)$ and $Al(OH)_3$. Chemical and mechanical enrichment of the ores is a common practice to increase the concentration of Al_2O_3 available to extraction (Totten et al. 2003). The main steps of aluminum extraction, still based on the Bayer process, developed and patented by Karl Bayer in 1888, are illustrated in Fig. 3.5. The output of the first step is hydrated alumina: $Al_2O_3 \cdot H_2O$. Pure aluminum requires the electrolytic reduction of Al_2O_3 dissolved in molten cryolite (Na_3AlF_6, Hall-Héroult process, see Fig. 3.5). Charles Hall and Paul Héroult developed independently this process in 1886, in Ohio (USA) and France, respectively (ASM International 1991). The overall electrochemical reaction involved in the extraction of aluminum is:

$$\frac{1}{2} Al_2O_3(\text{dissolved}) + \frac{3}{4} C(s) \rightarrow Al(l) + \frac{3}{4} CO_2(g) \tag{3.1}$$
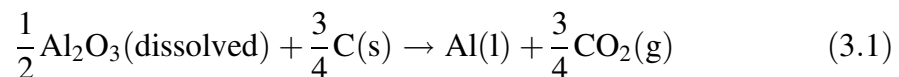
The electrolytic dissolution process is conducted at about 960 °C in the Hall-Héroult cells. Typically, for each kilogram of primary aluminum, 1.93 kg of Al_2O_3 is needed, while 0.40–0.45 kg of C and 1.5 kg of CO_2 are eliminated as secondary products (Lumely 2011).
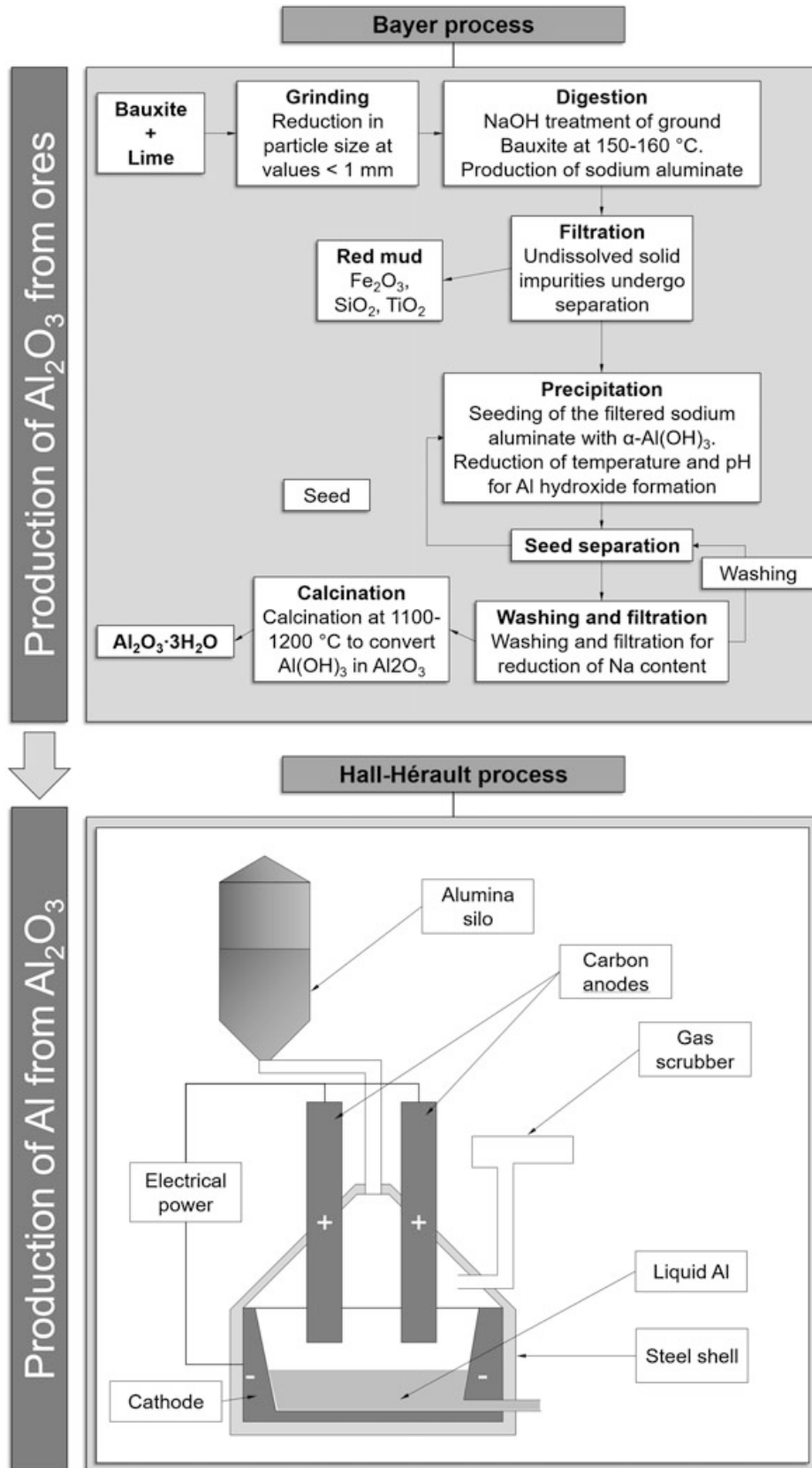
Fig. 3.5 Aluminum production route from ores to primary aluminum (Carter and Norton 2007; Lumely 2011)
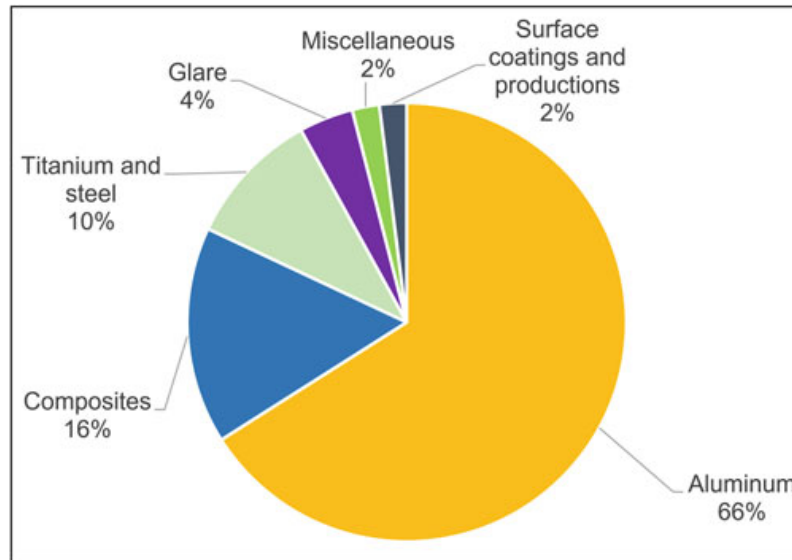
Fig. 3.6 Percentages of different materials used for the A380 Airbus, involving and promoting the development of the new materials and relevant processing routes. (Redrawn from Williams and Starke 2003)

Components made of aluminum alloys can sum up to more than a half of the total weight of a commercial airliner (see Fig. 3.6). Moreover, the possibility of varying and tailoring alloy's properties by suitable compositional changes, processing routes and post-processing thermomechanical treatments, is regarded as an attractive aspect of these materials, in addition to low density, a comparatively low cost, good availability, ease of manufacturing, reliability, and predictability of the in-service performances. Indeed, the leading role of Al-alloys in aerospace applications is mainly due to very well established alloy design principles. It is possible to obtain materials with specific properties for the different part requirements (see Table 3.1).

The density of Al-alloys, a primary selection criterion for these and other aerospace materials, varies from 2.643 g/cm^3 for commercially pure aluminum up to 2.803 g/cm^3 for highly alloyed compositions, like Al-Zn alloys. Metal working technologies, like milling, extrusion, and forging, lead to work-hardened products with higher specific strength (Starke and Staley 1996). The development occurring over the years that followed the end of World War II required a change of strategy after the accidents involving the Comet airliners at the Ciampino airport in Rome (1954, see Chap. 1). A premature fatigue failure was the main reason for the two accidents. However, an insufficient damage tolerance of the Al-Zn alloy, namely, the 7075 material used for the airframe of the Comet, was regarded as an additional factor behind the disasters. Therefore, these 7XXX alloys (see Sect. 3.2.3) were banned for several years from aerospace applications, and lower strength, but more damage-tolerant, Al-Cu alloys (precisely the 2024-T3 and 2014-T6) were used instead, with the exception for those components requiring highest tensile strength. The progress of commercial aviation has been accompanied by the request for larger payloads, larger number of passengers, and, thereby, larger airliners. Thicker sections of the structural parts started to be produced. At the same time,

Table 3.1 Summary table of the main properties of Al-alloys that can be attained by changing the composition and/or the microstructure of the alloy

Property	Desired microstructural feature	Function
Creep resistance	Thermally stable particles within the matrix and on the grain boundary	Inhibition of grain boundary sliding and coarse microstructure formation
Ductility and toughness	Fine structure with clean grain boundaries and absence of shearable precipitates or large particle	Encourage plasticity and work-hardening. Inhibition of void formation and growth
Fatigue crack initiation resistance	Fine grain size with absence of shearable particles. No surface defects	Prevent strain stress concentration, strain localization, and surface slip steps
Fatigue crack propagation resistance	Large grain size with shearable particles and no anodic phases or hydrogen traps	Encourage crack closure, branching, deflection, and slip reversibility
Pitting	Absence of anodic phases	Prevent preferential dissolution of second phase particles
Strength	Fine grain size with uniform dispersion of small, hard particles. Fine structure with clean grain boundaries and absence of shearable precipitates or large particles	Inhibition of dislocation motion
Stress corrosion cracking and HE	Hard particles and no anodic phases or interconnected hydrogen traps	Homogenization of slip and prevention of crack propagation due to anodic dissolution or HE

HE hydrogen embrittlement (Williams et al. 2003)

the incidence of damages due to stress corrosion started to be observed, with micro-cracks developing particularly when the load was applied along the short transverse direction. The most used alloys were 2014-T3, 7075-T6, and 7079-T6, where T3 and T6 represent two specific tempers, used to refine microstructure and relevant properties of aluminum alloys, as described in upcoming sections (Tables 3.9 and Table 3.10). Subsequently, thanks to alternative tempers for the 7075 alloy, codenamed T73 and T76, its stress and exfoliation corrosion problems were largely solved. These two tempers involve combinations of artificial aging at low and, as a subsequent step, at high temperature. The high-temperature treatment would generally result in a slight overaging of the alloy, with a consequent softening. However, the alternative beneficial effect of the treatment is the strengthening of the grain boundary region that enhances the fracture toughness of the alloy. This effect is determined by the enrichment of the grain boundary with Cu-rich precipitates. Nobler precipitates are less prone to microstructural changes and provide more effective obstacles to crack propagation. As an indirect toughening mechanism, there is also the lower affinity of the grain boundary precipitates and of the metallic matrix itself to hydrogen, whose embrittling action is thus neutralized or largely limited. In the A380, for assembling parts of the fuselage, laser beam welding (LBW) is used, with consequent requirements for a good weldability of the alloys. For this reason, Al-Mg-Si (6XXX alloys, see Sect. 3.2.3) materials have been considered. They exhibit excellent welding properties, and, in addition to that,

they have a comparatively lower density and price, as compared to Al-Cu materials. The reference alloy 6056-T78, featuring a relatively low density, i.e., 2.702 g/cm^3, in comparison with 2.781 g/cm^3 of the 2024 alloy, is also a laser-weldable product, developed at a later stage to comply with the elevated damage tolerance requirements. The outcome of the evolution of this material was the 6156 alloy, extensively used in lower shell fuselage applications. It is worth saying that also the temper (T78) developed for the 6XXX alloys played an important role in overcoming the problem of intergranular corrosion, which was observed in T6-treated parts made of the same materials. In the A380, notwithstanding the availability and actual use of other materials, like composites used already in the Boeing 787 Dreamliner (see Fig. 1.11), Al-alloys still retain a leading role, as shown in Fig. 3.6.

An indirect proof of the technological reliability of standard aluminum alloys, like the 2024 and 7050 materials, is provided by the improvements attained thanks to new processing and manufacturing steps, still using the same alloy compositions. This choice had to be made on several occasions to comply with requests from aircraft producers in terms of better properties but also for a faster and, therefore, cheaper production. Larger monoliths, machined from bulk thick plates and beams, have replaced assemblies and built-up structures. Machining may involve the removal by up to 95% of the original volume of the part. On the other hand, stress-free components can be obtained in this way, and the scraps can be recycled straightaway by remelting. Through the optimization of the alloy composition, in association with controlled conditions during temper treatments, important enhancement in alloy response to rolling can be achieved. Larger and thinner Al-alloy sheets are very much interesting for the process and manufacture optimization that they can bring about (Heinz et al. 2000).

Another issue that promoted important research efforts for developing special aluminum alloys was the expected heating associated with air drag in supersonic flight, which started to be considered also for commercial airliners. The Concorde project, started in 1962, required the development of quite stable alloys, not affected by any kind of long term, in-service aging, due to peak temperatures close to 100 °C, for exposure times of 20,000 h, out of the 50,000 h expected total service lifetime, at the highest Mach 2 speed. As seen in Chap. 1, based on the experience gained with military aircraft, Mach 2 is still a speed affordable to Al-alloys. The starting point of this material development was an alloy, codenamed RR58, originally designed for components of the compressor of the early gas turbine jet engines. The alloy, that in the end was employed for the fuselage panels and other structural parts of the Concorde, has a modified composition with respect to the parent material, i.e., the 2618 alloy, in which copper was the main alloying element. In particular, the ratios of copper to iron and nickel were fixed in the deliberate attempt to limit the formation of equilibrium intermetallics, typical of the overaging condition of these hardenable alloys. Moreover, an accurate microstructural refinement, inducing large grain size, was pursued to optimize creep resistance and to reduce exfoliation and stress corrosion. Subsequently, the alloy development regarded other critical mechanical properties, like strength and fracture toughness, leading to the design of several alloys not only of the 2XXX (Al-Cu, see Sect. 3.2.3) but also of the 7XXX (Al-Zn,
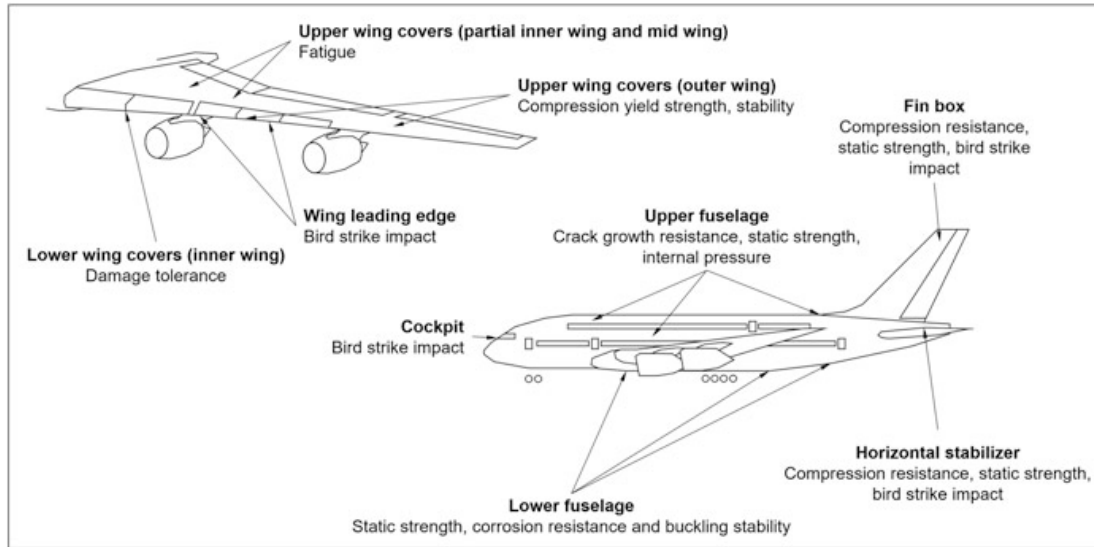
Fig. 3.7 General design aspects for the A380 Airbus aircraft, involving and promoting the development of the new materials and relevant processing routes. (Redrawn from Lequeu et al. 2007)

see Sect. 3.2.3) series, like the 7050-T74, 7050-T76, and 7150-T6, particularly recommended for the upper wing skin. For the Al-Cu series, it is worth mentioning the 2324-T39 and 2224-T351X materials, developed for the lower wing structures. The more recent developments of these alloys have been triggered by the design requirements for large size airliners, like the Airbus A380. Larger size and loads involved important improvements in static mechanical strength and damage tolerance, to be developed according to the leading selection criteria summarized in Fig. 3.7 for each specific component (Lequeu et al. 2007).

Moreover, thanks to a progressive implementation approach in alloy development, novel material products came up that could be processed relying on the knowledge background accumulated over the years. This is a fundamental prerequisite for a rapid technological transfer from research to applications. In this regard, to complete the picture of the main milestones in the development of aluminum-based materials, Al-Li alloys will be mentioned as well, together with the most recent class of aluminum alloys, containing scandium among alloying elements, and laminate composites, using aluminum as main metallic constituent, as illustrated in Sect. 3.4.

Al-alloys are generally divided into two large families: cast (see Sect. 3.2.2) and wrought (see Sect. 3.2.3) alloys. A great number of both cast and wrought alloys respond to thermal treatments that are essentially based on phase solubility, i.e., solutioning, quenching, and precipitation, and age hardening. These alloys are said to be *heat treatable* (or *hardenable*), since different phases and, thereby, different properties can be induced into the alloy through the control of the solid-state precipitation. Duralumin, the Al-3.5Cu-0.5Mg alloy (alloy 2017, according to the code that will be introduced in Sect. 3.2.3), already mentioned with reference to the early use of an aluminum alloys in aircraft structures (see Sect. 1.1), can be regarded

as the prototype of the heat treatable alloys. If the composition of the alloy does not offer this chance and no precipitate phases can be formed in the alloy matrix, the alloy is said to be *non-heat treatable*. Both wrought and cast alloys can be classified according to an alloy nomenclature system. This coding system was developed by the Aluminum Association (ASM International 1991). The nomenclature of both wrought and cast alloys, used already in some part of this section dealing with specific alloys, will be discussed in details in the relevant sections of this chapter. The aluminum parts and components of aircrafts are supplied either as wrought or cast products, these latter typically requiring some machining and surface finishing before installation. As already mentioned, the fuselage, the wings, the empennage, and the supporting structure of an aircraft are regarded as *primary structures*, since their failure would endanger the whole aircraft. Usually, wrought alloys are used for these parts, although for military airplanes highly controlled casting products are on some occasion employed. For *secondary structures* both cast and wrought products are used, depending on the shape and required part finishing.

Before entering this broad subject, a few bibliographic notes, which might interest the reader to widen the knowledge on this most important class of alloys, concern some of the properties of aluminum alloys that render these materials excellent candidates for aerospace applications and to complete the picture emerging from the former sections. Metal handbooks, such as that of ASM International (2015), offer a wide description of Al-alloy properties, relevant compositions, and tempers developed to attain alloy properties suitable for specific applications. Another essential reading is the handbook edited by Davis (2001). The textbook of Polmear (2006) is particularly recommended for a comprehensive treatment of the main themes concerning aluminum but also other *light alloys*, like magnesium, titanium, and derived alloys. A particular focus on the aerospace applications of all these *light alloys* can be found in the monographic chapter by Prasad and Wanhill (2017).

3.2.2   Cast Alloys

Aluminum and its alloys can virtually be subjected to any casting and forming process. However, early casting of aluminum has been characterized by several problems. Because of gas pick-up during melting, castings were often characterized by the presence of porosity and other defects, easily visible also on eye inspection. Porosity in aluminum castings is still an issue, and several techniques have been developed over the years to control its impact on the final products, if not to eliminate it at all. Some examples include degassing, filtration, improved handling of the molten alloy, even using low pressures, and solidification simulation, for predicting the potential effects of technological changes. Thanks to these contributions, aluminum is now regarded as one of the more versatile among the foundry metals, even considering the continuous progress in alloy design (ASM International 1991; Lumely 2011; Polmear 2006). Since casting techniques allow for the
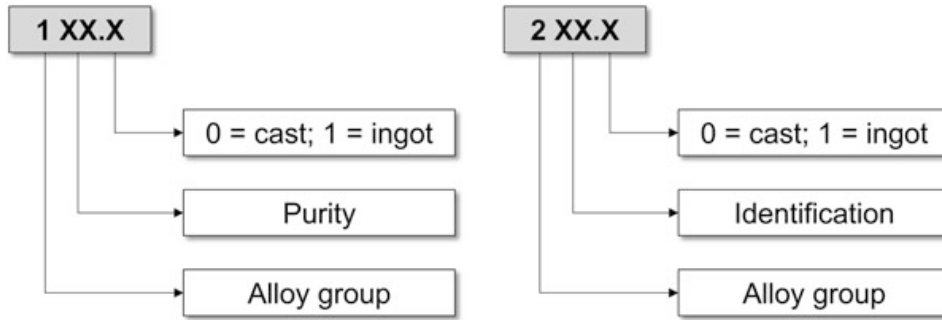
Fig. 3.8 Aluminum cast alloys nomenclature. Designation on the left is valid for 1XX.X alloys. Designation on the right holds for all the other cast aluminum alloys (ASM International 1991; Kaufman 2000). See also specifications in Table 3.2

Table 3.2 Aluminum cast alloy classification (ASM International 1991)

Series	Composition and brief description
1XX.X	Commercially pure aluminum with different grades
2XX.X	Copper is the main alloying element. Eventually, other alloying elements may be specified
3XX.X	Silicon is the main alloying element. Other alloying elements are present as specified, e.g., Cu and Mg
4XX.X	Silicon is the main alloying element
5XX.X	Magnesium is the main alloying element
6XX.X	The name of this series is not in use
7XX.X	Zinc is the main alloying element. Other elements, such as Mg, may be specified
8XX.X	Tin is the main alloying element
9XX.X	The name of this series is not in use

production of complex shapes and geometries, the choice of these materials is quite often driven by net shape considerations. Concerning the coding system for aluminum cast alloys, nine main groups do exist, although not all of them have been used so far: nXX.X, with n ranging from 1 to 9. The 1XX.X series is specific for the commercially pure (CP) aluminum alloys, whereas different codes have been developed for the other groups of alloys. The rationale of this coding system is provided in Fig. 3.8, together with the specification for the other alloy groups, listed in Table 3.2.

The selection of the best casting technique depends on the shape, the size, and the number of parts that have to be produced. High-pressure die-casting is used in more than 50% of the applications, whereas sand casting and permanent mold casting techniques are more often employed for the production of thick wall parts or for those characterized by internal hollow cavities for which high-pressure die-casting is

not a suitable choice. High-pressure die-casting implies that the molten aluminum alloy is forced into a steel die at high speeds, ranging from 20 to 100 m/s. This value can be achieved thanks to a piston-cylinder system, based on a hydraulic ram that is able to reach pressures up to 100 MPa on the metal (Polmear 2006). Aluminum castings are widely spread in the automotive industry, like for the fabrication of wheels, engine blocks, and pistons. About 2% of the products obtained via high-pressure die-casting is used in aerospace applications. The percentage raises up to 10% of the total when considering aerospace applications of castings obtained via permanent mold casting and sand casting techniques. Permanent mold casting is the preferred process for the production of wheels and suspension components (Lumely 2011). The chemical composition of some cast alloys is given in Table 3.3.

Usually, castings have mechanical properties that are lower if compared with the wrought counterparts, except for the creep resistance. Furthermore, properties tend to have a certain variability throughout the component (Polmear 2006). However, the ratio of cast to wrought aluminum alloys is increasing thanks to the push of the automotive industry (ASM International 1991).

3.2.3   Wrought Alloys

Wrought products include extrusions, foils, forgings, plates, sheets, stampings, and wires. The most common form is that of the non-heat treatable sheet, largely used in the construction, packaging, and transportation industry (Lumely 2011). The feed-stock for metal working is typically an alloy ingot produced with a direct chill casting. Wrought aluminum sheet products have usually a thickness in between 0.15 and 6.3 mm. Plates feature a thickness above 6.3 mm. Concerning specific aerospace applications of the wrought alloys, the fuselage skin can be made of sheets and plates with thickness ranging from 1 up to 10 mm. Otherwise, wing covers, that are load-bearing structures, are generally 25–50 mm thick. The largest thicknesses can be found in bulkheads, wing spars, and other structural parts. The classification of extruded products is still made referring to the part thickness or to the diameter of the smallest circle in which the cross section of the piece is contained. Open- or close-die forgings are the two main options for these products. Open-die forged parts are obtained by repeatedly deforming the alloy using flat dies or with very simple geometries. The alternative approach (close-die) is used for parts with more complex geometries, for which impression dies are needed. Wrought alloys can be classified in nine different families according to their composition and in accordance with the International Alloy Designation System (IADS), introduced in 1970 and now shared worldwide. The classification of these Al-alloys is presented in Table 3.4.

Apart from the 1XXX family, the international coding is essentially referred to the main alloying elements (see Fig. 3.9), according to the specifications in Table 3.4. The second figure indicates the degree of development of a specific alloy and, indirectly, the "age" of the alloy. For instance, the 2124 alloy has been

Table 3.3 Cast alloys chemical composition. Compositions are intended as maximum weight percentage unless shown as a range of values. Except for 150.1 alloy, Al content is balance (Polmear 2006)

International designation	Si	Fe	Cu	Mn	Mg	Cr	Zn	Ti	Others
150.1	a	a	0.10	–	–	–	0.05	–	Al = 99.50 min
201.0	0.10	0.15	4.0–5.2	0.20–0.50	0.15–0.55	–	–	0.15–0.35	Ag = 0.40–1.0
208.0	2.5–3.5	1.2	3.5–0.45	0.50	0.10	–	1.0	0.25	Ni = 0.35
213.0	1.0–3.0	1.2	6.0–8.0	0.6	0.10	–	2.5	0.25	Ni = 0.35
238.0	3.5–4.5	1.5	9.0–11.0	0.6	0.15–3.5	–	1.5	0.25	Ni = 1.0
242.0	0.7	1.0	3.5–4.5	0.35	0.15–0.35	0.25	0.35	0.35	Ni = 1.7–2.3
295.0	0.7–1.5	1.0	4.0–5.0	0.35	0.03	–	0.35	0.25	–
308.0	5.0–6.0	1.0	4.0–5.0	0.50	0.10	–	1.0	0.25	–
319.0	5.5–6.5	1.0	3.0–4.0	0.50	0.10	–	1.0	0.25	Ni = 0.35
328.0	7.5–8.5	1.0	1.0–2.0	0.20–0.60	0.20–0.60	0.35	1.5	0.25	Ni = 0.25
355.0	4.5–5.5	0.60[b]	1.0–1.5	0.50[b]	0.40–0.60	0.25	0.35	0.25	–
356.0	6.5–7.5	0.6	0.25	0.35	0.20–0.40	–	0.35	0.25	–
357.0	6.5–7.5	0.15	0.05	0.03	0.45–0.60	–	0.05	0.20	–
360.0	9.0–10.0	2.0	0.60	0.35	0.40–0.60	–	0.50	–	Ni = 0.50
380.0	7.5–9.5	2.0	3.0–4.0		0.50	0.10	3.0	–	Ni = 0.50
390.0	16.0–18.0	1.3	4.0–5.0	0.10	0.45–0.65	–	0.10	–	–
413.0	11.0–13.0	2.0	1.0	0.35	0.10	–	0.50	–	Ni = 0.50
443.0	4.5–6.5	0.8	0.6	0.50	0.05	0.25	0.50	0.25	–
514.0	0.35	0.50	0.15	0.35	3.5–4.5	–	0.15	0.25	–
518.0	0.35	1.8	0.25	0.35	7.5–8.5	–	0.15	–	Ni = 0.15
520.0	0.25	0.30	0.25	0.15	9.5–10.6	–	0.15	0.25	–
535.0	0.15	0.15	0.05	0.10–0.25	6.2–7.5	–	–	0.10–0.35	–

705.0	0.20	0.80	0.20	0.40–0.60	1.4–1.8	0.20–0.40	2.7–3.3	0.25	–
707.0	0.20	0.60	0.20	0.40–0.60	1.4–1.8	0.20–0.40	4.0–4.5	0.25	–
712.0	0.15	0.50	0.25	0.10	0.50–0.65	0.40–0.60	5.0–6.5	0.10–0.25	–
713.0	0.25	1.18	0.40–1.0	0.60	0.20–0.50	0.35	7.0–8.0	0.25	Ni = 0.15
850.0	0.70	0.70	0.70–1.3	0.10	0.10	–	–	0.20	Ni = 070–1.3 Sn = 5.5–7.0

[a]Ratio Fe/Si minimum 2:1

[b]In case Fe content exceeds 0.45%, Mn content must be less than 0.5 times the Fe content

Table 3.4 Wrought alloys classification (ASM International 1991; Lumely 2011)

Series	Information about the composition	Heat treatment
1XXX	Aluminum. CP – commercially pure with a purity degree higher than 99%	Non-treatable
2XXX	Copper is the main alloying element. However, other elements may be present (Mg in particular)	Treatable
3XXX	Manganese is the main alloying element	Non-treatable
4XXX	Silicon is the main alloying element	Generally non-treatable. Some exceptions do exist (e.g., 4032)
5XXX	Magnesium is the main alloying element	Non-treatable
6XXX	Magnesium and silicon are the principal alloying elements	Treatable
7XXX	Zinc is the main alloying element. However, other spices can be present. It is the case of Cr, Cu, Mg, and Zr	Treatable
8XXX	Alloys in which elements such as lithium and tin are present	Both treatable (e.g., 8090) and non-treatable
9XXX	The name of this series is reserved for future use	–

Fig. 3.9 Wrought alloy codename. Designation on the left is only valid for 1XXX alloys. Designation on the right holds for all the other wrought alloys (ASM International 1991; Kaufman 2000)

developed later, i.e., it is more recent, than 2024 alloy. However, both alloys have similar composition.

The latest two figures on the right indicate a serial number providing information on the specific set of alloying elements and relevant concentrations. For instance, alloy 7049 and 7050 are slightly different in composition. In case of 1XXX alloys, the last two figures of the code refer to the level of impurities of the alloy: e.g., 1155 alloy has a purity of at least 99.55% (Fig. 3.9). As seen in Table 3.4, concerning their composition, except for 1XXX series, wrought aluminum alloys can contain a wide range of alloying elements. The composition of selected wrought alloys of 1XXX series is given in Table 3.5.

A wider set of alloy compositions is given in Appendix 1; the indication of the main effect of any element on the alloy properties is given in Appendix 2. Aluminum wrought alloys can be split into two main subgroups: heat treatable and non-treatable alloys.

Heat treatments of aluminum alloys are used to improve two main properties: hardness and mechanical strength. This is attained through precipitation hardening, although other effects of thermomechanical treatments, e.g., strain hardening,

Table 3.5 1XXX alloys chemical composition. Compositions are intended as maximum weight percentage unless shown as a range of values

International designation	Si	Fe	Cu	Mn	Mg	Cr	Zn	Ti	Others
1050	0.25	0.40	0.05	0.05	0.05	–	0.05	0.03	Al = 99.50 V = 0.05
1070	0.20	0.25	0.04	0.03	0.03	–	0.04	0.03	Al = 99.70 V = 0.05
1098	0.01	0.006	0.003	–	–	–	0.015	0.003	Al = 99.98
1100	–	–	0.05–0.20	0.05	–	–	0.10	–	Al = 99.00
1275	0.08	0.12	0.05–0.10	0.02	0.02	–	0.03	0.02	Al = 99.75 Ga = 0.03 V = 0.03
1420	–	–	–	–	5.2	–	–	–	Li = 2.1 Zr = 0.11
1421	–	–	–	–	5.2	–	–	–	Li = 2.1 Sc = 0.17 Zr = 0.11
1440	–	–	1.5	–	0.80	–	–	–	Li = 2.4 Zr = 0.11
1441	–	–	1.65	–	0.90	–	–	–	Li = 2.4 Zr = 0.11
1450	0.25	0.40	0.05	0.05	0.05	–	0.07	0.10–0.20	–
1460	–	–	2.9	–	–	–	–	–	Li = 2.25 Sc = 0.09 Zr = 0.11

If not specified, Al content is balance (Polmear et al. 2017; Prasad et al. 2014; The International Aluminum Association 2015)

Table 3.6 Main families of wrought alloys and relevant strengthening mechanisms (ASM International 2015)

International designation	Alloys system	Strengthening mechanism
1XXX	Pure Al	Work-hardenable alloys
3XXX	Al-Mn	
4XXX	Al-Si	
5XXX	Al-Mg	
8XXX	Al-Fe	
8XXX	Al-Fe-Ni	
2XXX	Al-Cu	Precipitation-hardenable alloys
2XXX	Al-Cu-Mg	
2XXX	Al-Cu-Li	
6XXX	Al-Mg-Si	
7XXX	Al-Zn	
7XXX	Al-Zn-Mg	
7XXX	Al-Zn-Mg-Cu	
8XXX	Al-Li-Cu-Mg	

contribute to different extent to the overall characteristics of the alloys. Work-hardening is the main strengthening approach for non-heat treatable alloys. In Table 3.6, a further classification is proposed for the wrought alloys according to the main strengthening mechanisms and with the indication of the subgroups of the alloys depending on the reference compositional system.

3.2.3.1   Wrought Non-heat Treatable Alloys

Alloys of the series 1XXX, 3XXX, 4XXX, and 5XXX are non-treatable. This means that no alloy structural changes can be induced by thermal treatments so that the relevant properties are substantially insensitive to the thermal history of the alloy. In some respect, this is a positive feature, for instance, in applications involving uncontrolled thermal conditions, possibly inducing fast melting and solidification, like welding. On the other hand, cold working processes, even conducted on the component surface, like shot pinning and similar procedures, can drastically change the mechanical properties. Although not particularly used in aircraft structures, it is worth remembering some of their main application fields that are quite numerous and diverse (Davis 2001; Polmear 2006):

- **1XXX**: this family comprises un-alloyed aluminum alloys, with different grades of purity: commercially pure and super-pure aluminum (Belov et al. 2002). This series is used for the fabrication of several components, some interesting examples being architectural and decorations for structural parts in buildings, components of chemical plants, and electric wires and cables, considering the good electrical conductivity of pure aluminum.
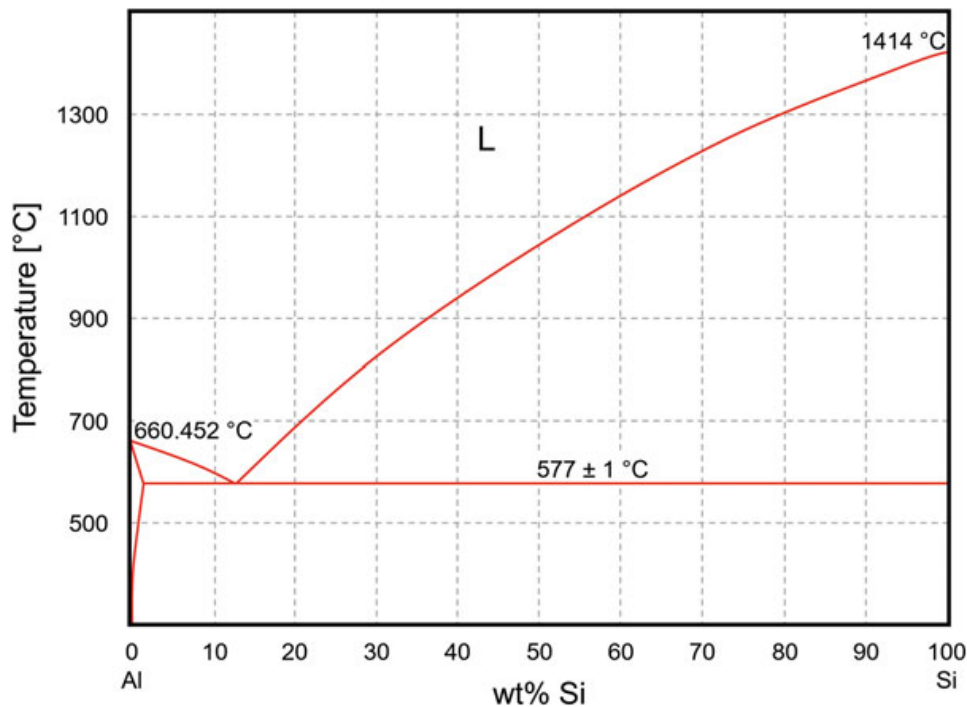
Fig. 3.10 Al-Si phase diagram. (Redrawn from ASM International 1992)

- **3XXX**: interesting characteristics of this family of alloys, having manganese as main addition, are a low mechanical resistance and a high ductility, in association with a good corrosion resistance. The most popular product is the 3003 alloy, whose strengthening mechanism relies on the formation of intermetallic compounds, e.g., Al_6Mn, dispersed within the alloy matrix. This intermetallic phase forms directly from the melt, and the structure of the phase diagram does not allow solutioning and thermal treatments inducing solid-state precipitation, necessary to refine the alloy microstructure and optimize its mechanical properties. Some common applications of the 3XXX alloys are production of multipurpose sheets, including building structures; furniture; cooking utensils, in particular pottery; cans for food and drinks; and thin foils.
- **4XXX**: the main alloying element is silicon, and these are two-phase alloys used for welding processes thanks to the presence of a low-temperature eutectic transformation (see Fig. 3.10). Silicon is not soluble in aluminum in the solid state, and this leads to the solidification of a two-phase mixture, consisting of mostly pure silicon grains dispersed into the aluminum matrix. The grain size and morphologies will depend upon the kinetic aspects of the transformation, although eutectic microstructures are very likely.
- **5XXX**: this series of alloys is characterized by the presence of magnesium as main alloying element. A particular feature of these alloys, interesting for some applications, is the fact that the *fcc* austenitic phase exhibits a very low ductile-to-brittle transition temperature. Therefore, these alloys are very much suitable for cryogenic use, like inner pressurized vessels for liquid nitrogen dewar containers, cryogenic sample holders, etc. They show a good weldability, so that complex

Table 3.7 Designation of the main temper condition used for all Al-alloys

Name	Main features
F	As fabricated. Corresponds to the strain-hardened condition due the production process. The letter F stands alone
O	Annealed condition to obtain the lowest strength temper, aiming at increasing the alloy workability. O can be applied to cast products that are annealed to improve dimensional stability and ductility. The letter O may be followed by a digit to indicate an annealed condition with special characteristics
H	Strain-hardened wrought products. Additional thermal treatment can be employed if a reduction of the alloy strength is needed. H is followed by two or more digits (see also Table 3.8)
W	Solution heat-treated alloys. This temper is applied only to alloys that undergo spontaneous aging after solution heat treatment. It induces a sort of metastable condition, followed by natural aging at room temperature. Digits to indicate the natural aging period, e.g., W1/2 h, are commonly used
T	Thermally heat-treated to produce stable tempers other than F, H, O. Supplementary strain hardening may be employed as well. The letter T is always followed by one or more digits (see Tables 3.9 and 3.10)

This scheme is adopted by the main international standards referring to these alloys (Benedyk 2010; Kaufman 2000)

structures and/or comparatively large pieces can be assembled: large tanks for milk but also petrol, oil, and other organic liquids. Small boat hulls have been also made using Al-Mg alloy sheets.

More information on wrought non-heat treatable alloys can be found in the references quoted at the end of the chapter.

3.2.3.2   Heat-Treatable Alloys and Designation of Tempers

Heat-treatable aluminum alloys are particularly interesting in aerospace applications. Different combinations of mechanical and corrosion resistance properties can be imparted to the same alloy thanks to suitable heat treatments. An international designation code, registered by the Aluminum Association, does exist for these tempers, and it is usually added to the alloy designation number. All changes induced into heat-treatable alloys are based on the solid-state formation of stable or metastable precipitates, as described in Sect. 3.2.3.3. The heat treatments are typically a combination of a solution stage and quenching, followed by natural and artificial aging. Considering the role that relevant defects may have in solid-state precipitation, cold-working is another aspect involved in the temper design. As shown by Table 3.7, the T temper is only one of the possible tempers used for Al-alloys. The designation, used since 1948 and updated over the years, is meant to assign to any heat-treatable alloy product the information on the thermal treatment used to set its properties.

Table 3.8 gives information about the codes used for strain-hardened, temper H, alloys.

Table 3.8 Description of the different "H" tempers. X indicates the residual strain hardening percentage, remaining in the alloy after each treatment, except that for H1X, where X is the percentage of imparted strain hardening

Type	Main features
H1X	Strain hardened only
H2X	Strain hardened and partially annealed. The strength acquired during strain hardening is reduced at the desired level by means of a partial annealing process. In this case X corresponds to the percentage of residual strain hardening after the partial annealing
H3X	Strain hardened and stabilized. Stabilization is used for improving ductility and can be carried out either thanks to heat introduced during the fabrication or thanks to a low temperature thermal treatment. Again, X corresponds to the percentage of residual strain hardening after the stabilization treatment
H4X	Strain hardened and lacquered or painted. It indicates the products that are strain hardened and subsequently subjected to heat during painting or lacquering. X corresponds to the percentage of residual strain hardening after lacquering or painting

The maximum value for $X = 8$ (Kaufman 2000)

As concerns the T tempers, a brief description is given in Table 3.9, with full details in Benedyk (2010). All T-treatments start with alloy solutioning. The subsequent quenching aims at freezing down to room temperature a super-saturated solid solution. The two main temper parameters are solution temperature and cooling rate. Precipitation occurs next, induced by either artificial or natural aging. Natural aging occurs spontaneously at room temperature, an aspect to be considered not only during the intermediate steps of the heat treatment but also as concerns the microstructural evolution occurring under operating conditions. Natural aging determines the useful lifetime of the alloy, corresponding to the time required to reach the overaging conditions, when material properties are no longer suitable for the relevant application.

The T tempers described in Table 3.9 can be rendered more complex by introducing further steps, mainly designed for relieving the stress accumulated into the alloy piece. Therefore, other digits can be added to the temper identification code, as specified in Table 3.10. In particular, stress relief by stretching is codenamed T51, by compressing T52, a combination of stretching and compressing T54. Stress relief can be performed either after solution heat treatment or after quenching, following a shaping process conducted at elevated temperatures. More digits can be used to provide additional information on other relevant parameters of the temper, like percentage of nominal permanent set, level of stress relieved, etc. (Table 3.10).

The selection of the right temper conditions is often the result of a compromise of diverging requirements. For example, tempers interesting for aircraft alloys of the 7XXX family are the T6 and T7. As shown by Fig. 3.11, T6 would induce excellent mechanical strength but a correspondingly lower corrosion resistance of the alloy. Intermediate conditions can be attained using suitable variants of the T7 temper.

Table 3.9 Description of the T temper treatments (Kaufman 2000)

Type	Main features
T1	Cooling from elevated temperature shaping process and natural aging. Natural aging leads to a substantially stable condition. Applications: products that do not undergo cold working after cooling from an elevated temperature shaping process
T2	Cooling from elevated temperature shaping process, cold working, and final natural aging process. Natural aging leads to a substantially stable condition. Applications: products that undergo cold working after cooling from an elevated temperature shaping process
T3	Solution treatment, cold working, and final natural aging process. Natural aging leads to a substantially stable condition. Applications: products that undergo cold working to improve the strength after being solution treated
T4	Solution treatment, natural aging. Natural aging leads to a substantially stable condition. Applications: products that do not undergo cold working after solution treatment
T5	Cooling from elevated temperature shaping process and artificial aging. Applications: products that do not undergo cold working after being cooled from elevated temperature shaping process
T6	Solution treatment and artificial aging. Applications: products that do not undergo cold working after solution treatment
T7	Solution treatment and overaging/stabilization. Applications: cast products that undergo artificial aging after solution treatment in order to give them stability in strength and dimension, wrought products that undergo artificial aging after solution treatment in order to give them an increase in strength beyond the maximum value achievable to control some specific characteristics or properties
T8	Solution treatment, cold working, and artificial aging. Applications: products that undergo cold working for increasing their strength
T9	Solution treatment, artificial aging, and cold working. Applications: products that undergo cold working operations for increasing their strength
T10	Cooling from elevated temperature shaping process, cold working, and artificial aging. Applications: products that undergo cold working for increasing their strength

For all T tempers, the solution heat treatment involves heating the alloy up to the solution temperature and holding at that temperature for a long enough time, so to obtain a complete solutioning of the alloying elements. The subsequent cooling (quenching) should be sufficiently fast to retain a supersaturated solid solution down to the quenching temperature, in order to have precipitation to take place during the subsequent artificial or natural aging

3.2.3.3   Precipitation Hardening

Solid-state precipitation is the phase transformation on which the hardening of *heat-treatable* Al-alloys is based. The same transformation and resulting strengthening mechanisms hold also for other classes of alloys that will be considered next: magnesium and titanium alloys (Sect. 3.3 and Chap. 4), PH stainless steels (Sect. 5.4.3.3), and iron- and nickel-based superalloys (Sects. 6.3 and 6.4). The fundamental aspects of these treatments, which will be illustrated herewith with reference to an aluminum alloy, are meant to provide indications, from the physical metallurgy point of view, for the heat treatments of the other alloy systems too, with obvious important differences as concerns both the process parameters and the precipitates that actually form in each specific alloy system.

Table 3.10 Additional digits for stress relief treatments in T-tempered aluminum alloy products (Kaufman 2000)

Additional digits for T tempers	Wrought product type	Stress relief process	Permanent set
TX51[a]	Plate	Stretching	1.5–3.0%
TX51[a]	Rolled or cold finished bars and rods	Stretching	1.0–3.0%
TX51[a]	Die or ring forgings and rolled rings	Stretching	1.0–5.0%
TX510[a]	Extruded bars, profiles, rods, and tubes	Stretching	1.2–3.0%
TX510[a]	Drawn tubes	Stretching	0.5–3.0%
TX511[b]	Extruded bars, profiles, rods, and tubes	Stretching	1.0–3.0%
TX511[b]	Drawn tubes	Stretching	0.5–3.0%
TX52	All products	Compressing	1.0–5.0%
TX54	Die forgings	Restriking cold in finish die	–

[a]No further straightening after stretching
[b]Minor straightening after stretching. This may be required by tolerance limitations
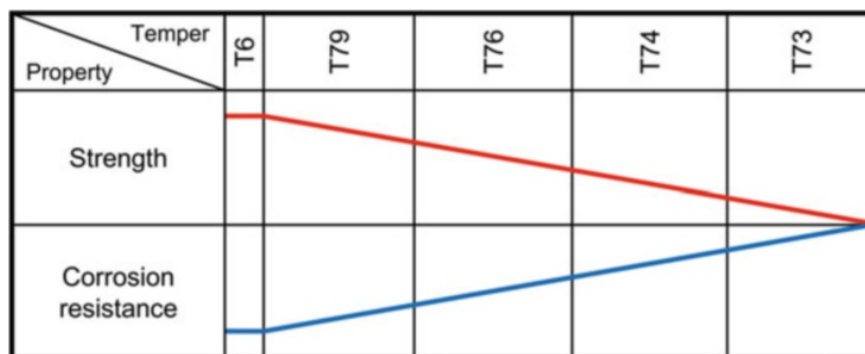
Fig. 3.11 Dependence of mechanical strength and corrosion resistance of the T6 and different T7 tempers. These tempers are typically used for alloys of the 7XXX group, including those for aircraft parts (redrawn from Benedyk 2010)

The main aspects of solid-state precipitation in hardenable aluminum alloys can be discussed considering the binary Al-Cu system, being an important reference also for alloys with more complex compositions. For technological purposes, the alloy composition never goes above the solubility limit of copper in aluminum (see Fig. 3.12); therefore the aluminum-rich corner is the interesting part of the phase diagram, as shown by Fig. 3.13. Solutioning of copper into the aluminum crystalline lattice results in a single-phase alloy, the α-phase in the phase diagram in Fig. 3.13. Quenching freezes the supersaturated alloy down to room temperature, and the subsequent aging, conducted either at room (natural aging) or higher (artificial aging) temperatures, is designed to reach the target conditions, in agreement with the requirements of the specific applications. The intermetallic compound θ-Al_2Cu, present in the Al-Cu equilibrium phase diagram, is not really interesting for the
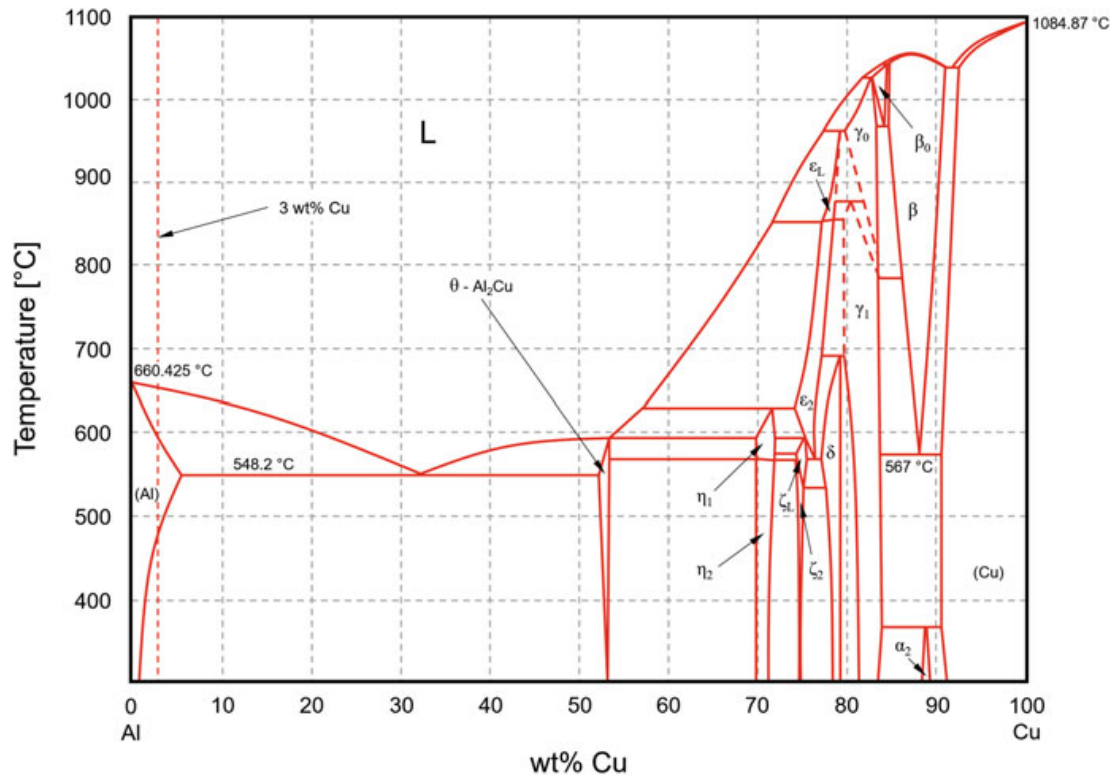
Fig. 3.12 Al-Cu phase diagram. (Redrawn from ASM International 1992)

improvement of the mechanical properties of the alloy and it is actually a typical phase observed in overaged conditions. Similar equilibrium phases, with different compositions, will form in other heat-treatable aluminum alloys (see Table 3.11). Several important metastable structures can be obtained indeed in real alloys, thanks to the kinetic constrains introduced by the heat treatment parameters. These structures, not present in the equilibrium phase diagram, are very important as concerns the alloy properties. In the Al-Cu system, these structures are θ', θ'', and GPZ (Guinier-Preston zone), described in the following.

The heat-treated condition of the alloy can be predicted from TTT curves (Fig. 3.14), once the main parameters of the treatment, like quenching rate, aging temperature, and time, have been selected. As illustrated in Fig. 3.14, there are two possibilities for obtaining GPZ. The first consists in quenching the alloy directly to the relevant GPZ field as shown by the cooling trajectory 1. A second approach is to cool down the alloy at a sufficiently high rate not to cut the GPZ directly from the solutioning temperature and then start an aging treatment, at constant temperature until the transformation is fully accomplished, according to the trajectory 2 in Fig. 3.14.
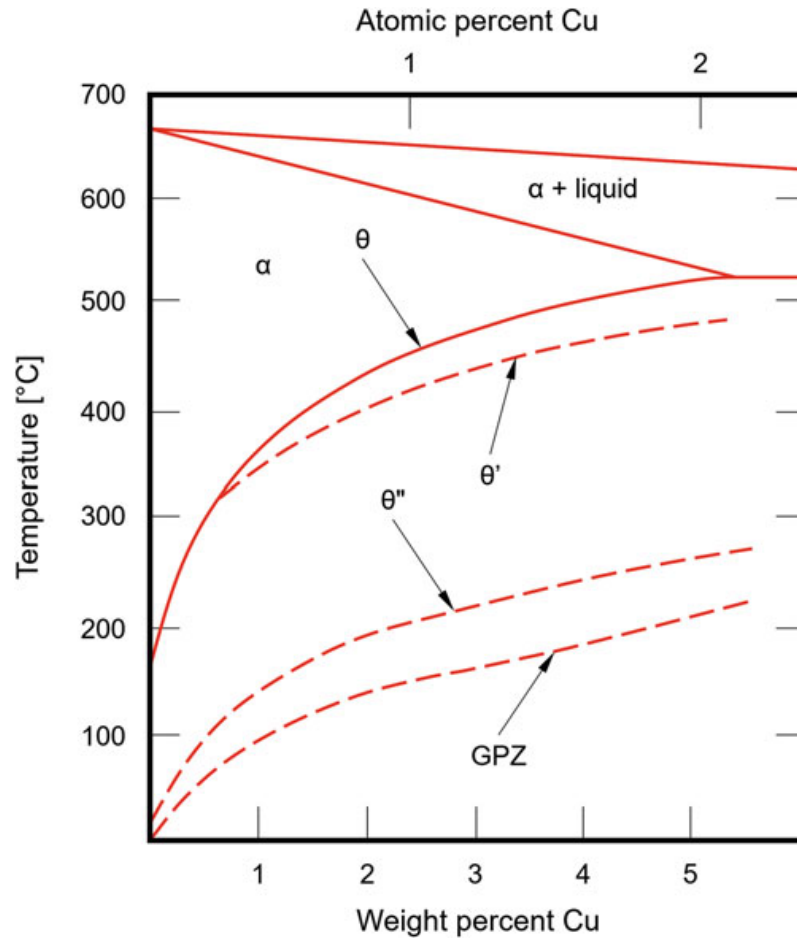
Fig. 3.13 Part of the Al-Cu phase diagram showing the stable θ-Al_2Cu precipitate and the metastable θ', θ'', and GPZ. (Redrawn from Porter et al. 2009)

Table 3.11 Solid-state precipitation in some alloy systems (Porter et al. 2009)

Base metal	Alloy	Precipitation sequence
Al	Al-Ag	GPZ (spheres) $\rightarrow$ γ' (plates) $\rightarrow$ γ (Ag_2Al)
	Al-Cu	GPZ (discs) $\rightarrow$ θ'' (discs) $\rightarrow$ θ' (plates) $\rightarrow$ θ (Cu Al_2)
	Al-Cu-Mg	GPZ (rods) $\rightarrow$ S' (laths) $\rightarrow$ S ($CuMgAl_2$, laths)
	Al-Zn-Mg	GPZ (spheres) $\rightarrow$ η' (plates) $\rightarrow$ η ($MhZn_2$, plates or rods)
	Al-Mg-Si	GPZ (rods) $\rightarrow$ β' (rods) $\rightarrow$ β (Mg_2Si, plates)
Cu	Cu-Be	GPZ (discs) $\rightarrow$ γ' $\rightarrow$ γ (CuBe)
	Cu-Co	GPZ (spheres) $\rightarrow$ β (Co, plates)
Fe	Fe-C	ε carbide (discs) $\rightarrow$ Fe_3C (plates)
	Fe-N	α'' (discs) $\rightarrow$ Fe_4N
Ni	Ni-Cr-Ti-Al	γ' (cubes or spheres)
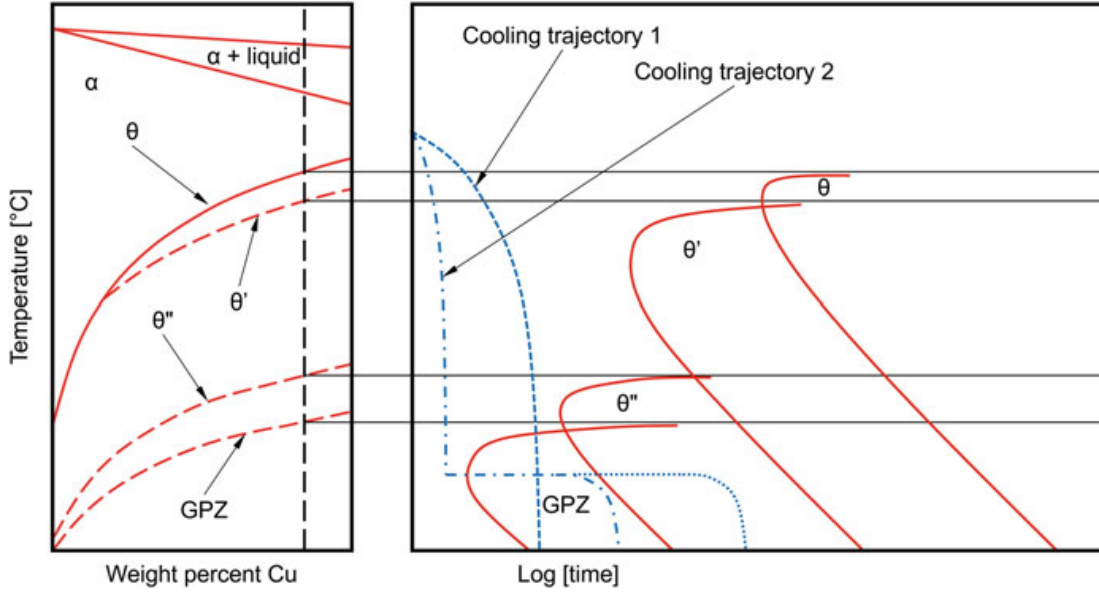
Fig. 3.14 Al-Cu phase diagram showing the stable θ precipitate and the metastable θ', θ'', and GPZ and related TTT diagram with different cooling trajectories. See main text for details. (Redrawn and adapted from Porter et al. 2009)

Similarly, the precipitation of other phases can be induced. Different precipitates feature different crystallographic structures that induce different kinds of interface with respect to the hosting aluminum matrix: coherent, semicoherent, or fully incoherent (Porter et al. 2009 – see also Sect. 6.4.1.1).

Figure 3.15 summarizes the situation for the precipitates' features in Al-Cu alloys. An important parameter that characterizes the matrix-precipitate interface is the lattice misfit δ (Geddes et al. 2010; Reed 2006):

$$\delta = \frac{a_{\theta''} - a_\alpha}{a_{\theta''} + a_\alpha} \times 2 \tag{3.2}$$

where

- δ is the lattice misfit.
- a_α is the lattice parameter of the matrix.
- $a_{\theta''}$ is the lattice parameter of the θ'' precipitate.

The lattice misfit depends on the difference of the lattice parameter, or interatomic distance, along specific crystallographic planes that are facing each other across the precipitate-matrix interface (see also Sect. 6.4.1.1). In the present example (Eq. 3.2), the lateral plane for the θ'' and cube plane for the α Al-*fcc* structure are considered. Other important features of the precipitates, like size, shape, composition, etc., are dependent on the overall alloy composition and on the elastic anisotropy along crystallographic directions. These intrinsic alloy parameters and the thermal treatment conditions act as kinetic constraints, so that not only stable but also metastable phases can form.
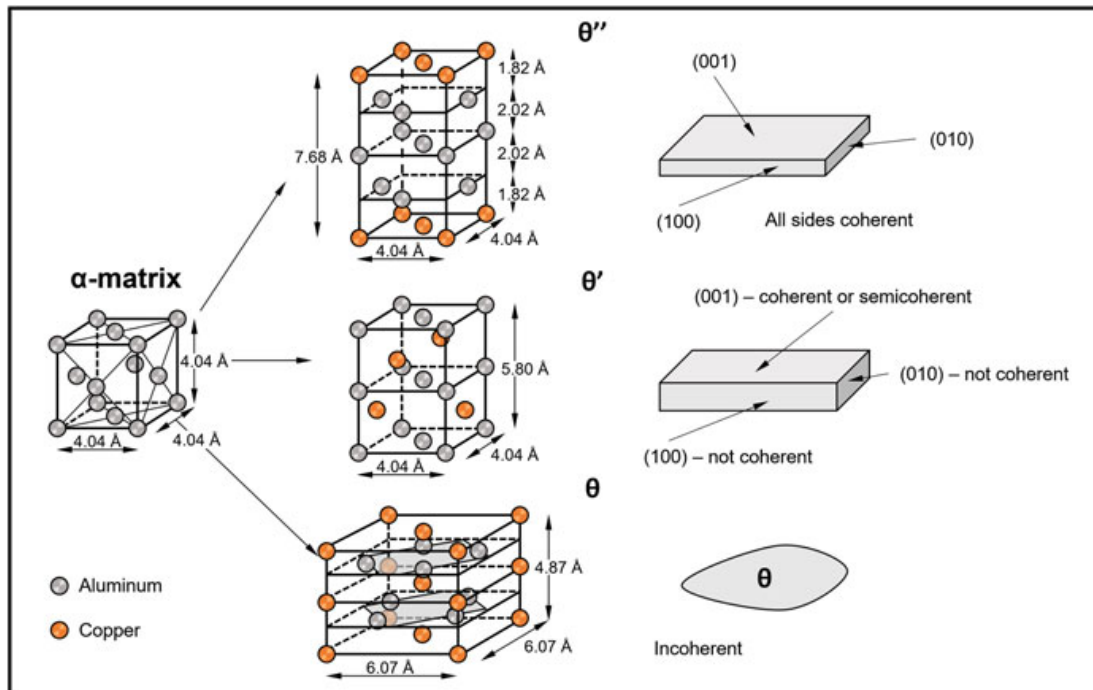
Fig. 3.15 α matrix, stable θ precipitate and metastable θ′, θ″ structure and morphology. (Redrawn from Porter et al. 2009)

In Table 3.11, the precipitation transformations for different alloy systems are summarized. In case of *heat-treatable* aluminum alloys, the formation of metastable structures is quite a general feature. This is the case of the β′ precipitates in the 6063 alloy (Al-Mg-Si group, Fig. 3.16). β′ (Mg_2Si composition) is a coherent precipitate with preferential orientation along the <100> direction of the aluminum matrix. The precipitates are aligned along this particular crystallographic direction since it turns out to be the more energetically favored, as compared to the others. In fact, along this direction there is the lowest atomic linear density, the interatomic distances are larger, and so the elastic constant is lower. The shape of the precipitate is sensitive to the elastic anisotropy as well. In fact, the interfaces with the aluminum matrix having a lower elastic strain energy term will be wider than those with a higher elastic energy term. The hardening induced by the alloy heat treatments will depend on the resulting microstructure that influences the way in which precipitates and dislocations interact.

In agreement with the TTT curves (Fig. 3.14), at an aging temperature of 190 °C, the GPZs cannot form, since the relevant aging trajectory is not cutting the stability domain of these structures, meaning that the aging temperature is larger than the GPZ *solvus*. Direct precipitation of θ″ can take place instead, and these precipitates for longer aging times may transform into θ′ precipitates. The peak hardness value scales up with the concentration of copper and, thereby, with the fraction of precipitates that may form. The hardening curves corresponding to a lower aging temperature (Fig. 3.17, $T = 130$ °C) may reach higher hardness peaks, for each one of the investigated alloys. This can be ascribed to the formation of finely
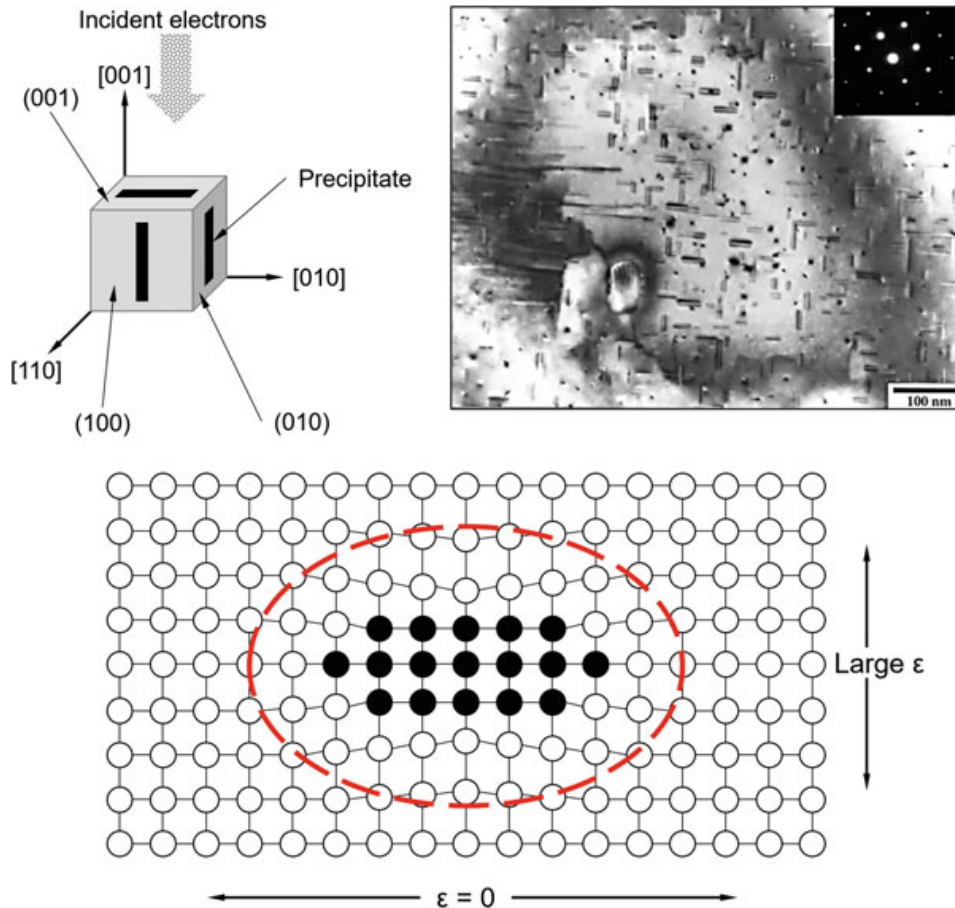
Fig. 3.16 Transmission electron microscopy micrograph of β' precipitate in 6063 alloy. The image contrast is due to the strain ε at the precipitate-alloy matrix coherent interface, as represented by the bottom scheme. (Photo property of the Authors, bottom scheme redrawn from Porter et al. 2009)

dispersed GPZs, not forming at the higher aging temperature. The evolution of hardness on aging is determined by the change of the dominant interaction mechanisms between dislocations and precipitates. In the early stages of the lower temperature aging, GPZs are the main strengthening agents. Dislocations are hindered in their movement by the elastically strained aluminum matrix. The same mechanism is active when the θ'' coherent precipitates start to form. Moreover, the coherency of the θ'' particles and their larger size, as compared to GPZs, allows also for the dislocation *cutting* mechanism to happen (Fig. 3.18). The resulting strengthening is due to the drag that the dislocations are subjected to when moving through the precipitates and to the resistance determined by the strain field at the precipitate-matrix interface.

The mechanisms described so far are responsible for the rising branch of the hardening curves in Fig. 3.17. Each one of these curves reaches a maximum and then starts to decrease. This is due to a change in the dislocation-precipitate interaction mechanism. The ripening of the precipitates with aging time results in a progressive alloying elements depletion from aluminum alloy matrix.
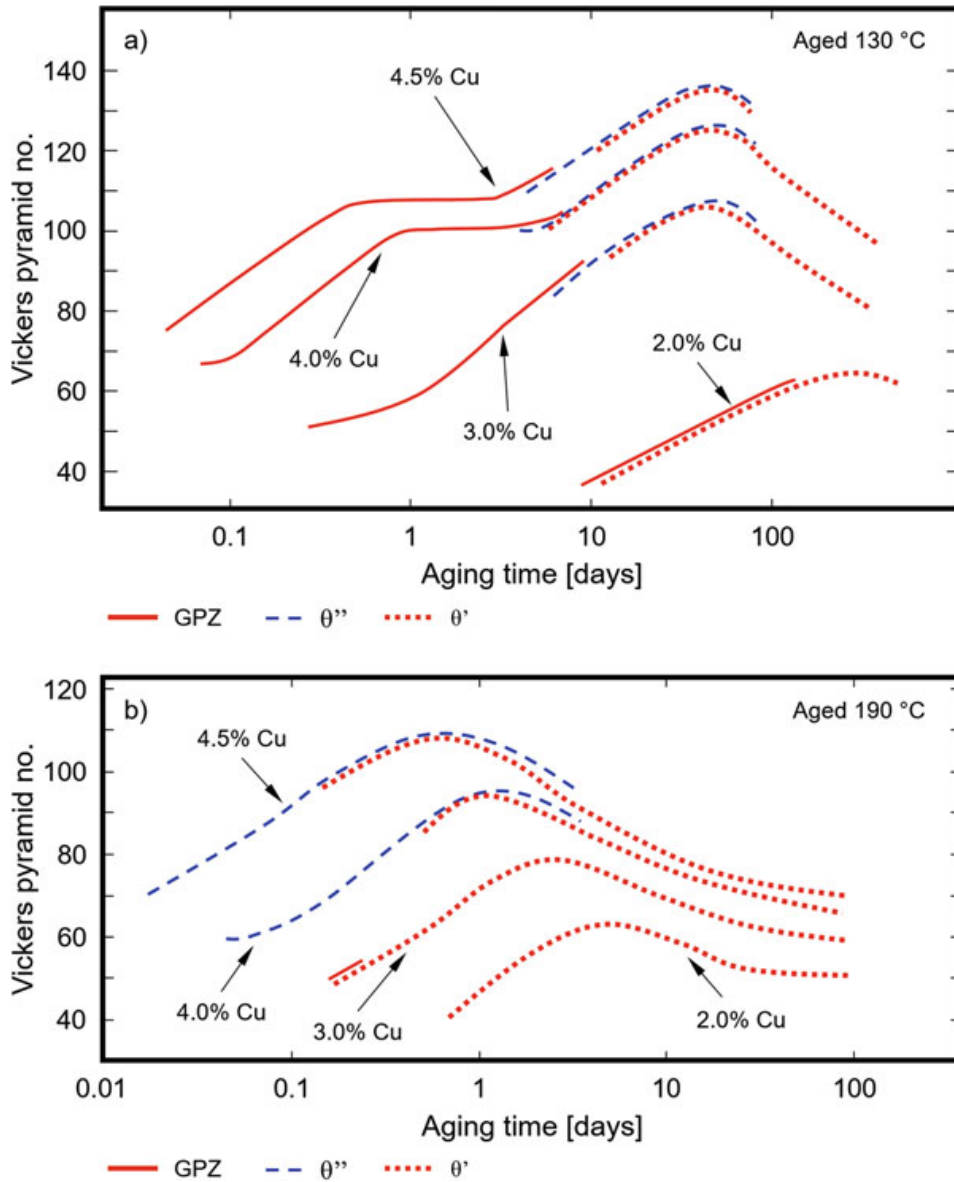
Fig. 3.17 Effect of the aging temperature on the hardness of binary Al-Cu alloys. (**a**) 130 °C aging; (**b**) 190 °C aging. Note that for the higher temperature, the precipitation of GPZ is nearly fully suppressed. (Redrawn from Porter et al. 2009)

This reduces the solid solution strengthening, and dislocations can now move more easily. Actually, they get pinned by the precipitates but can still continue to move if the applied stress is sufficient to increase their length. This is the strengthening mechanism active in the so-called dislocation *bowing* regime (also known as Orowan mechanism, Fig. 3.19; see Sect. 6.4.3 for further details).

Actually, additional strengthening may also come from the piling up of dislocation loops around each pinning precipitate. The Orowan mechanism is active in the Al-Cu alloys when incoherent θ' and equilibrium θ precipitates form. The occurrence of equilibrium precipitates in all hardenable aluminum alloys, i.e., those belonging to the 2XXX, 6XXX, and 7XXX groups (see Table 3.4), is often
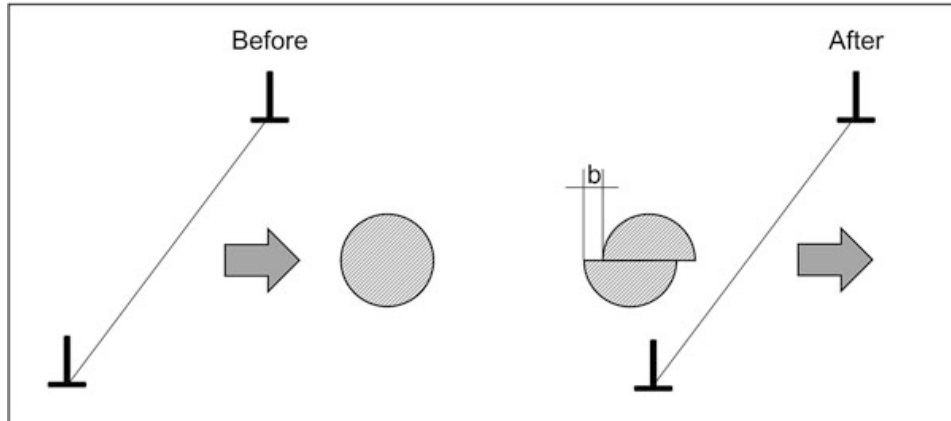
Fig. 3.18 Dislocation cutting through a spherical precipitate
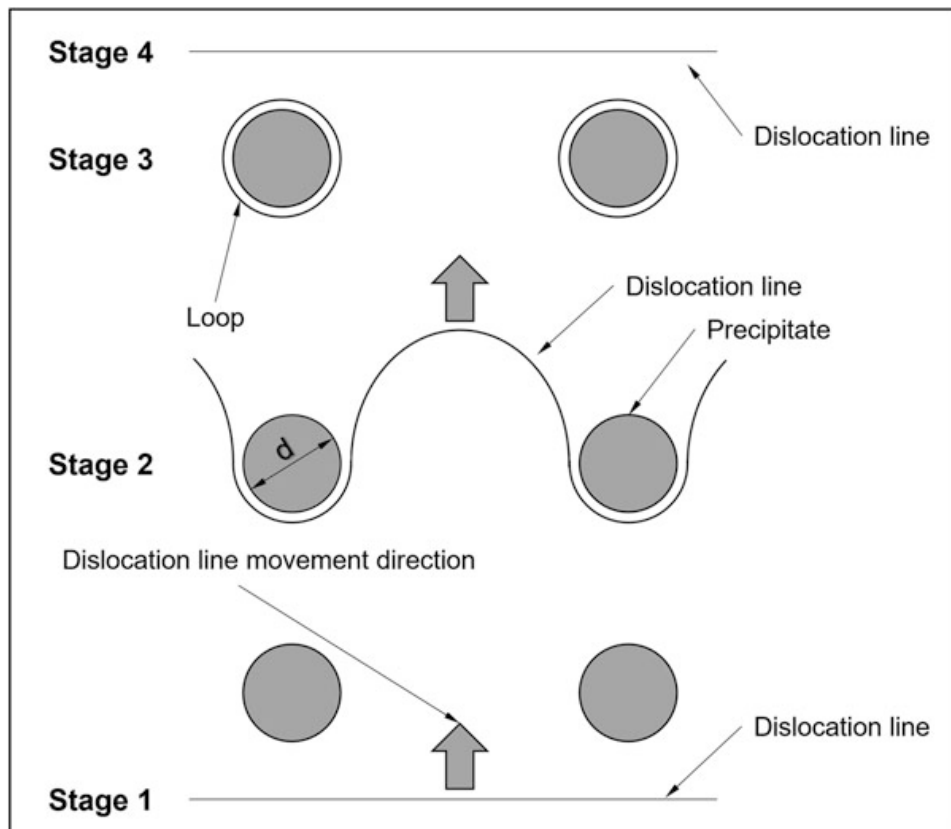
Fig. 3.19 Dislocation bowing. (Redrawn from Hull and Bacon 2011)

associated with the condition of overaging (Fig. 3.20 referring to a 6063 alloy with equilibrium Mg_2Si precipitates).

At this stage, which can be reached either for an incorrect heat treatment or for the prolonged exposure of the alloy to demanding servicing conditions, an important decay of the alloy hardness is observed. The transition from cutting to bowing as concerns the dominant dislocation-precipitate interaction mechanism is observed in other precipitation-hardened alloys, like Mg-alloys (see Sect. 3.3) and Ni-based

Fig. 3.20 Mg$_2$Si precipitate in an overaged 6063 alloy. (Photo property of the Authors)

superalloys (Chap. 6). For these latter, an important role as concerns strengthening is played by the atomic crystallographic order of the γ' precipitates (see Chap. 6 for further details). The heat treatments of aluminum alloys are important for the effects they have on the structure, composition, spatial distribution, and size of the strengthening precipitates. Also the microstructure of the alloy in the grain boundary regions is influenced by the heat treatment parameters and relevant precipitation kinetics. Figure 3.21 shows some examples of the so-called precipitation-free zone (PFZ) and relevant scheme.

Heterogeneous nucleation, driven by the grain boundary surface energy term, determines an anticipated precipitation along grain boundaries, which depletes the surrounding regions of alloying elements. When nucleation, mostly homogeneous, and subsequent growth of precipitates inside the grains start, they can no longer occur in the alloy-depleted regions that give place to the mentioned PFZs. As shown by the scheme in Fig. 3.21, PFZs become a preferential path for the movement of dislocations, resulting in a general weakening of the alloy. To get rid or at least to reduce the incidence of the PFZs, several approaches are possible. A higher undercooling, with respect to the solution temperature, enhances the homogeneous nucleation rate inside the grains. Alloying with insoluble atoms, like silicon, may introduce preferential nucleation sites in the alloy, which again favor a uniformly distributed precipitation within the alloy grains, by reducing the incidence of the preferential precipitation along grain boundaries. Another defect structure that can
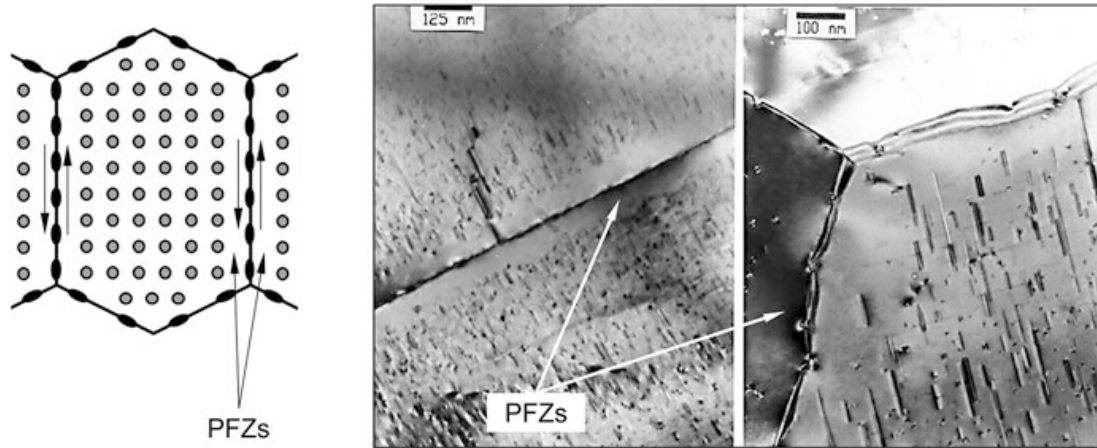
Fig. 3.21 Examples of precipitate-free zones. (Left picture redrawn from Polmear 2006; images on the right are photo property of the Authors)
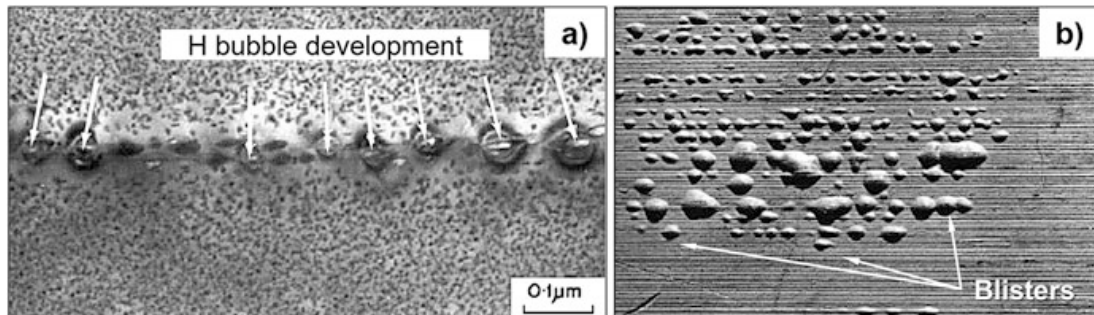
Fig. 3.22 (**a**) Transmission electron micrograph showing hydrogen inclusions development at the grain boundary of a thin foil of an artificially aged Al-Zn-Mg alloy; (**b**) blisters on the surface of an Al-alloy component after solution treatment in a humid atmosphere (Polmear 2006, reproduced with permission of the Publisher)

be observed along grain boundaries and subsurface regions is hydrogen micro-inclusions (Fig. 3.22). This phenomenon, called *blistering* for the particular morphology that induces on the alloy surface, occurs during water quenching as a consequence of the hydrolysis of H_2O catalyzed by the oxidation of aluminum, according to the reaction: $2Al + 3H_2O \rightarrow Al_2O_3 + 3H_2$.

The grade of the alloy, depending on the concentration of impurity elements, is very important because it determines the formation of intermetallic particles within the alloy itself (see Fig. 3.23). The size and intrinsic brittleness of these phases render their presence potentially detrimental for the properties of the alloy, in which they act as stress concentrators.

Fig. 3.23 Fe-rich inclusion in a 6063 alloy, isomorphous to the Al_3Fe intermetallic. (Photo property of the Authors)
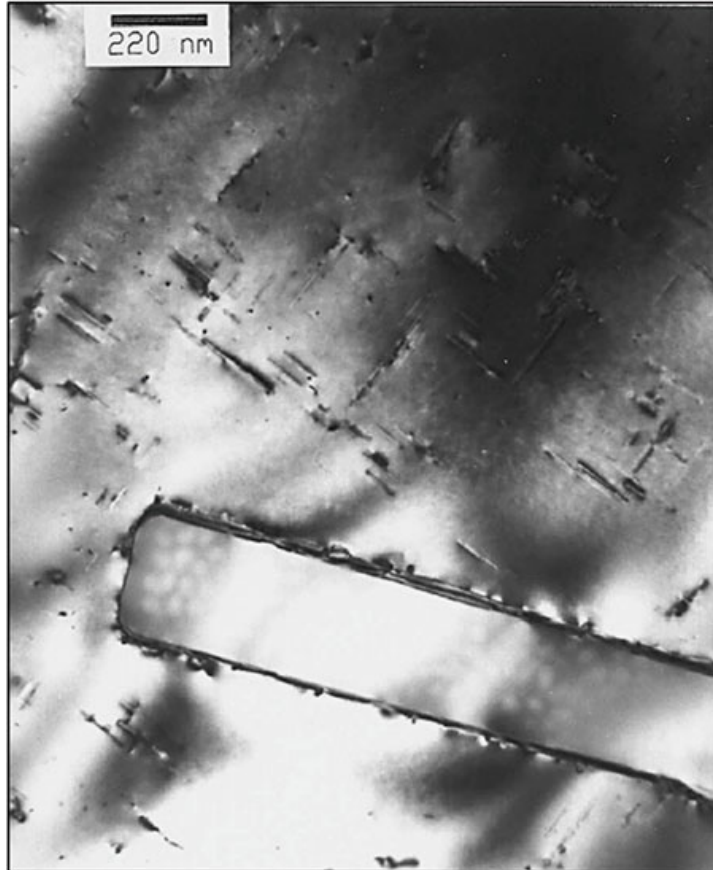
3.2.4 Aluminum-Lithium Alloys

Lithium is present in several Al-alloys, but since it is not necessarily the majority alloying element, wrought Li-containing Al-alloys can be found in different alloy groups: 1XXX, 2XXX, and, finally, 8XXX, being the alloys of this latter group, those featuring larger Li concentrations (Table 3.12).

Although regarded as the most recently developed of the Al-alloys, actually, Al-Li alloys started their metallurgical history back in the 1920s, and lithium additions were used to enhance the strengthening of age-hardenable alloys (Starke et al. 1981). The very first Li-containing Al-alloy was developed in Germany in 1924 with the commercial name Scleron and nominal composition Al-12Zn-3Cu-0.6Mn-0.1Li (Prasad et al. 2014). The first results were very encouraging indeed, since the expected improvement in strength was accompanied also by a higher stiffness and, obviously, lower density (see Fig. 3.24). The production of Al-Li alloys requires a careful working condition control, in order to avoid the losses of lithium during melting, for which vacuum induction melting is regarded as a safe route (for additional information see Sect. 5.3.2) (ASM International 2008). Lithium content in the main Al-Li alloys is given in Table 3.12, while the complete chemical composition of the main alloys of the family can be found in Table 3.5 and Appendix 1. Three main different development stages can be identified. The *first-generation*

Table 3.12 Designation, Li content, density, and introduction of some relevant Al-Li alloys

Alloy	Generation	wt% Li	Density [g/cm³]	Producer (introduction year)
2020	1	1.00	2.71	Alcoa (1958)
1420		2.10	2.47	Soviet (1965)
1421		2.10	2.47	Soviet (1965)
2090	2	2.10	2.59	Alcoa (1984)
2091	(Li ≥ 2%)	2.00	2.58	Pechiney (1985)
8090		2.40	2.54	EAA (1984)
1440		2.40	2.55	Soviet (1980s)
1441		1.95	2.59	Soviet (1980s)
1450		2.10	2.60	Soviet (1980s)
1460		2.25	2.60	Soviet (1980s)
2195	3	1.00	2.71	Lockheed Martin Corporation/Reynolds (1992)
2196	(Li ≤ 2%)	1.75	2.63	Lockheed Martin Corporation/Reynolds/McCook Metals (2000)
2297		1.40	2.65	Lockheed Martin Corporation/Reynolds (1997)
2397		1.40	2.65	Alcoa (1993)
2098		1.05	2.70	McCook Metals (2000)
2198		1.00	2.69	Reynolds/McCook Metals/Alcan (2005)
2099		1.80	2.63	Alcoa (2003)
2199		1.60	2.64	Alcoa (2005)
2050		1.00	2.70	Pechiney/Alcan (2004)
2296		1.60	2.63	Constellium Alcan (2010)
2060		0.75	2.72	Alcoa (2011)
2055		1.15	2.70	Alcoa (2011)
2065		1.20	2.70	Constellium (2012)
2079		1.50	2.64	Constellium (2012)

The complete chemical composition is given in Table 3.5 and Appendix 1 (Prasad and Wanhill 2017)
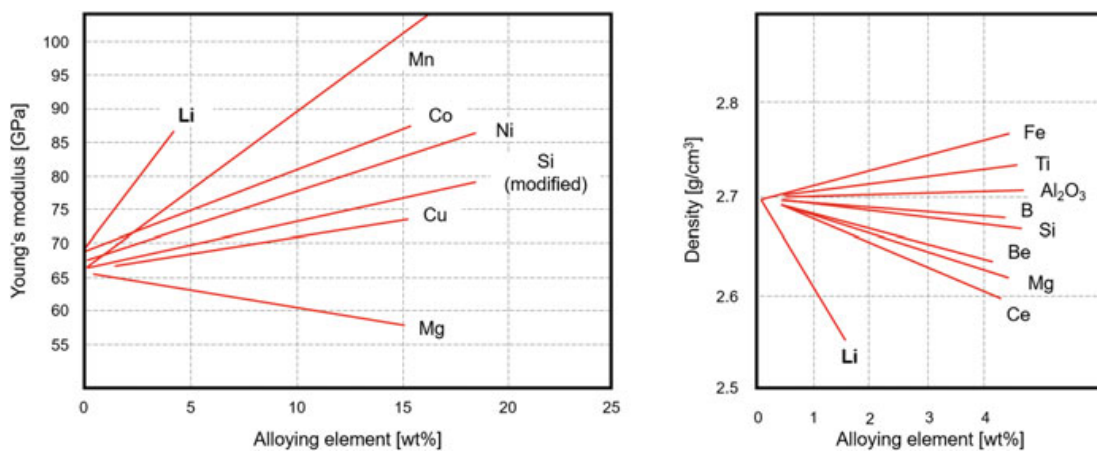
Fig. 3.24 Dependence of the Young's modulus and density of aluminum as a function of the concentration of different alloying elements. (Redrawn from Polmear et al. 2017)

Table 3.13 Main precipitate phases encountered in commercial Al-Li alloys (Prasad et al. 2014)

Phase	Chemistry	Crystal structure	Lattice parameters [nm]	Main features
δ	AlLi	Cubic (NaCl)	$a = 0.638$	Equilibrium phase with a plate morphology
δ'	Al_3Li	Cubic ($L1_2$)	$a = 0.401$	Non-equilibrium ordered phase, usually with spherical shape and coherent interface with the aluminum matrix
T_1	Al_2CuLi	Hexagonal	$a = 0.4965$ $c = 0.9345$	Equilibrium phase. Partially coherent interfaces
T_2	Al_6CuLi_3	Cubic	$a = 1.3914$	Please note: the cubic structure displays icosahedral symmetry
S'	Al_2CuMg	Orthorhombic	$a = 0.401$ $b = 0.925$ $c = 0.715$	Semicoherent phase
θ'	Al_2Cu	Tetragonal	$a = 0.404$ $c = 0.580$	–
–	Al_3Zr	Cubic ($L1_2$)	$a = 0.405$	Coherent, ordered, spherical dispersoids

alloys were developed over a decade across 1960. The potential of these materials was demonstrated and the critical aspects of their processing emerged. The *second-generation* Al-Li alloys featured a Li content in excess, or equal to, 2 wt% and were produced either via ingot metallurgy, mainly, or powder metallurgy. The development of the *third-generation* was initiated in the late 1980s, when the Martin Marietta Corporation was engaged in the design of a weldable, low-density aluminum alloy for cryogenic tanks and other components of aerospace vehicles (Prasad et al. 2014).

Lithium alloying reduces aluminum density and increases its stiffness (Fig. 3.24). The higher stiffness and, most importantly, the enhancement of the alloy strength are due to the formation of the ordered δ'-Al_3Li precipitates. These precipitates have the same $L1_2$ structure as the ordered γ' precipitates in Ni-based superalloys (see Chap. 6). The partial covalent character of the chemical bonds in the intermetallic phase enhances the Young's modulus of the alloy and, as counterpart, reduces the alloy ductility and its fracture toughness. Moreover, fracture toughness of Al-Li alloys is extremely sensitive to the content of alkali metal impurities. A few tens of ppm of Na and K, introduced during the ingot metallurgy casting for the production of the primary alloy, are sufficient to reduce the alloy fracture toughness below the safety values compatible with structural applications (Polmear 2006).

The main strengthening mechanism active in the early compositions (first generation, Table 3.12) of the Al-Li alloys is based on the dislocations cutting through the δ'-Al_3Li precipitates (Table 3.13). This intermetallic, not present in the relevant equilibrium phase diagram (Fig. 3.25), can be stabilized though using suitable thermal treatments.

The ordered structure of the δ'-Al_3Li precipitates introduces a further strengthening factor, associated with their interaction with dislocations and with the formation
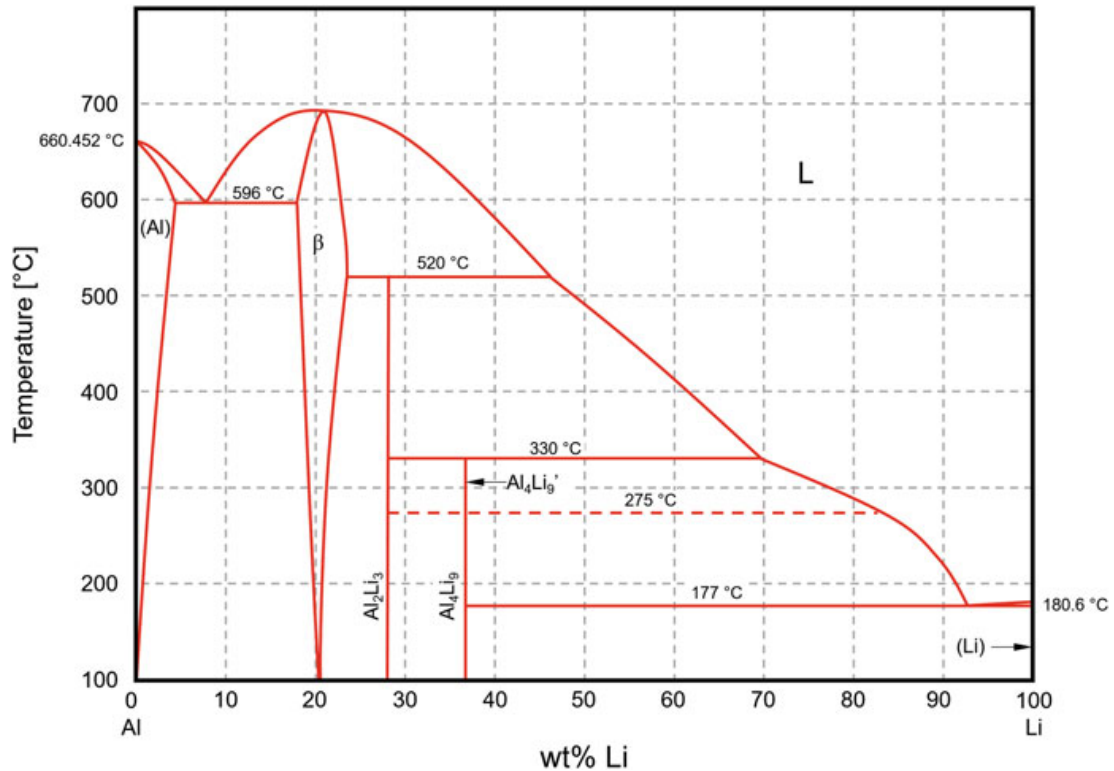
Fig. 3.25 Al-Li phase diagram. (Redrawn from ASM International 1992)

of complex defect structures, involving antiphase boundaries and super-dislocations, as in Ni-based superalloys (see Sect. 6.4.3). However, the localized shearing across the ordered precipitates may produce excessive strain hardening concentrated close to grain boundary, leading in the long run to diffuse cracking. This was one of the main reasons for the withdrawal of the *first-generation* alloys, e.g., the A2020 (see Table 3.12), used for the wing skin of the Northrop RA-5C Vigilante aircraft. The alloy compositions and relevant annealing treatments were developed further, aiming at the formation of other precipitates and dispersoids, capable to homogenize the dislocation structures. The reinforcing phases that formed in the novel alloy formulations were either finely distributed inside the alloy matrix, like the θ'-Al_2Cu, introducing lattice strain as obstacle to dislocation movement, or were semicoherent grains with a limited number of slip systems. This is the case of the T_1-Al_2CuLi and S'-Al_2CuMg intermetallics, not easily cut by dislocations, that thereby remain stuck at the precipitate-alloy interface. The formation of these phases is favored by the presence of alloying elements, like silver and zirconium, introduced in several of the *third-generation* Al-Li alloys. Another feature of these alloys is the optimum concentration of lithium, typically ranging from 1.0 to 1.3 wt%, anyway lower than 2.0%, or more, typical of the *second-generation* Al-Li alloys, for this reason featuring extremely low-density values and regarded as a promising metallurgical response to the early encouraging results obtained with the extra-light polymer matrix structural composites. Notwithstanding the interest in these alloys, their elevated brittleness and low toughness lead to a rapid abandon of these formulations

and stopped any further development. A definitely better outcome was faced by the *third-generation* Al-Li alloys. Although relatively heavier, for the smaller concentrations of lithium, these alloys exhibited the right balance between workability and in-service performances. The development of these alloys received an important boost also from the results of the research conducted by metallurgists in the Soviet Union in the 1970s. The most recent Al-Li products, featuring the constant presence of copper, have been qualified for high strength and high damage-tolerant applications in aircraft structures, exhibiting even interesting corrosion resistance properties (Lequeu et al. 2010). Altogether the Al-Li alloys represent an important step in the development of light alloys. In fact, several Al-Li products have reached similar or better properties than the 2XXX and 7XXX traditional alloys, of which they represent excellent candidates for substitution (Table 3.14).

3.2.5 Aluminum Alloys in Aircraft Structures: Present State and Perspectives

The capability to meet quite complex and diverse requirements is an important aspect of the aluminum alloys and probably one of the main reasons for their success in aircraft structures. The situation is well depicted by the scheme in Fig. 3.26, summarizing the main properties for the principal parts and components of an aircraft structure, for which aluminum alloy represents an excellent choice.

Possible candidates like magnesium alloys (see Sect. 3.3) and structural polymer matrix composites that in the long run might take over the role of aluminum alloys are emerging. The B787-Dreamliner has demonstrated the possibility of using structural composites as reliable replacements for aluminum alloys (see Fig. 1.11 in Chap. 1). This result has been possible thanks to an integrated production approach, involving materials development and the implementation of novel manufacturing technologies. In some respect, this is what has also been made for the Airbus A380, this time with a priority for structural aluminum alloys. In this aircraft, an intelligent mix of improved new composition and workhorse alloys have been largely employed, as indicated by the list of aluminum parts given in Table 3.15 (Lequeu et al. 2007).

The large dimensions of the A380 (Fig. 3.27) and the optimization of the production costs, have required the development of new equipment for casting the primary alloys, for machining, for hot-rolling, and for handling the super-size slabs and plates (Lequeu et al. 2007). The use of several Al-Li alloys is coherent with the Airbus strategy that over the years has progressively reduced the percentage of conventional aluminum alloys used in their airplane structures and at the same time has increased the fraction of the lighter Al-Li alloys.

In other commercial airliners, like the B777 and A460-600, high strength and high damage-tolerant aluminum alloys belonging to the 2XXX and 7XXX groups, as those listed in Table 3.16, have been selected for the airframes, using products

Table 3.14 Products, requirements, applications of selected Al-Li alloys, with reference also to the substitution of alloys from other groups (Prasad et al. 2014)

Generation	Alloy	Temper	Product	Alloys to substitute	Requirements	Applications
2	8090	T3	Sheet	–	–	Floor installations, brackets, stiffeners, frames, spars, stringers, longerons, ribs, bulkheads
	8090C	T8		2014-T6	Medium strength	Flying control systems, avionics bay structures, cabin roof frames
	8090C	T81		2024-T3 2024-T42	Damage tolerance	Lower fuselage skin panels, flat roof panels, flying control structures
	8090	T852	Forgings	7010-T7451	Medium/high strength	Cabin roof and side frames
	8090	T8511	Extrusions	7075	Medium strength	Frames, brackets, stringers, bulkheads, door rails
3	2098	T8511	Sheet	2024-T3 2524-T3	Damage tolerance, medium strength	Fuselage/pressure cabin skin
	2198	T8		2524-T351		
	2199	T8E74				
	2060	T8E30				
	2199	T86	Plate	2024-T351 2324-T39	Damage tolerance	Lower wing covers
	2050	T84				
	2060	T8E86		2624-T351 2624-T39		
	2098	T82P		2024-T62	Medium strength	F-16 fuselage panels
	2297	T87		2124-T851		F-16 fuselage bulkheads
	2397	T87				
	2050	T84		7150-T7751 7055-T7751 7055-T7951 7255-T7951	High strength	Upper wing covers
	2055	T8X				
	2195	T82P				

				High strength	Wing/fuselage attachments, windows frames, crown frames
2050	T852	Forgings	7175-T7351 7050-T7452	High strength	Wing/fuselage attachments, windows frames, crown frames
2099	T81	Extrusions	2024-T3511 2026-T3511 2024-T4312 6110-T6511	Damage tolerance	Lower wing stringers, fuselage/pressure cabin stringers
2099	T83		7075-T73511 7075-T79511 7150-T6511 7175-T79511 7055-T77511 7055-T79511	Medium/high strength	Fuselage/pressure cabin stringers and frames, upper wing stringers, Airbus A380 floor beams and seat rails
2055	T8R83				
2065	T8511				
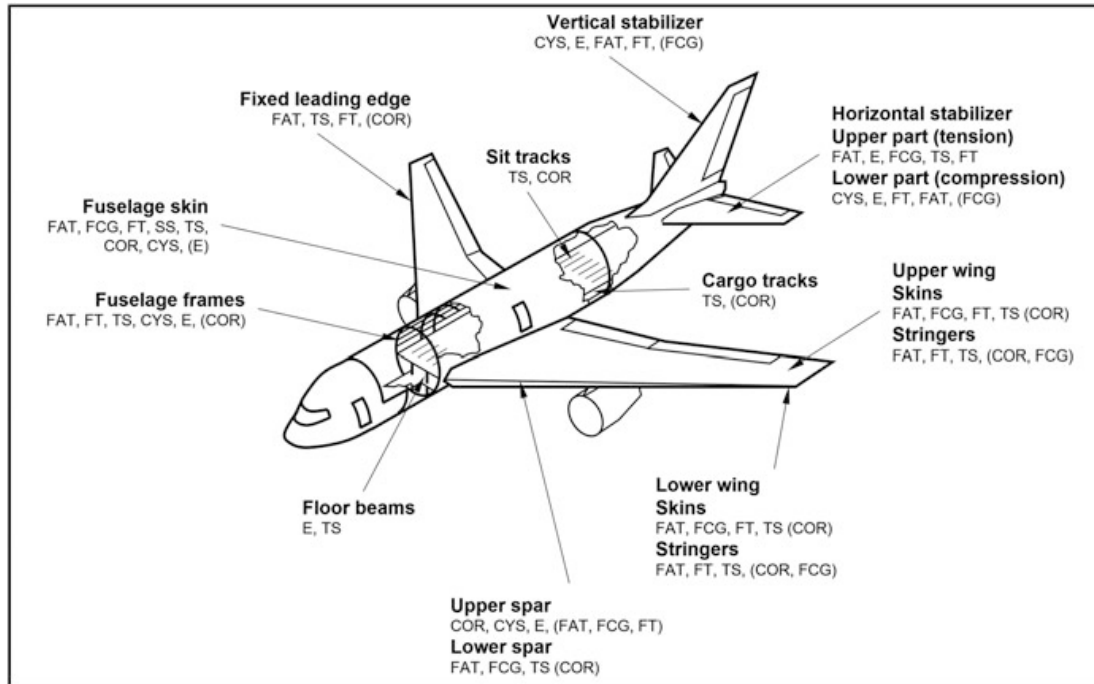
Fig. 3.26 Materials property requirements for a commercial airliner. Material properties abbreviations: *COR* corrosion, *CYS* compressive yield strength, *E* modulus, *FAT* fatigue, *FCG* fatigue crack growth, *FT* fracture toughness, *SS* shear strength, *TS* tensile strength. Material properties in brackets ( ) are regarded as important, but not critical, design requirements. (Redrawn from Polmear et al. 2006)

obtained by rolling, extrusion, or forging. In most cases, the starting batch is an ingot semi-continually direct-chill cast.

The extreme reliability of the conventional Al-alloys and the knowledge that has been accumulated over the years in more than one century represent also an important benchmarking for the development of new wrought alloys, like the recent formulations and tempers of Al-Li alloys discussed in Sect. 3.2.4 (Lequeu et al. 2010), particularly as concerns those mechanical properties important both for processing and in-service performances (Table 3.17).

Some structural aircraft components made of aluminum alloys are produced also by casting: sand casting, investment casting, and permanent mold casting. In this way, single-part components have been obtained, thus reducing or eliminating at all joining steps. The cast components are particularly well suited for replacing parts with complex geometries, requiring time-consuming and expensive machining. Another advantage of cast components is the elimination of all those defects that are typically associated with joints, like structural flaws and corrosion-initiation regions. However, since the resulting mechanical properties of cast products are on average lower than those of the corresponding wrought counterparts (see Sect. 3.2.2), the so-called *casting factor* (CF) has been introduced. This is a sort of safety factor, ranging from 1.0 to 2.0 used to scale down the reliable strength of the cast components, any time the material has an assigned CF value in excess of 1.0. A

Table 3.15 Aluminum alloy products used for different parts and components of the A380 (Lequeu et al. 2007)

Alloy	Temper	Form	A380 application
2024A	T351	Plates	Lower wing reinforcement
2027	T351		Lower outer wing panel (A380-800F)
2050	T84		Lower wing reinforcement
7010	T7651		Upper outer wing panel, heavier gauge wing ribs
7040	T7451		Fuselage main frames, cockpit, window frames, beams, fittings
7040	T7651		Wing spars (inner front and inner center part)
7056	T7951		Upper wing panels (A380-800F)
7449	T7951		Upper wing
7449	T7651		Lower gauge wing rib
2027	T3511	Heavy sections	Lower wing stringers
2196	T8511		Floor beams
7449	T79511		Upper wing stringers
2024HS	T432	Small sections	Fuselage frames
2196	T8511		Floor structure, fuselage stiffeners
6056	T78		Fuselage stiffeners
6056	T6		Fuselage stiffeners
7349	T6511		Seat rails, stiffeners of center wing box
7349	T76511		Fuselage stiffeners
6056	T78	Sheet	Pressure bulkhead below cockpit floor
6156Cl	T6		Fuselage panels

consolidated experience in using castings has been developed for military aircrafts. A few examples of quite an extensive use of Al-alloy castings in military aircrafts and helicopters are:

- The inlet duct of the General Dynamics F-16 Fighting Falcon.
- The pave tack pod of the General Dynamics F-111 and of the McDonnel Douglas F-4.
- The main support of the sensor for night vision in the Apache helicopter (Starke and Staley 1996).

The experience with military aircrafts has been exploited in the first place to reduce the impact of CF. Therefore, the use of castings has become a valuable and reliable choice also for primary structures. This has indeed happened for several Airbus aircrafts, starting from the A320 onward with the following main components:

- Baggage compartment door.
- Flap tracks.
- The inner structure of the passenger door.

The same choice has been adopted by Boeing too and has now become a standard (Rendigs 1994).
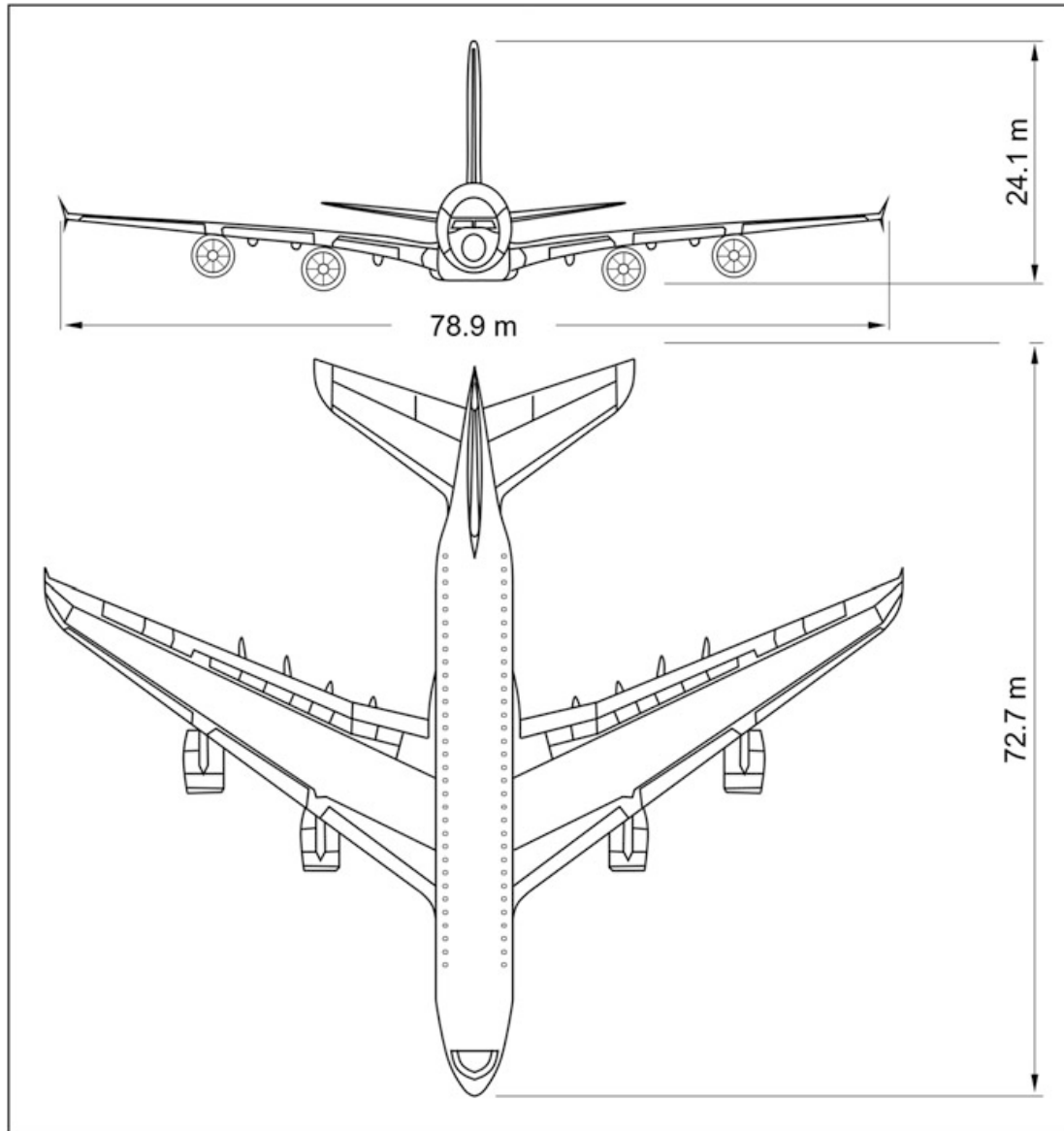
Fig. 3.27 Schematic of the Airbus A380

To complete the picture concerning the perspectives of aluminum alloys, a further alloying element is being considered for improving their structural properties: this is scandium. Scandium ($Z = 21$) is a light metal, having a density of 2.985 g/cm^3, and it is often associated with the group of RE elements, although it is not really part of this group. The early reported results on aluminum-scandium alloys date back to the early 1970s, both in the USA and in the Soviet Union. In 1971, the early Al-Sc alloys were patented. Meanwhile, several studies started at the VILS (All-Russian Institute of Light Alloys), demonstrating that it was possible to produce rather thick ingots of Sc-bearing Al-Mg alloys with non-dendritic structures. Subsequently, the investigations proceeded to assess the potential of these alloys in the aerospace field (Djukanovic 2017; Filatov et al. 2000; Röyset and Ryum 2005). The interest for Sc-containing alloys relies on the improved mechanical properties and processing

Table 3.16 Conventional wrought Al-alloys used for commercial aircraft parts (Polmear 2006; Staley and Lege 1993)

Alloy	Temper	Application	Alloy	Temper	Application
7090	T7E71	Aircraft parts	2024	T3	Fuselage skin
7091	T7E69		7075	T6	
2618	T61	Aircraft parts and structures for high-temperature applications	7475	T6	
2219	T62		7075	T6	Fuselage stringers
2219	T87		7075	T73	
2025	T6	Aircraft propellers, forgings	7475	T76	
6013	T4	Aircraft sheet	7150	T77	
2014	T6	Aircraft structures	6005	T5	General purpose extrusions
2124	T8		6060	T5	General purpose extrusions
2048	T85		6151	T6	Medium-strength forgings
7001	T6		2024	T3	Ribs and spars
7009	T6		7010	T76	
7010	T6		7150	T77	
7049	T73		2017	T4	Screw machine fittings
7050	T736		2011	T6	Screw machine parts
7075	T6		6061	T6	Welded structures
7075	T73		2024	T3	Wing lower panels
7075	T76		7075	T6	
7475	T7651		7175	T73	
7178	T6		2024	T3	Wing lower skin
7055	T7751		7475	T73	
7085	T7651		2024	T3	Wing lower stringers
2024	T4	Aircraft structures and sheets	7075	T6	
2024	T6		2224	T39	
2024	T73	Empennage (tail)	7075	T6	Wing upper skin
7075	T6		7150	T6	
7050	T76		7055	T77	
6063	T6	Extrusions	7075	T6	Wing upper stringers
2024	T6	Fuselage frames/bulkheads	7150	T6	
7075	T6		7055	T77	
7050	T6		7150	T77	

possibilities. In fact, scandium additions determine the highest specific increment of tensile strength in aluminum alloys than any other alloying element. Scandium has also attracted interest because its presence can lead to:

Table 3.17 Tensile properties of selected wrought Al-alloys and relevant tempers, widely used in aircraft structures (Polmear 2006)

Alloy	Temper	Tensile strength [MPa]	Yield strength [MPa]	%Elongation in 50 mm
2011	T6	390	295	17
2014	T6	480	410	13
2017	T4	425	275	22
2618	T61	435	330	10
2219	T62	415	290	10
2219	T87	475	395	10
2024	T4	470	325	20
2024	T6	475	395	10
2124	T8	490	440	8
2025	T6	400	255	19
2048	T85	480	440	10
6005	T5	305	270	12
6060	T5	215	195	17
6063	T6	240	215	12
6061	T6	310	275	12
6151	T6	330	295	17
6013	T4	315	185	25
7001	T6	675	625	9
7009	T6	535	470	12
7010	T6	545	485	12
7049	T73	530	470	11
7050	T736	550	510	11
7075	T6	570	500	11
7075	T73	500	430	13
7075	T76	540	470	12
7475	T7651	590	560	12
7178	T6	610	540	10
7055	T7751	630	610	12
7085	T7651	510	475	7
7090[a]	T7E71	620	580	9
7091[a]	T7E69	590	545	11

[a]Refers to alloys produced via powder metallurgy

- Better quality of welded joints due to the reduction in the incidence of cracks, with a consequent increase, up to 200%, in the fatigue life of the joints.
- Grain refinement during both casting and welding processes.
- Precipitation hardening.
- Recrystallization inhibition.

As concerns recrystallization, its temperature can be as high as 600 °C when scandium is added. This value is definitely above the typical heat treatment

temperatures of aluminum alloys. A better understanding of grain refinement and hardening can be inferred from the Al-Sc phase diagram (see Fig. 3.28), featuring an eutectic on the Al-rich side, at 659 °C and 0.56 wt% scandium. On cooling from the melt a hypereutectic composition, the Al_3Sc intermetallic forms. This phase contributes to the strengthening of the alloy and also to the grain refinement during the solidification process. In fact, the intermetallic grains are preferred nucleation sites for the solidifying alloy, owing to the crystallographic affinity to aluminum. This aspect can be improved by the addition of titanium or zirconium, resulting in the formation of $Al_3(Sc, Ti)$ or $Al_3(Sc, Zr)$ particles, that, as shown by high resolution atom probe investigations, improves the control of the intermetallic formation kinetics, in agreement with the relevant transformation curves in Fig. 3.29 (Röyset and Ryum 2005).

Scandium has been added to non-heat treatable alloys of the 1XXX, 3XXX, 4XXX, and 5XXX series (Röyset and Ryum 2005). The percentage of added scandium goes from 0.1% to 0.45% (Scandium International Mining Corp 2017). The best combination of strength and other structural properties has been obtained with the Al-Mg alloys (5XXX series – Filatov et al. 2000). Thanks to the homogenous, fine-grained microstructure of the alloys, tensile strengths in the 300–450 MPa range are obtained, still retaining a 12–15% elongation, depending on the actual scandium concentration. The fine grain size has also positive effects on the extrusion flow rate (Scandium International Mining Corp 2017). Sc-containing Al-alloys are interesting for aerospace applications, with particular regard to non-treatable alloys, like welded gas tanks, structures for dashboard panels and compartments, fuselage stringers, and large stamped and welded structures (Djukanovic 2017; Röyset and Ryum 2005). The Russian military aircraft MIG 29 has the largest use of Sc-containing Al-alloys so far (Djukanovic 2017; Röyset and Ryum 2005). Airbus Group APWORKS Gmbh, in association with Airbus Group R&D, has developed recently the Scalmalloy®, a high-performance Al-Mg-Sc alloy specifically designed for the production of high-strength aerospace structures via laser powder bed additive manufacturing (see Table 3.18). The result is a material with exceptional high fatigue strength and specific strength approaching that of titanium alloys (APWORKS 2017; Djukanovic 2017).

It has been estimated that the use of high-strength Sc-containing alloys in aircrafts would afford a 10–15% weight reduction (Djukanovic 2017). Unfortunately, the extremely high cost of scandium (now higher than 2000 USD/kg) and its relatively low abundance and the relevant extraction difficulties (Djukanovic 2017) seem to be an important obstacle to a widespread application of this element, unless novel extraction technologies will maintain their improvement promises (Röyset and Ryum 2005). One approach is based on using, as raw material, ScO_3 from the "red mud" coming from the Bayer process (see Sect. 3.2.1). Alternatively, ScO_3 may be reduced directly in the liquid aluminum alloy. In this way the production cost is cut by one order of magnitude approximately (Röyset and Ryum 2005). Sc-containing alloys already on the market are the 1460, 2023, 5024, and 5025 (for full composition see Table 3.5 and Appendix 1). Other alloys, whose designation is not present in the IADS, are 1515 and 1570 (5XXX series; 0.30–0.50% and 0.15–0.35% Sc, respectively) and 1970 (7XXX series; 0.25% Sc).
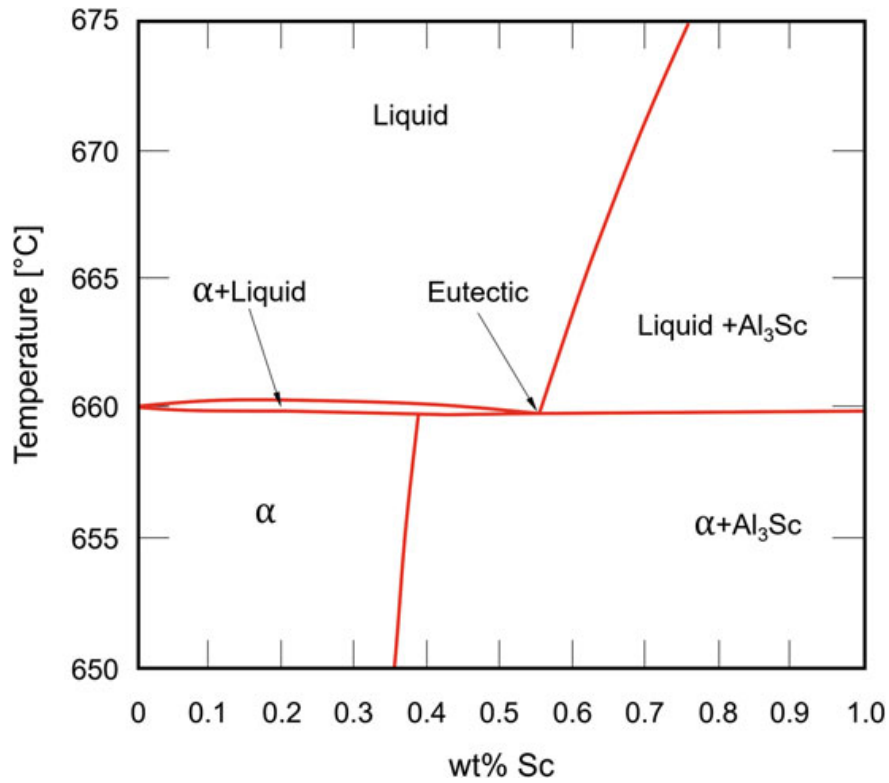
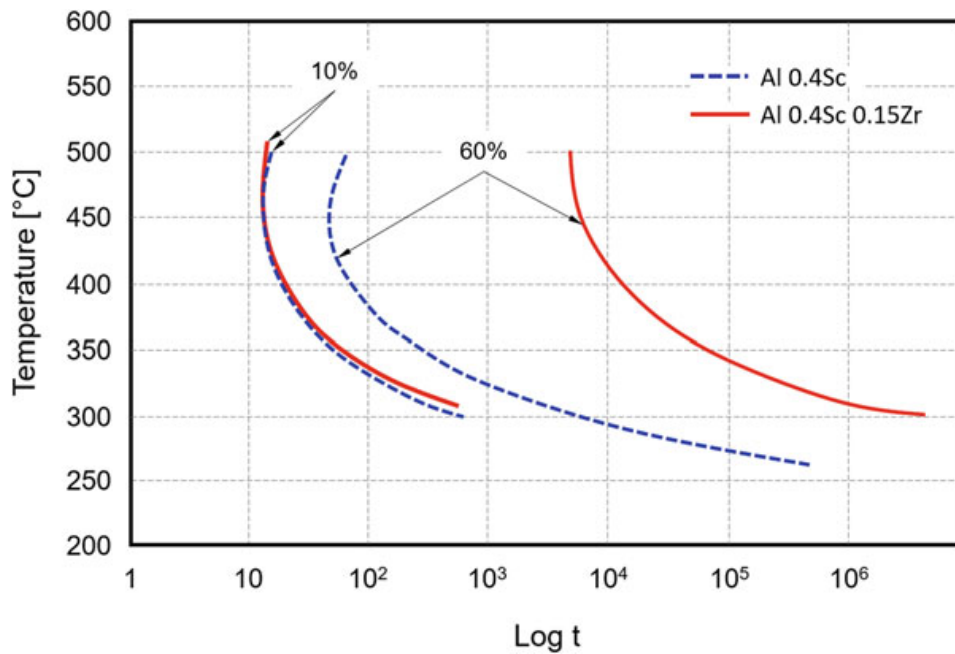**Fig. 3.28** Al-rich part of the Al-Sc phase diagram. (Redrawn from Röyset and Ryum 2005)

Fig. 3.29 Transformation curves for the formation of the intermetallic phases in Al-0.4Sc and Al-0.4Sc-0.15Zr (see main text for details). In the plot, the completion percentage of the transformation is also indicated. (Redrawn from Röyset and Ryum 2005)

Table 3.18 Typical mechanical properties of Scalmalloy[®]

Density [g/cm^3]	Young's modulus [GPa]	Ultimate tensile strength [MPa]	Yield strength [MPa]	% Elongation	Hardness vickers (HV 0.3)
2.67	70	520	470	13.0	180

Values are obtained according to the DIN EN ISO 2002-001 standard and measured from specimens that have been heat treated and machined. Values are typical of products obtained via ALM (Additive Layer Manufacturing) and are measured in the least strong direction (APWORKS 2017)

3.3   Magnesium Alloys

3.3.1   Introduction

Magnesium (atomic number $Z = 12$) is in the second group, third period of the periodic table. It is characterized by a density of 1.738 g/cm^3 and a Young's modulus of 45 GPa. Magnesium has several applications in the modern industry (e.g., steelmaking processes, Kroll's process for titanium extraction and alloying element in Al-alloys), and it is also an interesting metal for aerospace applications. Although aluminum and its alloys are holding a leading role in aerospace structures, this has not always been the case. Indeed, magnesium can be regarded as the less dense of the metals interesting for structural applications, leaving aside lithium and beryllium, not suited for bulk structural uses. The name magnesium derives from the Greek name *Magnesia*, a district of Thessaly, a traditional geographic and modern region of Greece (Davy 1808; Perkguleryuz et al. 2013). The existence of elemental magnesium was first claimed in 1755 by Joseph Black, who pointed out that magnesia mineral (MgO) contained a new element that, unfortunately, he was not able to isolate. In the past, magnesia was known as *white earth* or *white stone*. Magnesium was discovered by Sir Humphry Davy in 1775 (Davy also discovered aluminum, see Sect. 3.2.1). Sir Davy also suggested the name *magnium* for the metal, but magnesium was adopted instead. First extraction of the metal by Davy occurred in 1808, thanks to the electrolysis of moistened magnesium sulfate. A mercury cathode was employed in the process. The resulting product was a magnesium amalgam, from which magnesium was distilled by removing mercury. In 1828, Antoine Alexandre Brutus Bussy was able to isolate magnesium thanks to the fusion of dehydrated $MgCl_2$ with potassium at high temperature. Some years later, in 1833, Michael Faraday obtained metallic magnesium from the electrolysis of impure magnesium chloride in a molten state. However, it took two more decades to achieve production capabilities of commercially relevant quantities of metallic magnesium. The first who achieved this result was Robert Bunsen, who obtained pure magnesium using a small laboratory cell starting from anhydrous $MgCl_2$. At the beginning of its history, magnesium found considerable interest in Germany only, that in 1868 was the only producer in the world. The application of magnesium was not focused on structural components but on the production of powder for flash-lights and fireworks. Industrial production of magnesium started around the late 1920s in several countries.

Magnesium Elektron, a still existing company, was founded in 1934 and started its production 2 years later, using magnesia coming from Greece as raw material. However, when World War II was about to start, magnesia was directly extracted from seawater. In Italy, the SAMIS company built a production plant in Sardinia in 1935. The first owner was very much related to the aerospace field. His name was Giovanni Caproni regarded as one of the originators of the newborn Italian aircraft industry. In 1939 the production of magnesium also started in Bolzano, a town located in the Dolomites in the northern part of Italy. The plant was owned by the company Società Magnesio e Leghe di Magnesio. One interesting peculiarity of the Bolzano plant was its silicothermic production process, named Bolzano process (Horst and Mordike 2006; Perkguleryuz et al. 2013).

Magnesium is one of the most common elements on the Earth: according to the estimated total abundance, it is in the fourth place, after iron, oxygen, and silicon. Magnesium occupies the eighth position in the list of the most abundant elements in the Earth's crust (lithosphere), considering its actual availability to mining and extraction processes, using the so-called Clarke number. This is the concentration of each element referred to a surface crustal layer, and although magnesium is preceded by metals like iron and aluminum, it still has a larger Clarke number than other strategic raw materials, like nickel, chromium, and so on (Parker 1967). Furthermore, magnesium is the second most abundant metal in seawater, the first being sodium (Perkguleryuz et al. 2013). Primary magnesium can be extracted from very common carbonate ores, like magnesite ($MgCO_3$) and dolomite ($CaCO_3 \cdot MgCO_3$). In other words, the availability of magnesium as raw material seems not to be an issue, even in view of future developments and increase in the production. The extraction metallurgy of metallic magnesium is based on two main processes: electrolysis and thermal reduction of the ores.

The extraction of magnesium requires a relatively high energy consumption for the strong chemical bonds it has with other elements in the ores. From the 1970s to the 1990s, the production of Mg was primarily performed according to the electrolytic route (Table 3.19). Since the chemical reaction that takes place during the electrolytic process is a redox process, it can be considered as made of two semi-reactions, the cathodic and the anodic one (see Chap. 8). The electrolytic route for the production of magnesium is well established for both $MgCl_2$ coming from traditional raw materials (see Table 3.19) and for the recycled molten anhydrous magnesium chloride deriving from the Kroll's process used for the extraction of titanium (see Sect. 4.1). A few details on the thermal reduction of magnesium ores and major process parameters are given in Table 3.20.

As concerns the silicothermic extraction process, it is based on two main approaches: the Bolzano process and the Pidgeon process. In both cases, silicon coming from a ferroalloy, named ferrosilicon (FeSi), is used as reducing agent. This same agent is used for steel deoxidation and in the reduction stage during the steel conversion process (see Sect. 5.3) (Gasik 2013). The Bolzano process, using dolomite as raw material, was initiated by Edoardo Ravelli, who industrialized it on the basis of the silicothermic reduction process developed by Amati in 1938 at the University of Padua (Italy). The plant, based in Bolzano (Italy, from which the name

Table 3.19 Electrolytic processes for the production of magnesium

Process	Raw material	Raw material preparation	Chemical reactions involved	Temperature [°C]	Pressure [kPa]
AM	Magnesite	Mining, leaching with HCl, dehydration	Cathode semi-reaction $2Cl^- \rightarrow Cl_2 + 2e^-$ Anode semi-reaction $Mg^{2+} + 2e^- \rightarrow Mg$ Global redox reaction $MgCl_{2(l)} \rightarrow Mg_{(l)} + Cl_{2(g)}$	700–800	101.325
Dow	Seawater/ desalination brine	Neutralization, purification, dehydration			
IG Farben		Neutralization, prilling, dehydration chlorination			

AM indicates a process based on the chlorination of MgO obtained from thermal decomposition of magnesite ($MgCO_3$). In the IG Farben process, the dehydration step is optimized by prilling (Wulandari et al. 2010)

of the process comes), used ferrosilicon to reduce calcined dolomite. The production reached a peak in 1981 with 10,700 metric tons and continued until the closing down of the plant in 1992, when the costs of magnesium production became too high, thus not profitable any longer. In the Bolzano process, still used in Brazil by a company named Bramag, dolomite undergoes a calcination first, and it is then mixed and compacted with the ferrosilicon reduction agent. Bauxite may be employed as an additive in the process. The resulting material is prepared in the form of large blocks that are connected to the electric-heating conductors. Thanks to this particular design, the blocks only are heated up, thus avoiding heat dispersion over the entire furnace. The process is carried out at a pressure of about 0.4 kPa and at a temperature of 1200 °C, a relatively low value if compared to the typical values for non-silicothermic-based processes (Table 3.20), so that also the energy consumption is comparatively lower with respect to other thermal reduction processes. The alternative silicothermic extraction process for magnesium, i.e., the Pidgeon process, was developed by Lloyd Montgomery Pidgeon in the late 1940s. The reduction of dolomite, like in the Bolzano process, is carried out in a reactor using ferrosilicon. The process uses a furnace (retort) in which a briquetted mixture of ferrosilicon and calcined dolomite powder are heated in order to obtain the reduction of magnesium oxide coming from the carbonate decomposition. High-purity magnesium is produced and then remelted and cast in form of ingots. The process is carried out at a temperature of about 1500 °C, thus higher than that of the Bolzano process, and over a pressure range of 0.013–0.4 kPa. The retort can be coal-fired, gas-fired, or electrically heated (Horst and Mordike 2006). Notwithstanding specific differences, all magnesium extraction processes can be traced back to the same main functional stages, according to the schematic in Fig. 3.30.

Magnesium has a hexagonal close-packed (*hcp*) structure, whose limited number of slip systems (three slip systems) renders this metal and its alloys intrinsically difficult to be deformed, definitely more difficult than austenitic *fcc* alloys.

Table 3.20 Processes involving thermal reduction of Mg-containing ores (Horst and Mordike 2006; Wulandari et al. 2010)

Process	Raw materials	Raw material preparation	Main chemical reactions involved	Temperature [°C]	Pressure [kPa]
Aluminothermic	Dolomite, Al scrap	Calcination	$4MgO + 2Al \rightarrow 3Mg + MgAl_2O_4$	1700	86.126–101.325
Carbothermic	Magnesite, carbon	Calcination and pelleting	$MgO + C \rightarrow Mg + CO$	1700	101.325
Magnetherm	Dolomite, bauxite, FeSi	Calcination and FeSi formation	$2CaO \cdot MgO + (xFe)$ $Si + nAl_2O_3 \rightarrow 2CaO \cdot SiO_2 \cdot nAl_2O_3 + 2Mg + xFe$	1550	5.066
Mintek	Dolomite, bauxite, FeSi, Al scrap	Calcination	$2CaO \cdot MgO + (xFe)$ $Si + nAl_2O_3 \rightarrow 2CaO \cdot SiO_2 \cdot nAl_2O_3 + 2Mg + xFe$ $4MgO + 2Al \rightarrow 3Mg + MgAl_2O_4$	1700	86.126
Silicothermic	Dolomite, FeSi	Calcination, FeSi formation, pelleting	$MgO + CaO + FeSi \rightarrow Mg + Ca_2SiO + Fe$	1160–1500	0.013–0.4
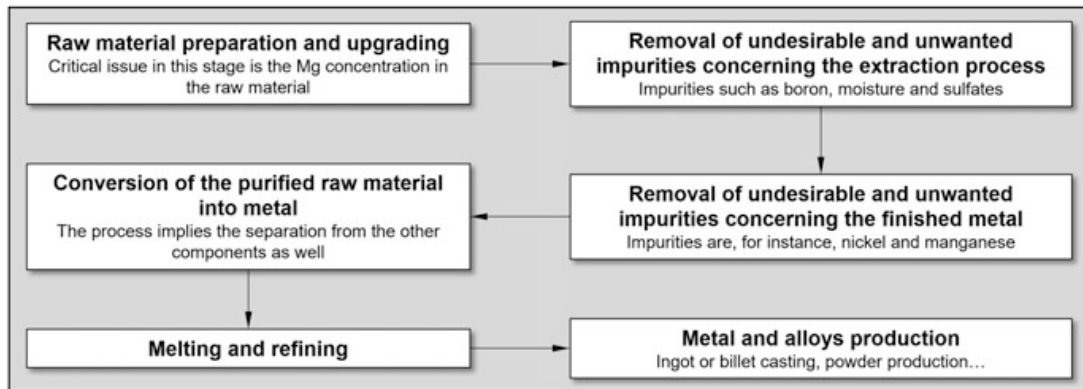
Fig. 3.30 Flowchart for a general magnesium production process (Perkguleryuz et al. 2013)

Table 3.21 A comparison among properties of key elements for structural alloys, including magnesium

Property	Mg	Al	Ti	Fe
Density [g/cm^3]	1.74	2.70	4.51	7.87
Melting T [°C]	650	660	1670	1538
Boiling T [°C]	1105	2470	3287	2862
Thermal conductivity (RT) [W/ °C · m]	160	235	22	80
Specific heat (RT) [J/kg °C]	1025	904	520	449
Young's modulus [GPa]	45	70	120	210
UTS [MPa]	90	98	150	275

UTS indicates the ultimate tensile strength (Donachie 2000; Pepperhoff and Acet 2001; Perkguleryuz et al. 2013)

Table 3.21 gives some properties of this metal, as compared with the same properties of other key metals: aluminum, titanium, and iron. The low density of magnesium stimulated the interest for this metal in the early days of the aerospace industry.

Starting from the military field, the first important example of the use of Mg-alloys in aeronautic structures was probably the prototype concept of all-magnesium aircraft, the Northrop XP-56, the so-called Black Bullet. It was tested in experimental flights in the latest years of World War II. The Black Bullet was important, since it demonstrated the real potentials of Mg-alloys in aircraft structures. Another full magnesium structure was there in the Lockheed F-80C. Magnesium and its alloys started to be used in large military transportation airplanes, like the Convair B-36, with a total amount of 8600 kg of magnesium, of which about 5600 kg of magnesium sheet and 700 kg of forged parts and 300 kg of castings (Ostrovsky and Henn 2007). Another notable example of application of Mg-alloys to aircraft structures is the Convair XC 99, which serviced from 1949 until 1957, and is considered as the first double-deck airliner. This airplane had several components of the structure and fuselage skin made of Mg-alloys. The exceptional payload and passenger capacity (i.e., 400 fully equipped troupes), allowed by the double-deck design, rendered this aircraft particularly attractive also for civil and commercial
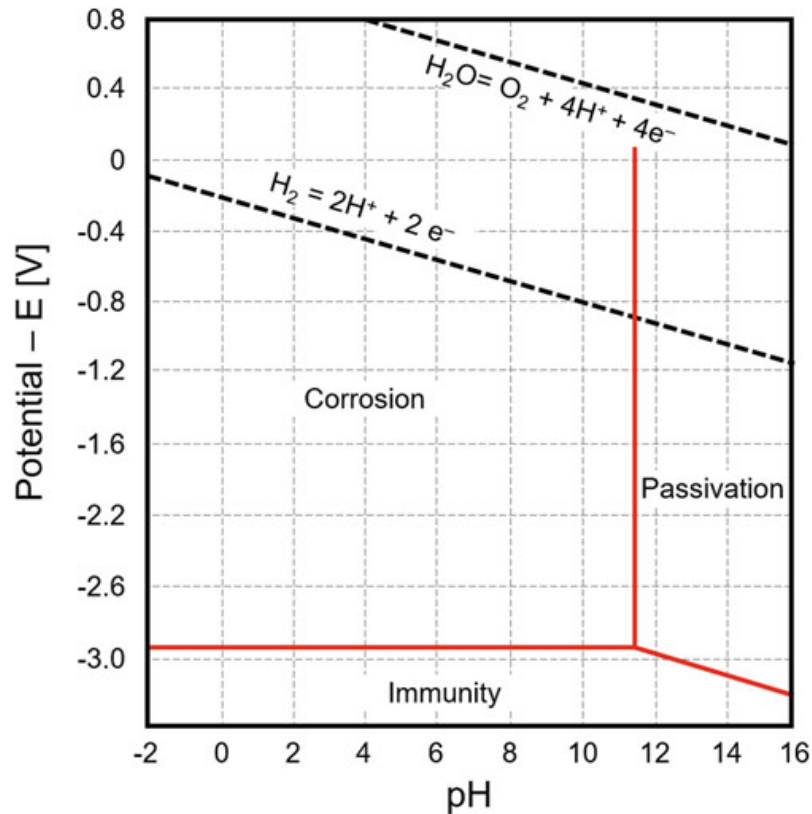
Fig. 3.31 Pourbaix diagram of pure magnesium. (Redrawn from ASM International 2003)

purposes. In fact, Pan Am ordered 15 of these aircrafts for its fleet, although no one of them was delivered and never started its service, because the program was first suspended and then cancelled. Among the reasons for this change of plans, there were the emerging limitations and critical aspects exhibited by magnesium alloys available at the time, particularly as concerns their surface durability.

The poor corrosion resistance is particularly evident when analyzing the Pourbaix diagram of pure Mg in aqueous environment (Fig. 3.31), where corrosion takes place over a wide range of pH and potential. Since it was not an issue in the military field, this feature was initially overlooked, although it emerged soon as an important aspect for commercial fleets in terms of reliability and costs associated with maintenance and repair. These aspects and the contemporary rapid, solid evolution of new aluminum alloys determined the progressive abandon of magnesium in air transportation. Quite different was the situation in the Soviet Union, where military aircraft structures were systematically used for prototyping solutions to be used for civil transportation purposes, with the possibility of faster development and validation loops for new materials. The Boeing 737 (produced since 1967) features an extremely limited number of magnesium components, summing up to a total weight of a few tens of kilograms, much lower if compared to the Tupolev TU-134,
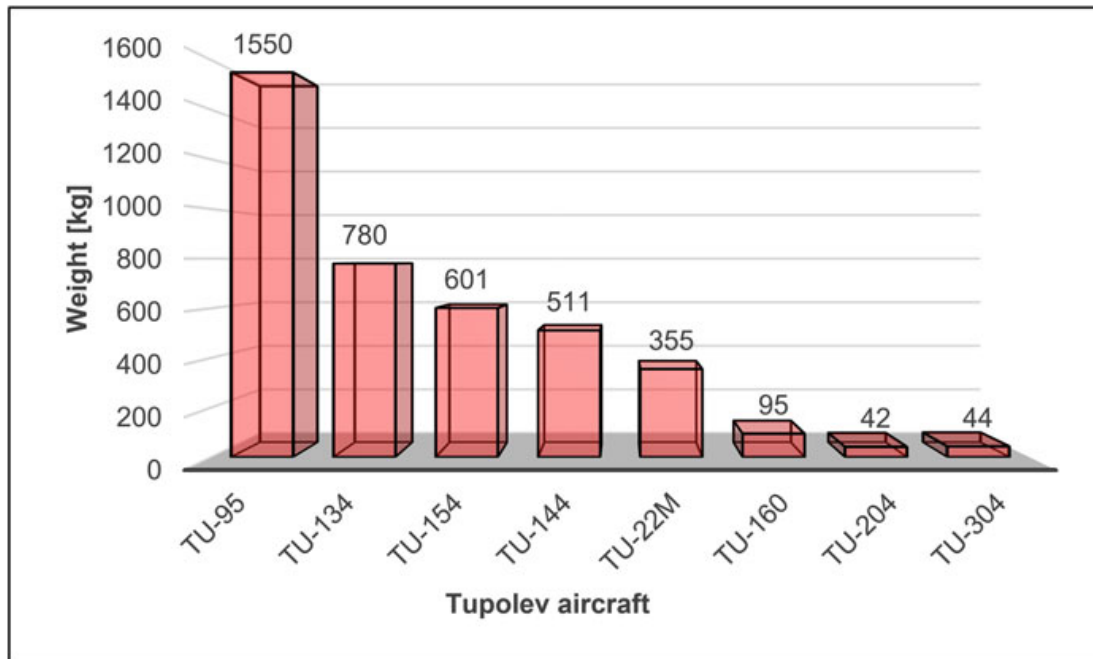
Fig. 3.32 Evolution of the weight of magnesium used for the different models of Tupolev planes, developed over the years (Gupta and Gupta 2017; Ostrovsky and Henn 2007)

developed over the same years (early production date 1963). In this case, the components made of magnesium alloys had a total weight of 780 kg. The Tupolev planes can be taken as important witnesses of the use of magnesium alloys for civilian air transportation. After the golden years for magnesium, 1960s and 1970s, a progressive reduction has been observed also in the Soviet Union, as can be seen in Fig. 3.32, referring to the use of magnesium in Tupolev airplanes. The situation in Russia in the 1990s was substantially similar to that of the Western aerospace industry, whose main players never used magnesium in their commercial and passenger airplanes intensively. The same is not true for helicopters, for which magnesium is a standard choice for gearboxes, transmission between engine and rotor, and other components, mainly nonstructural. In this case, weight saving is a decisive selection parameter. The comparatively limited applications of magnesium in aeronautic structures, if compared to aluminum alloys and notwithstanding the interesting properties and potential of this class of materials, can be ascribed to a set of concurrent reasons, in addition to the already mentioned poor corrosion resistance. The elevated oxidation kinetics, resembling combustion under particular conditions, has been obviously regarded as a negative issue in applications for which safety and reliability are paramount, although the magnesium combustion issue is to be regarded as an example of misconception. In real terms, combustion may become an actual risk for magnesium powder samples only and requiring some precautions in handling, for instance, scraps from machining of magnesium parts.

All commercial magnesium alloys are compliant and fully certified as concerns the resistance to ignition, although limitations to their use in specific components have been imposed, owing to the strict safety standards and legislation adopted for aerospace products. However, in recent times, a ban on the use of magnesium alloys for aircraft seats has been lifted, once the presumed flammability risk of candidate magnesium alloys has been ruled out with lab size and full-scale experiments (Marker 2013; Nature Materials 2016).

In addition to the limited corrosion resistance, the inadequate mechanical strength was identified as another key property to be improved in order to enable a wider use of magnesium alloys also in the aerospace industry. The important research efforts resulted in the developments of the main classes of alloys, described in the following with regard to specific aerospace applications. As concerns processing, casting appeared from the beginning as the obvious choice, considering the comparatively low-melting temperature of magnesium and its low latent heat of fusion, which renders solidification and cooling rather fast. The role of casting techniques was strengthened further by the intrinsically low deformability of magnesium for its limited number of slip systems. The development of more ductile alloys with novel compositions has incremented the number of wrought magnesium alloys available on the market. In this regard, the mechanical properties achieved by the state-of-the-art magnesium alloys, like the high-strength Elektron 21 and Elektron 675 materials, make them potential valid replacements for aluminum alloys, laminate, and polymer matrix composites in aeronautic structures (Lyon et al. 2007). This trend is encouraged by the always standing issue of the weight reduction, that is, nowadays considered also for the important beneficial effects, concerning fuel saving and consequent reduction of environmental pollution (see Chap. 2). Since the 1990s, there has been renewed interest in magnesium alloys for weight-sensitive applications, including the aerospace field. At the beginning of that period, there were a few commercial magnesium alloys systems: Mg-Al, Mg-Al-Zn, Mg-Zn-RE, and Mg-REs. Most magnesium alloys usage for structural applications was in die-casting, and a single alloy (AZ91D) accounted for around the 90% of the total market. A clear indication of the increasing, renewed interest for magnesium can be also inferred by the growing trend of magnesium production, started in the early 1990s, under the incisive drive by China, that is holding nowadays 80% of the global supply of this element (see the historical development in Fig. 3.33). When China entered the global economy in the early 1990s, it made magnesium one of the fundamental items of the raw materials and metallurgy industry portfolio. The base approach is the silicothermic Pidgeon production process, facilitated by the large availability of low-cost ferrosilicon and using coal as main heat source. This evolution has probably fostered the interest in magnesium also in the rest of the world, particularly as concerns its use in civilian transportation, as reported, for instance, in the research documents by the European Community AEROMAG program for the aerospace application of magnesium alloys (Perkguleryuz et al. 2013).
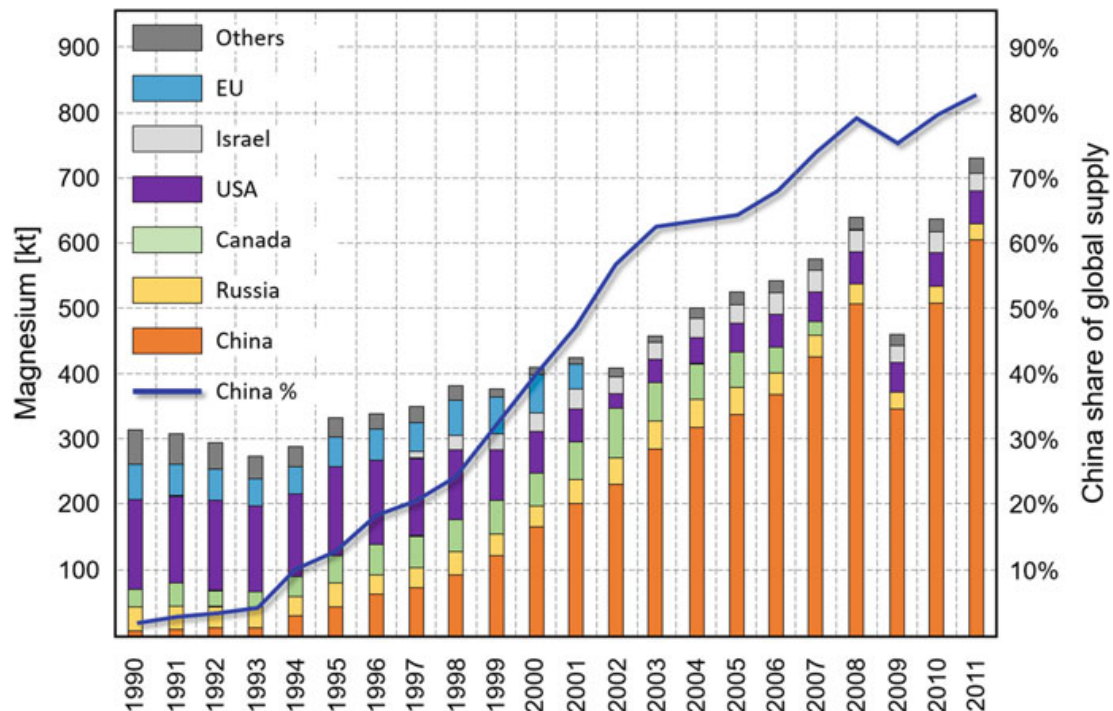
Fig. 3.33 The global magnesium industry in 2011. Quantities are expressed in thousands of metric tons. (Redrawn from The CM Group 2012)

3.3.2 Aerospace Magnesium Alloys: Metallurgy, Main Designation System, and Tempers

The ASTM (American Society for Testing and Materials) international designation system is the most widely accepted for both cast and wrought magnesium alloys, although it is not the only one, being a possible alternative of the so-called British system. The alphabetic part of the alloy name refers to the main alloying elements, according to the symbols listed in Table 3.22. The first digit of the code represents the rounded off concentration (in wt%) of the majority alloying element, identified by the first letter. The second figure corresponds to the concentration of the second element and so on. Additional letters, following the concentration reference numbers, represent possible modifications to the same alloy material. Some discrepancies are there, but it is not difficult to sort them out and identify the actual alloy product, also thanks to the conspicuous available literature on this matter (Cahn et al. 2005; Cardarelli 2008).

The AZ91 code indicates the Mg-9Al-1Zn cast alloy, with the relevant composition range and minority elements indicated in Table 3.23. The ZMC711 indicates the wrought alloy with composition: for Zn-6.5-Mn 0.75-Cu-1.25 (Polmear 2006). Therefore, there is no specific differentiation between the cast and wrought products, as seen instead for aluminum alloys. Other magnesium alloys are simply identified by the relevant trademark, like the Elektron alloys produced by Magnesium Elektron, and codenamed using a reference number, like the Elektron 21 alloy. A

Table 3.22 ASTM designation code for the main classes of magnesium alloys (ASM International 1991)

Code letter	Alloying element	Code letter	Alloying element
A	Aluminum	M	Manganese
B	Bismuth	N	Nickel
C	Copper	P	Lead
D	Cadmium	Q	Silver
E	Rare earths	R	Chromium
F	Iron	S	Silicon
G	Magnesium	T	Tin
H	Thorium	W	Yttrium
K	Zirconium	Y	Antimony
L	Lithium	Z	Zinc

Table 3.23 Chemical composition of some magnesium alloys

Alloy	Al	Mn	Th	Zn	Zr	Other elements
AM50	5.0	0.30	–	–	–	–
AZ31	3.0	0.20	–	1.0	–	–
AZ61	6.5	0.15	–	1.0	–	–
AZ81	7.0–8.0	0.13–0.35	–	0.40–1.0	–	Be = 0.0008 max
AZ91	8.1–9.2	0.17–0.35	–	0.40–1.0	–	–
AZ91E	9.0	0.10	–	0.50	–	–
AZ92	8.3–9.7	0.15–0.50	–	1.7–2.3	–	Be = 0.0008 max
AZ92A	9.0	0.10	–	2.0	–	–
ELECTRON 675	General chemical composition is property of Magnesium Elektron					
ELEKTRON 21	–	–	–	0.50	0.20–0.50	Gd = 1.0–1.7 Nd = 2.6–3.1
EZ33	–	–	–	2.0–3.0	0.50–1.0	RE = 2.5–4.0
EZ33A	–	–	–	2.0–3.0	0.40–1.0	RE = 2.5–4.0
HK31	3.0	–	3.25	0.30	0.70	–
HM21	–	0.45	2.0	–	–	–
LA141	1.0	–	–	–	–	Li = 14.0
LS141A	0.50–0.80	–	–	–	–	Li = 13–15
QE22	–	–	–	–	0.40–1.0	Ag = 2.0–2.7 RE = 2.0–3.0
WE43A	–	–	–	–	0.70	RE = 3.4; Y = 4.0
WE54	–	–	–	–	0.50	Ag = 5.25 Nd = 3.5
ZE41	–	–	–	4.2	–	RE = 1.2
ZE63	–	–	–	5.5–6.0	0.40–1.0	Cu = 0.10 max Nd = 2.1–3.0
ZK60	–	–	–	5.5	0.45	–
ZMC711	–	0.75	–	6.5	–	Cu = 1.25

Chemical compositions can slightly change according to the type of product (i.e., sheets, forgings, extrusions) (ASM International 1991; Czerwinski 2011; Magnesium Elektron 2012; Magnesium Elektron 2014, 2015; Perkguleryuz et al. 2013; Polmear et al. 2017; Prasad and Wanhill 2017)
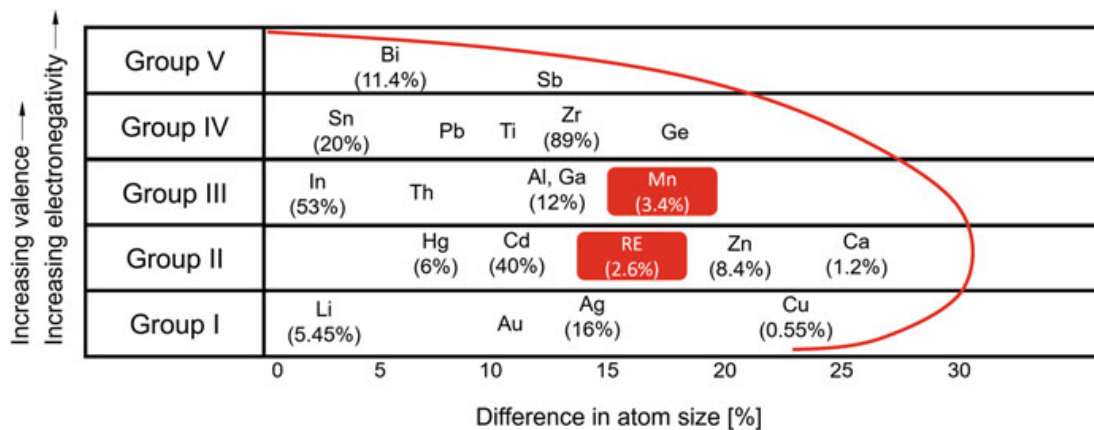
Fig. 3.34 Alloying behavior of magnesium. Values among brackets are the solid solubility limits of the element in Mg. (Redrawn from Pekguleryuz et al. 2013)

list of some of the most common magnesium alloys is given in Table 3.23, including their compositions.

The compositions of the magnesium alloys are designed according to the standard physical metallurgy principles for the formation of solid solutions and intermetallic phases, aiming at the optimization of the structural properties and corrosion resistance under different operating conditions. The graph in Fig. 3.34 shows how atomic size, electronegativity, and valence influence the solid solubility of several elements in magnesium, providing different effects, as specified in Appendix 3. Elements to the left of the curve have at least 0.5% maximum solid solubility in magnesium. The highest solubility belongs to those elements showing favorable size factor and valence, meaning a low difference in atom size and a valence equal to 2 or 3. Considerable solid solution strengthening occurs at around 12–15% size factor values, for instance, with Al, REs, and Zn. When Hume-Rothery rules are not satisfied, second phase formation occurs (Perkguleryuz et al. 2013). An important difference with respect to the tempers of Al-alloys is that the equilibrium phases foreseen by the relevant phase diagrams are not to be regarded as detrimental, as in the case of overaged aluminum alloy, but absolutely beneficial, being important strengthening agents. The equilibrium phases that are interesting as concerns precipitation hardening of magnesium alloys belong to three main intermetallic types. The first is the simple cubic CsCl structure such as that of MgTl, MgAg, CeMg, and SnMg. The second is that of the Laves phases, with an AB_2 stoichiometry like $MgCu_2$, $MgZn_2$, and $MgNi_2$, each featuring a different stacking sequence of the closest packed planes. Finally, the third type is that of the compounds with the antifluorite structure, like Mg_2Si, and with the fluorite structure, like Mg_2Sn. The equilibrium phases used as strengthening agents demonstrate the intrinsic stability of the alloy conditions induced by treatments in these alloys.

The equilibrium intermetallic phases are important in magnesium alloys also for their beneficial effect on creep resistance and for hindering alloy recrystallization (Pekguleryuz et al. 2013). Concerning the heat treatments of Mg-alloys, the temper condition is indicated in the alloy designation code, according to the specifications

Table 3.24 Designation letters of the main tempers for magnesium alloys (ASM International 1991; Pekguleryuz et al. 2013)

Code	Temper description	Details
F	As-fabricated	–
O	Annealed	–
H	Strain hardened	H1: strain-hardened only
		H2: strain-hardened and partially annealed
		H3: strain-hardened and stabilized
		The number following the letter H indicates the degree of strain hardening remaining in the alloy. Additional digits (H2X) indicate a subdivision of the H tempers giving information about the final degree of strain hardening between 0 (annealed) and 8 (totally hard)
T	Tempered	T4: solution heat treatment
		T5: artificial age hardening
		T6: solution heat treatment followed by artificial aging
		T7: solution heat treatment and subsequent stabilization
		T8: solution heat treatment, cold working, and artificial aging
W	Solution heat treated	–

contained in Table 3.24 with the main temper treatments for magnesium alloys. Those more commonly used for aerospace alloys are the T4 (solution-treated alloy), T5 (direct cooling and artificially aged), and T6 (solution-treated and artificially aged) (Eswara Prasad and Wanhill 2017).

3.3.3 Magnesium Alloy Processing

The alloy design and development have essentially concerned cast products, which still cover the majority of magnesium alloy production, notwithstanding the continuous progress in the development of deformable alloys, as discussed in the next section. Casting, using different techniques, with some restrictions and recommendations determined by the target grade and by other properties required by specific applications, is still the most flexible processing route for magnesium alloys. The main casting methods that are used for processing magnesium alloy parts are:

- Investment and die-casting.
- Permanent and semi-permanent mold casting.
- Sand casting.

A full description of these technologies, specifically applied to magnesium and its alloys, can be found in Polmear (2006), in the *ASM Specialty Handbook: Magnesium and Magnesium Alloys* (1999) and in the *ASM Handbook: Volume 15 – Casting* (2008). Wrought magnesium alloys, featuring in general better mechanical properties than cast alloys, although more challenging to be produced for the objective

difficulties concerning their formability and therefore production costs, are gaining increasing importance. In fact, the possibility of using magnesium alloys as wrought products is paramount to sustain the general tendency to increase further the overall volume of magnesium products. As concerns aerospace applications, with particular regard to civil and commercial aircrafts, it is clear that the enhancement in the workability of magnesium alloys is a necessary step forward to widen the possibilities of these alloys in this field. Considering the standard parts of a commercial airliner, like the B757, it turns out that only 1% in weight are castings, whereas worked parts are the majority: 28% extruded components, 20% sheets, 18% forgings, 16% plates, and 13% bars (Kettner et al. 2007). The interesting aspect is that the main materials of which magnesium alloys are potential replacements, aluminum alloys and structural composites, sum up in this case to 78% and 3%, respectively, which is an extremely large volume. Continuous research efforts, backed by industrial and scientific projects, are actively working to find reliable solutions to this strategic issue. The EU project AEROMAG (6th Framework Program of the European Commission 2005) can be regarded as an interesting example of this challenge. The program was aimed at developing new magnesium wrought products (sheets and extrusions), particularly for aerospace structures and components, with excellent static strength and fatigue resistance. The benchmarks for these novel materials were two aluminum alloys: 5038 for nonstructural applications and 2024 for secondary structures. The three independent slip systems of the *hcp* Mg crystallographic structure are not sufficient to guarantee the homogeneous polycrystalline plastic deformation, since, according to the von Mises criterion, at least five of these slip systems are necessary (Hosford 2010). To overcome this intrinsic obstacle, higher temperatures are required to achieve adequate workability. Accordingly, temperatures close to 300 °C are absolutely recommended, and, indeed, magnesium alloys used in the aircraft industry are mechanically formed over a temperature range between 290 and 450 °C (Davis et al. 2007). Similarly, to make the process more effective, accurate, and fast, a preliminary heating up of the working tools at temperatures ranging from 250 to 350 °C is adopted, if necessary. In general, these temperatures are kept constant during the entire process, which is thus conducted under nearly isothermal conditions.

3.3.4   Development of Aerospace Magnesium Alloys

As seen, magnesium alloys experienced an alternating interest in the field of aerospace applications since the beginning of the aerospace era. Early compositions showed, in fact, several features that, in the long run, limited their application in aircraft structures. The main development lines of these alloys have been focused on the improvement of the following properties:

- Corrosion resistance, that in the early formulations was relatively poor.

- High-temperature creep resistance, a property that is particularly interesting for the relatively high-temperature applications of magnesium alloys, ranging from 150 up to 350 °C.
- Strength and elongation (Pekguleryuz and Celikin 2010).

A galvanic attack (see Sect. 8.1) is often observed at the contact region of a magnesium alloy part with dissimilar alloys. Heavy metals, reaching the magnesium surface from atmospheric deposition, may produce a generalized pitting attack, due to a localized galvanic coupling (Esmaily et al. 2017). The protection of the alloy surface by suitable coating systems, namely, synthetic and electrical insulating ones, is probably the most effective and practical strategy. Corrosion failures are usually associated with internal or surface contamination. In the first case, copper, iron, and nickel contamination can be introduced during casting operations. Another internal contamination phenomenon can be due to the inclusions coming from salt fluxing employed during casting and recycling operations. On the other side, concerning surface contamination, blast residues can have detrimental effects on the corrosion resistance of the material. These residues would typically come from blasting operations, used for improving the surface uniformity and appearance (Horst and Mordike 2006). In this case, a twofold corrosion protection strategy can be implemented: firstly, through the removal of the surface contaminants by surface treatments (e.g., chemical etching and sand blasting), possibly in association with the deposition of protective coatings. Secondly, a better control of the processing conditions, particularly during casting operations, will reduce the occurrence of contaminants and impurities automatically. The improvement in the alloy grade has generally resulted in better performing materials, also as concerns corrosion resistance. Of course, the search for better magnesium alloys, in terms of corrosion resistance, has been also the opportunity for developing novel coating systems and surface treatments. The surface protection strategies developed for these alloys are based on:

- Anodizing.
- Cold-spraying deposition.
- Conversion coatings.
- Electrochemical plating.
- Gas-phase deposition.
- Laser surface alloying and/or cladding.
- Organic coatings and paints.
- Plasma gel coatings.

Organic and composite coatings have also been specifically designed for aerospace industry and then transferred to other fields of applications. These coatings, being directly exposed to external conditions and undergoing structural and chemical evolution under environmental and operating conditions, are prone to release degradation products. Of course, also for organic coatings, the weight issue is important. Therefore, single rather than multiple layers are preferable. Possible

alternatives are the wet methods, like conversion coatings, electrochemical plating, anodizing treatments, etc. (Blawert et al. 2006).

They are in general less expensive than advanced organic coatings, although still requiring particular precautions for the presence in their formulations of chromates and cyanides, both toxic to the environment and human health. In this regard, dry methods, using thermal spraying, laser melting, physical and chemical vapor deposition, and solid diffusion, are certainly more appealing. The best choice, as usual, is a trade-off of several factors, including the costs of the infrastructures and consumables. Considering the complexity of the requirements and conditions, composite coatings, like the Gardobond® coating, and surface treatments, like PGA ALGAN 2M, are attracting specific research interests in this field (Ostrovsky and Henn 2007). These coatings would not only make magnesium alloys as stable as aluminum but provide also an excellent surface finish for subsequent application of paints for an improvement of the surface barrier effect and also for decorative purposes.

In the aerospace industry, the first magnesium alloys that were developed contained Al, Mn, and Zn. AZ81, AZ91, and AZ92 are important early representatives of this group (Table 3.23). Referring the reader to Appendix 3 for a complete description of role of alloying elements, it is herewith reminded, as concerns these important aerospace alloys, that aluminum has positive effects on the mechanical properties of the alloy, enhancing its ultimate strength. Furthermore, aluminum improves creep resistance and the mechanical properties at elevated temperatures. Zinc has a strengthening effect too, although it is also important for the grain refinement, in particular, by preventing excessive grain growth during solidification and cooling. Zinc-containing alloys also show improved workability, quite a critical issue for these alloys. Zinc is generally associated to manganese. This latter element, in addition to the enhancement of the creep resistance of the alloy, has a central role in improving its corrosion resistance. It is now clear that even very little concentrations of iron (a tolerance level of 170 ppm of Fe is reported), generally deriving from contamination during primary casting, have an essential role in the corrosion behavior of magnesium alloys (Atrens et al. 2015). By controlling the alloy grade and the formation of stable Mn-Fe intermetallic phases, that neutralize the galvanic action of iron, a significant improvement in the corrosion resistance of the alloy can be attained. Very much the same effect of iron has been observed also with other impurities, particularly transition metals, determining detrimental galvanic couplings with the alloy. The intermetallic precipitates and secondary phases, like those obtained with temper treatments (Table 3.24) and having in general a higher electrochemical potential than the magnesium alloy matrix, affect the corrosion behavior of the alloy. Also in this case, the prevailing mechanism is a localized corrosion attack. Actually, the effect of impurity and secondary phases can be inhibited if their average grain size is kept below a critical value, estimated in 4 nm for standard aluminum alloys. The same can be assumed for magnesium alloys, considering that on this length scale, the effects of corrosion can be mended by the growth of surface reaction layers. The beneficial effects of a controlled refinement of the alloy microstructure will be recalled next with reference to Mg-Li alloys, being both these elements particularly reactive, and with a low
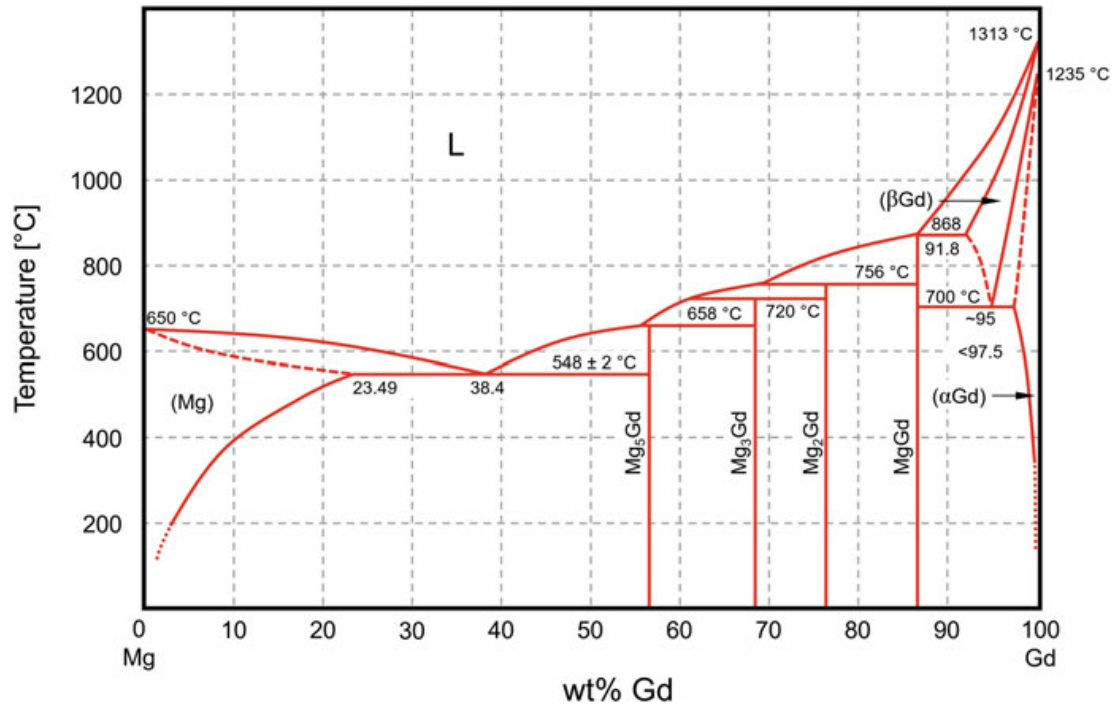
Fig. 3.35 Mg-Gd phase diagram. (Redrawn from ASM International 1992)

position in the galvanic series. Another important class of Mg-alloys, developed next, featured as main alloying elements rare earth (REs) elements and zirconium, in addition to zinc that is still present.

RE elements are interesting for their good solubility in magnesium (see Fig. 3.34). This aspect can be seen in the Mg-Gd phase diagram in Fig. 3.35, exhibiting also a low-temperature eutectic. A technological consequence of this behavior is an excellent castability of RE-containing Mg-alloys. To reduce the costs of the raw materials, RE elements are used in these alloys in the form of the so-called *misch* metals. These are mixtures of several RE elements based either on cerium (Ce55-La20-Nd15-Pr5) or neodymium and praseodymium. This latter mixture is often designated as *didymium misch* metal. This name derives from that of didymium, a mixture of neodymium and praseodymium that, in a first attempt, was considered as a new metal when Gustav Carl Mosander discovered it in 1840. Few years later, it was demonstrated that didymium was not really a new element in the periodic table but a mixture of oxides of the two elements, i.e., neodymium and praseodymium (Meyer 2001). The optimization of the mechanical properties, strength and creep resistance in particular, required alloying with zinc and zirconium, as anticipated. The already attested beneficial effect of zinc is enhanced by zirconium, which is added both as a grain refiner and a precipitation hardener. A refined and homogeneous microstructure, attained thanks to the right selection of the composition and subsequent temper, can stabilize the alloy microstructure and prevent fast recrystallization, an important aspect when the component is bound to be serviced in creep conditions. To this group of alloys, whose development started quite early (1940s) and continued until recently, belong several materials used in
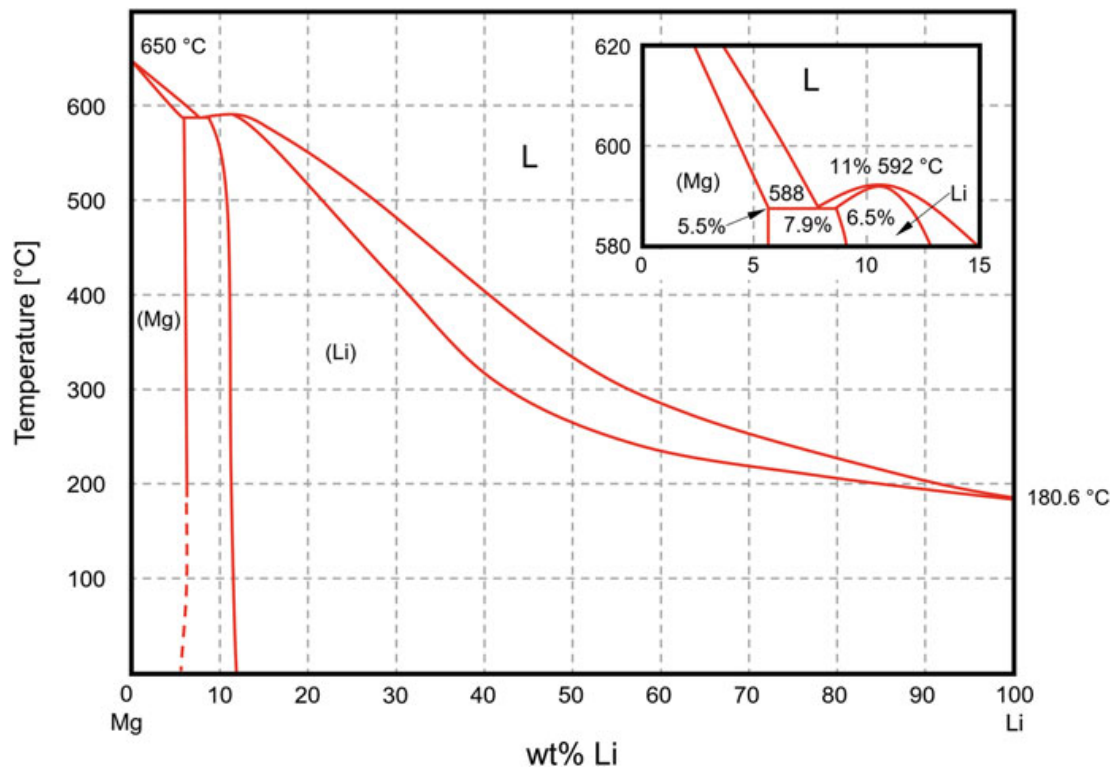
Fig. 3.36 Mg-Li phase diagram. (Redrawn from ASM International 1992; Perkguleryuz et al. 2013)

aircraft structures, like the EZ33, ZE41, ZE63, and the more recent ELEKTRON 21 (see Table 3.23). Strictly associated with REs-Mg-alloys are the alloys of the Mg-Ag system. The central feature of these alloys is the remarkable improvement of the mechanical properties, in particular tensile strength, observed, particularly in Mg-REs-Zr materials, with silver addition in concentrations close to 2.0%, which seems to be a critical value to differentiate Mg-Ag-REs-Zr alloys from standard Mg-REs-Zr (Polmear 2006). In fact, in the QE22 alloy (Table 3.23), one of the most used of this family, a concentration of silver equal to 2.5% is present. For silver-containing alloys, the use of the *didymium misch* metal is particularly recommended. Alloys combining excellent mechanical properties, also in creep regime up to 300 °C, and corrosion resistance have been obtained using yttrium as majority alloying element. In the WE54 alloy, for instance, a concentration of yttrium equal to 5.1% is present, attained using a particular *misch* metal, dominated by the presence of yttrium (75% approx.), in association with gadolinium and erbium. In analogy with Al-alloys, for which Al-Li compositions represent the latest development of their design; lithium has also been selected as alloying element for magnesium alloys. The addition of lithium reduces further the already low density of these systems, which represent at the present time the lightest metallic structural materials (Wu et al. 2015).

In the binary Mg-Li phase diagram (Fig. 3.36), the α-phase, i.e., the hexagonal solid solution of lithium in magnesium, is stable up to a concentration of 5.5 wt% Li

in the phase diagram. Above this limit and up to 10.3 wt% Li, a mixture of α + β phases is present, being β a *bcc* solid solution of magnesium in lithium, (Li) in the phase diagram. The β-phase is the only one present at room temperature above 10.3 wt% up to pure lithium axis. Any raise in the concentration of β-phase improves the ductility of the alloy, an aspect that renders the Mg-Li alloys ideal candidates for metal forming, although strength and creep resistance tend to be reduced by the presence of the β-phase. Moreover, the high chemical reactivity of lithium, particularly in association with magnesium, requires a particular attention in managing the oxidation and corrosion resistance of these alloys. Initially, the alloy design regarded compositions in which standard alloying elements, already encountered in magnesium alloys, are present. Several families of alloys were developed: LA (Mg-Li-Al), LZ (Mg-Li-Zn), and LAZ (Mg-Li-Al-Zn), strengthened by the formation of intermetallics, like $MgLi_2Al$, $MgLi_2Zn$, AlLi, and MgLiZn (see Sect. 3.3.2). Specific additions have been explored in the attempt to improve the alloy properties and compensate for the partial instability exhibited by some of the above strengthening intermetallic phases. Starting from the reference compositions of the LA and LAZ alloys, the formation of stable intermetallic phases was attained thanks to the addition of Ag, Ca, Cu, and REs (Zhang et al. 2013). These alloy developments indeed achieved the expected results, although some limitations, pertaining surface stability, are still there and hinder the widespread, safe use of these alloys. However, strengthening mechanisms, which already proved successful in other Mg-alloys, have been applied to improve the properties of Mg-Li alloys too. Mg-RE-Zn alloys, in particular those with RE concentration in excess of the zinc concentration, exhibit an improved room- and high-temperature mechanical strength for the presence of the so-called long-period stacking ordered (LPSO) structures (Zhu et al. 2010). LPSO structures are based on intermetallic compositions, like $Mg_{96}Y_2Zn_2$, featuring a peculiar crystalline superlattice, as results from electron diffraction investigations. TEM observations have also demonstrated that the LPSO determine a fine lamellar structure within the relevant domains. The formation of the LPSO structures has been reported to occur in as-cast alloys, although not with optimized properties. For a complete exploitation of the benefits introduced by these ordered phases, solution heat treatments, possibly followed by extrusion, are recommended. The first reported application of this approach to Mg-Li alloys is the study on the cast Mg-8Li-6Y-2Zn (wt%) alloy, solution treated at 500 °C for 6 h in an inert atmosphere and then hot-extruded with an extrusion ratio of 14:1 (Zhang et al. 2013). The resulting mechanical properties turned out to be particularly good, as concerns the ultimate tensile strength, the tensile yield strength, and the elongation to fracture. If extrusion is preceded by the above mentioned thermal treatment, the refined microstructure shows mechanical properties up to 243 MPa, 187 MPa, and 30%, starting from 202 MPa, 142 MPa, to 19%, respectively, in alloy samples that were just extruded but not heat-treated. The microstructural refinement, resulting from the thermomechanical treatments imparted to the alloy samples, has also an indirect beneficial influence on its corrosion behavior, since it reduces the detrimental micro-galvanic effect associated with presence in the alloy of intermetallic particles and unwanted impurities. A similar approach has been applied also to fully β Mg-Li

alloys, as reported in (Xu et al. 2015). Again, using specific thermomechanical treatments, remarkable improvements in the alloy mechanical strength and corrosion resistance have been achieved retaining at the same time an excellent ductility. The main processing steps adopted for Mg-Li alloy materials comprise hot-extrusion and solution heat treatments, followed by water quenching. Furthermore, aging treatments, conducted at low temperatures (<100 °C), and cold-rolling are imparted to the alloy in order to stabilize the microstructure and relevant properties. The newly developed alloy exhibits also a very attractive corrosion behavior that overcomes the intrinsic weakness of α- and α + β alloys, which is determined by combined effect of the alloy composition, in particular the elevated concentration of lithium, and the microstructural refinement induced by the processing treatments. The investigated Li-rich alloy is characterized by a single-phase *bcc* microstructure containing a fine Li-rich solute nanostructure. The solute nanostructure is likely to be formed thanks to the high diffusivity of Li in the Mg lattice at low temperatures. Furthermore, the most interesting feature of this alloy is probably its corrosion behavior, being the Li-rich solute nanostructure substantially electrochemically homogeneous, thus increasing the intrinsic corrosion resistance of the alloy, in which inhomogeneities acting as preferential corrosion nucleation sites have been eliminated (Xu et al. 2015). A comparative picture of the way Mg-Li alloys perform in air is shown in Fig. 3.37. The scheme illustrates how the surface region of different Mg-alloys reacts to standard atmospheric conditions. The poor oxidation resistance of Mg-rich α-alloy is due to the incomplete coverage by the oxide layer that spontaneously forms on the alloy surface (Fig. 3.37, *incomplete coverage*). Therefore, the alloy is not insulated from the surrounding environment, and oxidation can proceed, possibly accompanied by the hydration of the outer oxide. Higher concentrations of lithium, like in two-phase α + β alloys, result in the oxidation of this element too, to form Li_2O (Fig. 3.37, *preferential attack*). The α-grains, which are still present, behave similarly to what is observed in the case of a fully α-alloy. From the scheme, it is also evident that the finer is the microstructure of the alloy, the more homogeneous is the coverage of the alloy itself produced by the outer reaction layer. The interesting novelty introduced by these advanced Mg-Li alloys is the active role of lithium, which, thanks to the refined microstructure of the alloy, better if with a nanometric grain size, forms together with Mg a compact mixed oxide layer. Moreover, lithium oxide (Li_2O), reacting with carbon dioxide to form Li_2CO_3, improves the protection performances of the outer reaction layer. Thanks to the combined oxidation and carbonation reactions, a complete coverage of the metallic surface can be achieved in case of the fully *bcc* nanostructured Mg-Li alloy (Fig. 3.37, *complete coverage*). This latter alloy is definitely better performing as concerns corrosion resistance, and this is due both to the complete surface coverage and to the underlying matrix with the nanostructured features avoiding corrosion to initiate at inhomogeneities contained in the material (Xu et al. 2015).

Moreover, it turns out that this reaction layer has excellent self-healing features, so that it can also stand possible damages, thus behaving very much like the self-passivating film of native oxides, which form on the surface of aluminum, stainless steels, and titanium alloys. These novel Mg-Li alloys exhibit structural properties
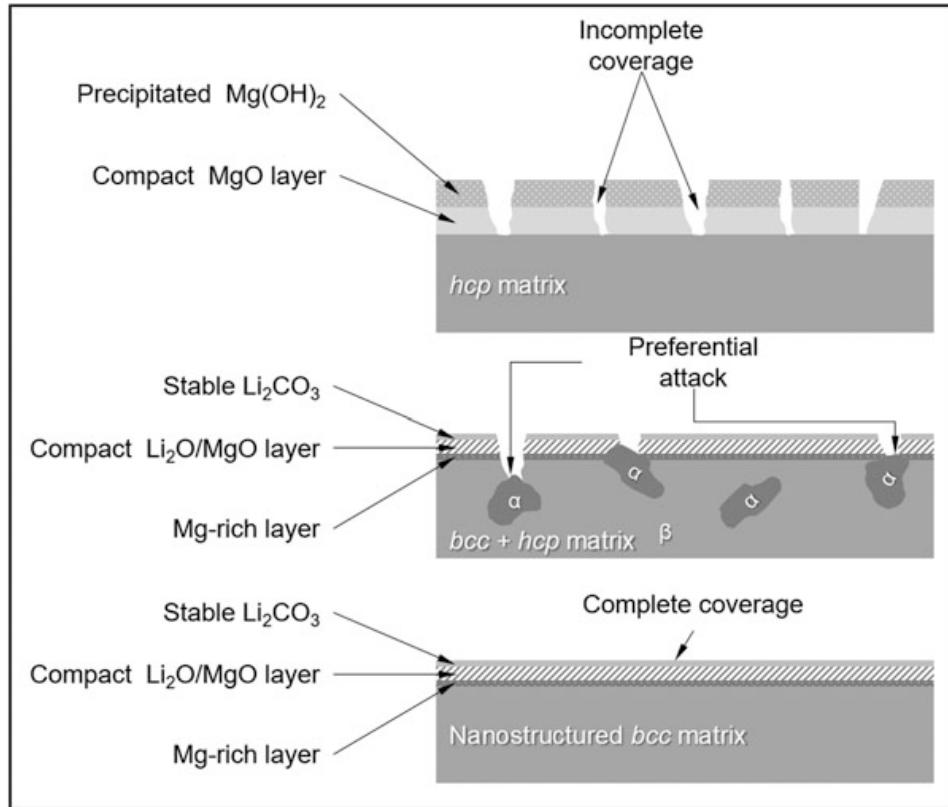
Fig. 3.37 Schemes of the surface reactions of different Mg-Li alloys when exposed to air with reference to three matrix conditions: conventional *hcp* Mg-rich α-alloy, *bcc* + *hcp* Mg-Li extruded alloy, and *bcc* nanostructured Mg-Li alloy. (Redrawn from Xu et al. 2015)

and surface stability that render them potentially interesting for real applications, including aerospace ones.

The research efforts that have been spent for this task indicate anyway the growing, in some respect, renovated interest for Mg-alloys, as proved also by the ever-growing trend in Mg production shares (Fig. 3.33) and by the variety of available mechanical properties, and related tempers, provided by state-of-the-art magnesium alloys (Table 3.25).

3.3.5 Current Aerospace Applications

The aircraft components in Fig. 3.38 provide an interesting overview of the potential afforded by metal working technologies of magnesium alloys. These encouraging results are promoting new investigations for the development of fully enabled production routes, suitable also for the aerospace field. The explorative manufacturing of aircraft brackets, with different geometries, has attained excellent results in terms of part control and resulting properties, absolutely comparable, if not better than those of the benchmark cast counterparts, that still represent the larger part of

Table 3.25 Selected Mg-alloys and tempers with resulting mechanical properties

Alloy	Thermal treatment	Tensile strength [MPa]	Tensile yield strength [MPa]	Compressive yield strength [MPa]	Elongation [%]	Hardness	Product form
AM50	F	268	168	–	18.0	–	Extrusions
AZ31	F	245	165	–	12.0	–	Extrusions
AZ31	H24	325	180	–	15.0	–	Sheets
AZ61	F	280	165	–	14.0	–	Extrusions
AZ91A	F	230	150	165	3.0	63 HRB	Castings
AZ92A	T6	275	150	150	3.0	84 HRB	Castings
ELEKTRON 21	T6	248–280	145–170	168	2.0–5.0	–	Castings
ELEKTRON 675	T5A	300–350[a]	200–230[a]	–	1.0–5.0[a]	–	Extrusions
ELEKTRON 675	T5B	340–400[a]	230–260[a]	–	1.0–3.0[a]	–	Extrusions
HK31	H24	285	160	–	9.0	–	Sheets
HM21	T8	270	130	–	11.0	–	Sheets
LA141	T7	132–165	105–160	–	11.0–24.0	–	Sheets
WE43A	T6	250	165	–	2.0	75–95 HRB	Castings
WE54A	T6	250	172	172	2.0	75–95 HRB	Castings
ZE41A	T5	205	140	140	3.5	62 HRB	Castings
ZE63A	T6	300	190	195	10.0	60–85 HRB	Castings

(continued)

Table 3.25 (continued)

Alloy	Thermal treatment	Tensile strength [MPa]	Tensile yield strength [MPa]	Compressive yield strength [MPa]	Elongation [%]	Hardness	Product form
ZK60	F	325	240	–	13.0	–	Extrusions
ZK60	T5	330	268	–	12.0	–	Extrusions
ZK60A	T5	365	305	250	11.0	88 HRB	Extrusions
ZMC711	T6	325	300	–	3.0	–	Extrusions

References and details about temper treatments are given in Table 3.24 (ASM International 1991; Magnesium Elektron 2014, 2016; Pekguleryuz et al. 2013)
[a]Properties of samples up to 100 mm in diameter. Lower value is measured in transverse direction, while higher value is measured in longitudinal direction
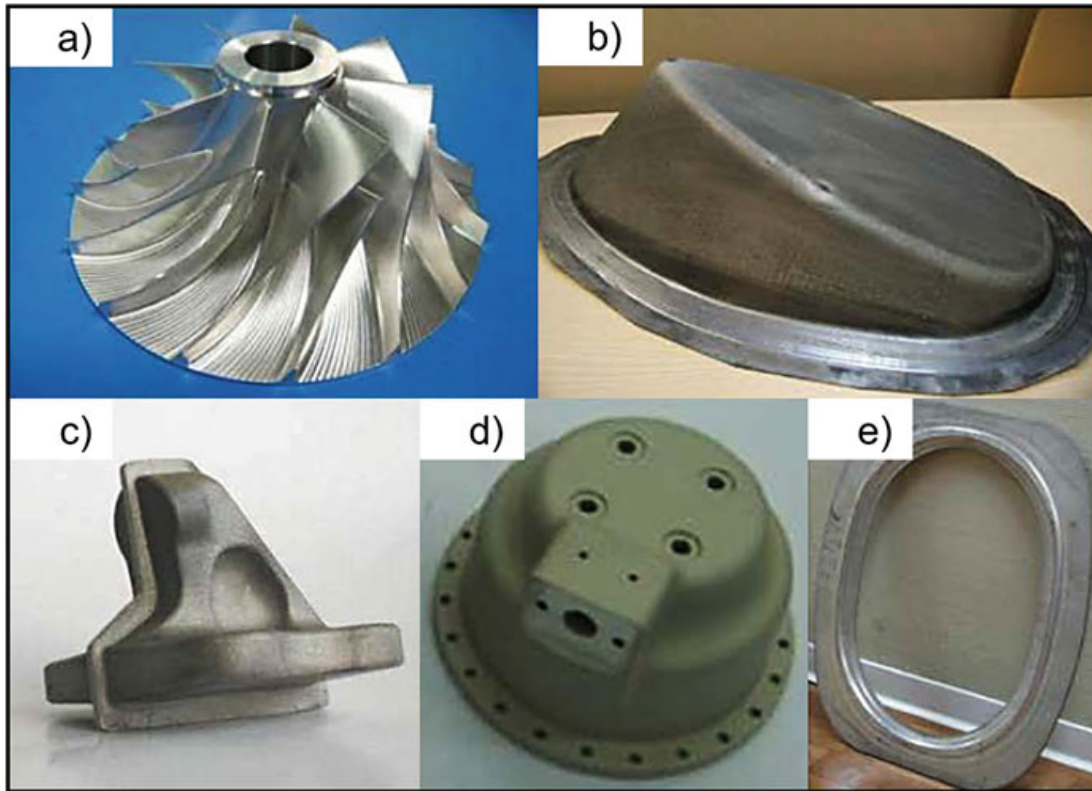
Fig. 3.38 Some aircraft components obtained by different forming techniques and made of different Mg-alloys, as specified in the following. (**a**) WE43 impeller with twisted blades; (**b**) AZ31B support of the Eurocopter antenna – deep drawing; (**c**) AZ80 door stop fitting – forging; (**d**) WE43 compressor upper case for air conditioning plant – closed-die forging; (**e**) AZ80 window frame for Airbus plane – forging (Dziubinska and Gontarz 2015, reproduced with permission of the Publisher)

magnesium alloy components (Dziubinska and Gontarz 2015; Dziubinska and Gontarz 2016). The weight saving introduced by magnesium alloys encouraged their widespread and successful use for helicopters. Some examples of applications of magnesium alloys for helicopter and airplane components are given in Table 3.26.

The future applications of magnesium alloys in the aerospace field seem to be liable of important expansion. In fact, as suggested by the examples in Fig. 3.38 and Table 3.26, the consolidation of metal working technologies for the manufacture of magnesium alloy components is widening the application possibilities of these materials. This process route is certainly benefitting from the established use of these alloys in the automotive industry and in other large-scale production industrial fields, leading to the creation of knowledge and solutions for high-quality components.

Table 3.26 List of some magnesium alloys used in the fabrication of components of helicopters and aircrafts (Gupta and Gupta 2017)

Alloy	Applications
AZ19E	Sikorsky CH33D-Seastallion with a part weight of 238 kg
	After the T6 temper, it is used for the sump of the six-cylinder 540 Lycoming engine used to power the Piper Chieftain
	Fabrication of some components for the Piper Comanche
	Fabrication of some components for the Sikorsky CH53D
AZ92A	Thrust reverser panels obtained by cascade casting used in the Boeing B737, B747, B757, and B767 airliners
ELEKTRON 21	Parts of the Boeing AH64D Apache
EZ33A	Parts of the gearbox of the Rolls-Royce turbofan engine RB211
QE22	Compressor casing of the ALF 507s engine
	Gearbox of the General Electric F110 engine
WE43	Parts of the MD 600 and Sikorsky S92
WE43	Pratt & Whitney F119 auxiliary casing
WE43	Castings used in the gearbox of the Bell Augusta 609 twin engine tilt rotor VTOL (vertical take-off and landing) aircraft
ZE41	Parts of the Sud-Aviation Super Frelon helicopter
	Parts of the Boeing AH 64 Apache
	Parts of the Boeing CH47 (Chinook)
	Parts of the Sikorsky UH60 (Black Hawk)
	Parts of the Pratt & Whitney PW 305 turbofan
	Castings used in the Rolls-Royce Allison AE-3007 engine

3.4   Composite Materials

3.4.1   Introduction

Composites are materials made of at least two phases, which are physically distinct. In general terms, any two or multiphase material can be classified as a composite, including the precipitation-hardened aluminum and magnesium alloys, discussed in Sects. 3.2 and 3.3, and other multiphase alloy systems that will be discussed next. A particular group of composites will be considered in this section, belonging to the broader family of structural composites. Structural composites are materials designed to respond better to specific requirements regarding mechanical properties and realized by mixing together two or more phases in order to achieve these properties, which each single component would not be able to reach by itself (Hull 1981). This aspect together with the low-density values of the main composite systems are the main reasons for the strong interest for structural composites in aircraft applications. The main classes of composites used in aircraft structures are based on epoxy polymer matrix, reinforced with carbon, glass, or aramid fibers. Since the early use of composites in aircraft structures, dating back to the end of the

1990s, their shares have continuously increased, starting, as usual, from military fighter airplanes and spreading to any aircraft and spacecraft. Actually, the path was not straight, and some diverting accident occurred. This is the case of the low toughness and impact resistance exhibited by the carbon fiber fans and blades of the early stages of the compressor of the RB211 Rolls-Royce engine, which did not resist bird strikes and for this reason had to be temporarily abandoned (see *fail safe* concept, Sect. 1.2). Moreover, the quest for a reliable assessment of the useful lifetime (*life safe* criterion, Sect. 1.2), especially, of primary structures, like wings and empennages, was not always met, particularly in case of early composites based on carbon fibers, not displaying any fatigue limit. The situation evolved positively, following two parallel paths: materials based on alternative reinforcements and better grade and microstructural control on carbon fibers. One interesting example of novel design component is the single-shell monocoque that provides higher strength and lower total weight, as compared to the same part assembled by joining together several parts. In addition to the improvement in the specific mechanical properties obtained both from the adoption of new materials and of the new structures that they allow to realize, the rapid spread of epoxy matrix structural composites has been sustained by other important advantages. With reference to the B787-Dreamliner (Sect. 1.2, Fig. 1.11), the use of composites requires also novel processing and manufacturing technologies that result in important cost reduction, thanks to the optimization of the material use. In fact, once the target properties (strength, stiffness, toughness, etc.) have been set, the lay-up design indicates precisely the necessary production steps and relevant materials quantities. The composite parts produced in this way can easily be assembled using lay-up machinery and rotational molding process. In general, composites exhibit a larger mechanical stability as a consequence of their relatively low coefficient of thermal expansion. Lighter structures obviously result in a reduction in fuel consumption and an increase in the payload and/or passenger number. The latest generation of composite materials, featuring high damage tolerance, has also improved the accident survivability of the components. Eventually, the electrically insulating character of the polymer matrix structural composites eliminates all drawbacks pertaining galvanic corrosion, typically initiated at the contact regions between dissimilar metal alloys, particularly in marine environments, featuring high concentrations of water vapor and salty aerosols. For the same reasons, the incidence of fatigue/corrosion problems is virtually eliminated. These latter aspects, influencing materials and structural durability, are of course very positive for the maintenance programs that may potentially result in important reduction in the fleet management costs.

For the military field, other benefits can be considered, related not only, or not necessarily, to the increase the payload, but also operational range, flight performances, and maneuverability under extreme conditions. Polymer matrix structural composites definitely have a number of interesting properties, and this can explain their continuously increasing usage in aerospace structures. However, a specific aspect descending from the electrically insulating character of these materials has to be underlined. Whereas an aircraft with fuselage and skin made of aluminum alloys is quite conductive so that it can dissipate the electrical currents produced by

lightning strikes, the same would not be possible for a polymer matrix composite, unless some alternative solutions are implemented. In fact, all structural composites used for the outer surfaces of an airplane, those directly exposed to possible lightning strike, have in their lay-up a protection system, consisting of a ply of metallic mesh or other kinds of conductive layers. These metallic components have essentially a functional role, i.e., improving electrical conductivity, and their relative concentrations are comparatively small. A class of composites that has been specifically developed for aircraft structures and that features major fractions of metallic components are the *fiber-metal laminates* (FMLs). These materials are composed of stacks of metal sheets, made of aluminum or titanium alloys, and prepreg layers, made of continuous felts of aramid, glass, or carbon fibers. The potential of FMLs in aerospace structures appeared evident since the beginning, even considering the low density of their component phases: metallic alloys, reinforcing fibers (see next), and epoxy resin. The possibility to produce anisotropic parts through a suitable fiber orientation and to optimize the stress distribution within the load-bearing section is another positive feature of these important structural composites (Botelho et al. 2006; Vermeeren 2003).

3.4.2   Fiber-Metal Laminates: Development and Designation

The early developed FML was the aramid-fiber-reinforced Al-laminate, ARALL, for which the Dutch University of Delft and the AKZO company filed two patents in 1981. One of the patents covered the general concept of the FML, based on the combination of metal sheets and prepreg fiber felts. The other patent regarded the so-called *stretch forming* (stretching) process. Although flying components of this prototype FML were actually produced, any further development of ARALL was interrupted at the time, due to an insufficient fatigue resistance, particularly under compressive and tensile load conditions. A new class of laminates was developed next, whose name was GLARE, i.e., glass-fiber-reinforced Al-laminate. Also for this material, there is a patent by AKZO, now AKZO Nobel (1987). The general layout of an FML is shown in Fig. 3.39.

Further developments of FML were composites reinforced by carbon fibers:

- CARALL – carbon fiber reinforced aluminum laminate.
- Ti-Gr (titanium-graphite composites).

In this latter, developed by the Boeing company, aluminum is replaced by titanium. Other materials systems have been considered, but their actual use in aircraft structures is still far to come. This is the case of the composites like ALLIC (Al-Li reinforced by carbon fibers), VIRALL (Al-alloy reinforced by Vinylon), BRALL (Al-alloy reinforced by bamboo), and RAFAL (Al-alloy reinforced by ramie) (Laliberte et al. 2000).

For the identification of the different products, an international designation code has been established, according to the scheme illustrated in Fig. 3.40.
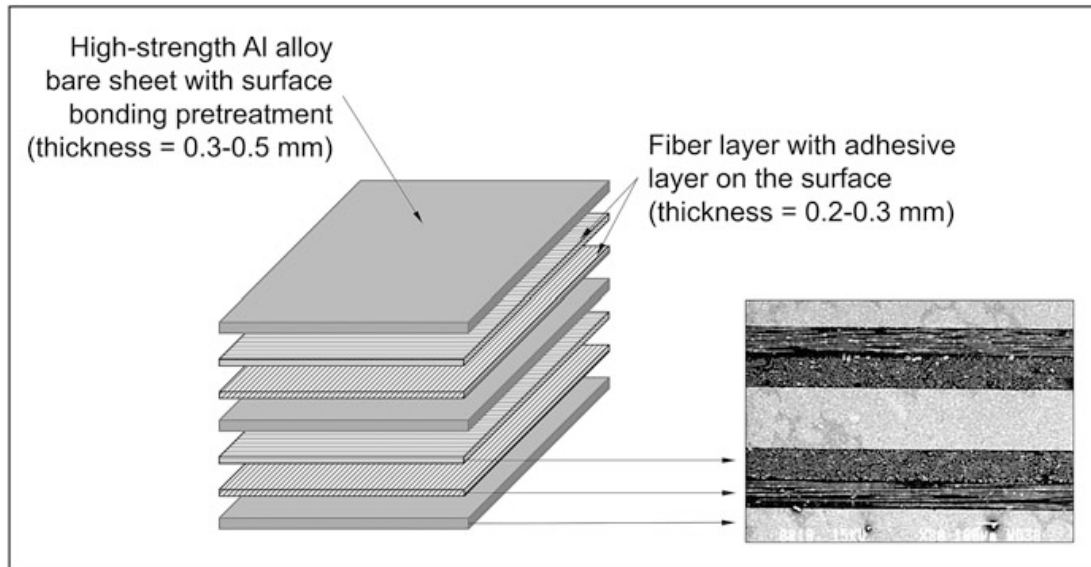
Fig. 3.39 General layout of a FML composite. On the right the cross-sectional view of a real FML. Please note the different orientation of each layer of fibers (Vermeeren 2003, reproduced with permission of the Publisher)
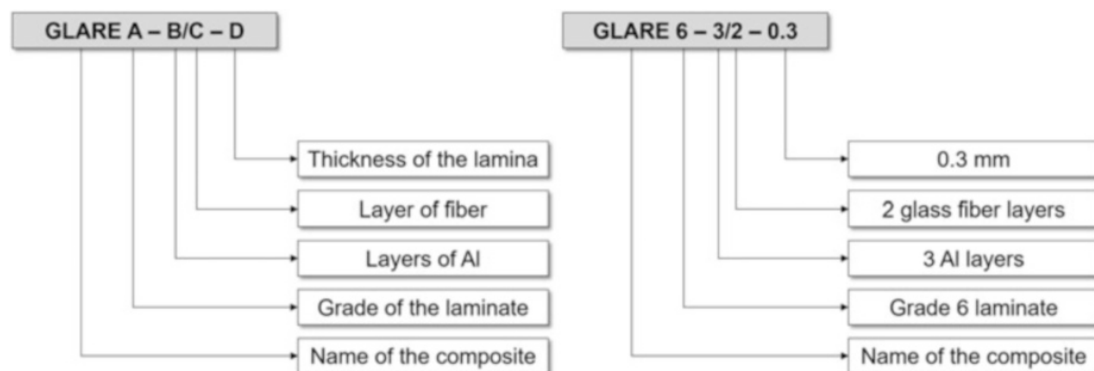

Fig. 3.40 Scheme for the FML international designation code, with an example

For a full qualification of FMLs, other features are important, in particular the orientation of the fibers (Table 3.27).

3.4.3 Main Production Steps and Resulting Characteristics

The processing of FML components typically involves the following steps: surface preparation, lay-up preparation, preparation of the lay-up for the curing treatment, curing treatment, inspection, and post-processing operations (Botelho et al. 2006). During the first step (surface preparation), the metallic surfaces are pre-treated in order to improve the bonding efficiency with the prepreg layer. Different approaches

Table 3.27 Specifications of the GLARE composites (Wu and Yang 2005)

Type	Typical density (g/cm^3)	Al layers characteristics			Fiber layer characteristics	
		Alloy	Temper	Thickness [mm]	Orientation	Thickness [mm]
GLARE 1	2.52	7475	T76	0.3–0.4	Unidirectional	0.25
GLARE 2	2.52	2024	T3	0.2–0.5	Unidirectional	0.25
GLARE 3	2.52	2024	T3	0.2–0.5	0°/90° cross-ply (50%)	0.25
GLARE 4	2.45	2024	T3	0.2–0.5	0°/90°/0° cross-ply (67%–33%)	0.375
GLARE 5	2.38	2024	T3	0.2–0.5	0°/90°/90°/0° cross-ply (50%)	0.50
GLARE 6	2.52	2024	T3	0.2–0.5	+45°/−45° cross-ply (50%)	0.25

have been developed in this regard, which can be grouped into the following main categories: mechanical, chemical, and electrochemical (Sinmazçelik et al. 2011).

The effects of a chemical etching, carried out on an aluminum alloy (2024-T3) foil, using a sulfuric acid solution, are visible in the SEM micrographs in Fig. 3.41. The increase in the surface irregularity and, consequently, in the specific surface area is an important parameter used to improve the adhesion between the aluminum foil and the prepreg fiber felt.

After treating the metallic surfaces, the lay-up of the composite is assembled. At this stage, the choice of the right orientation of the fiber layers is paramount to obtain the expected properties.

Some indications have been developed over the years as concerns this aspect, depending on the different loading conditions:

- 0°/0° to enhance fatigue resistance, ultimate tensile strength and yield strength;
- 0°/90° to obtain fatigue resistance, impact resistance;
- +45°/−45° to obtain shear resistance.

Concerning the metallic alloy layers, they are integrated into the composite starting from already formed foils. The alternative involves the direct deposition of Al-foil directly from the melt using a method that will be fully discussed next. Once the composite lay-up has been prepared, it is transferred to a vacuum bag for the curing treatment (Fig. 3.42). The vacuum bag is typically made of nylon with rubber seals. A release film, e.g., fluorinated ethylene propylene, wraps the composite stacks and helps its detachment from the vacuum bag and other parts of the set up at the end of the curing. A bleeder, that might be woven fabric or felts, adsorbs the excess of resin, possibly ejected during the treatment (Gutowski 1997). The autoclave curing occurs at pressures and temperatures suitable for a full consolidation of the composite. Temperature and pressure profiles suitable for ARALL (2024 alloy, with a T3 temper) composites are shown by the graph in Fig. 3.42, as a function of
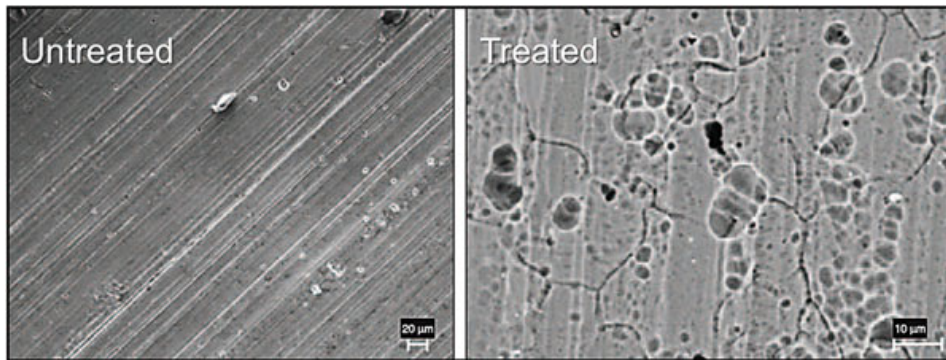
Fig. 3.41 SEM micrograph showing the surface of a 2024 T3 alloy before (untreated) and after a H_2SO_4 chemical etching used to improve the adhesion with the prepreg fibers. (Bothelo et al. 2009, reproduced with permission of the Publisher)
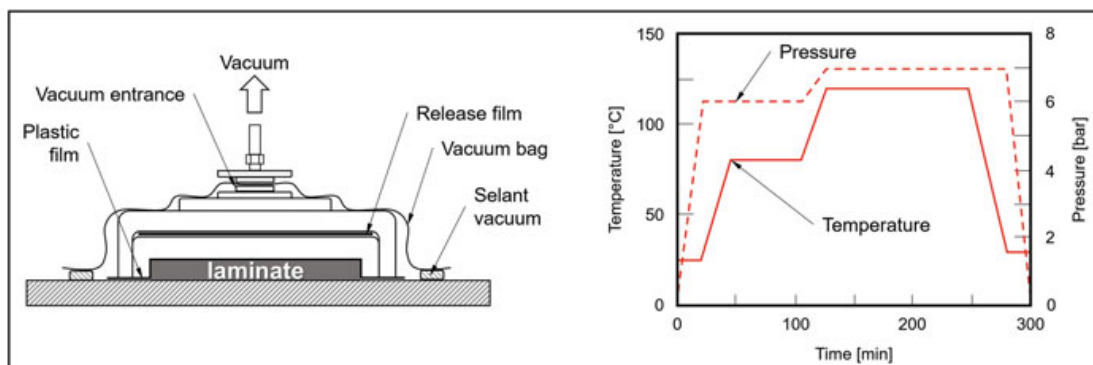

Fig. 3.42 Vacuum-bag setup for the impregnation and curing treatment of the composite lay-up. (Redrawn from Bothelo et al. 2006)

the time of curing, which is the most critical part of the production process. Thanks to the removal of air via a vacuum system, this procedure allows to press the multilayer and helps the spread of the resin and the elimination of excess residues and volatile components. Limits and possible problems at this stage of the process are essentially two: firstly, curing temperature can be comparable with the temper treatment temperature of the selected aluminum alloy, being the use of aged and stabilized alloys a possible remediation. Secondly, an optimal distribution of the resin can be achieved only if dimensions of the workpiece are not too big.

To overcome these limitations and to render the whole production process less expensive and applicable to relatively larger pieces too, the *vacuum-assisted resin transfer molding* (VARTM) process has been developed (Jensen et al. 2009). In this process, the resin is injected into the fiber preform and spreads through the metal and fiber layers. This is a fundamental step of the process, since a great deal of the final mechanical properties of the FML is dependent on the homogeneous spread of the resin within the fiber felt and at the interfaces with the metal foils. During the VARTM process, any excess resin is sucked away from the opposite side, with respect to the inlet duct of the vacuum bag (Fig. 3.43).
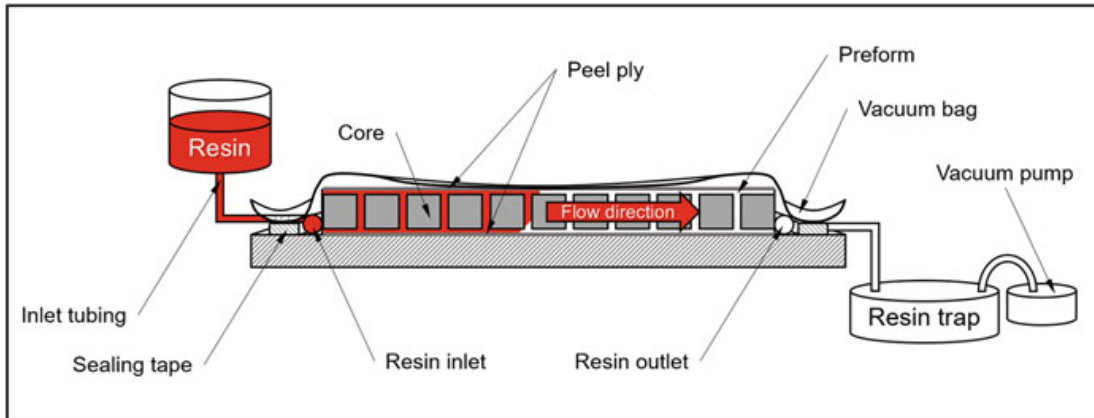
Fig. 3.43 Scheme of the fabrication set up for the VARTM. (Redrawn from Jensen et al. 2010)
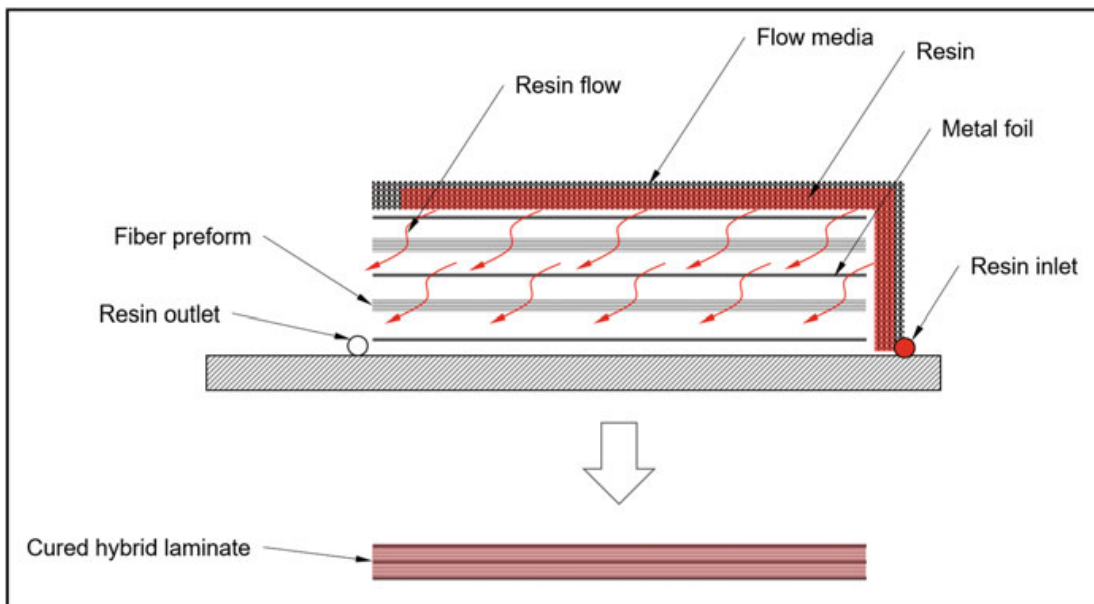

Fig. 3.44 Sequence of resin infiltration and curing for the VARTMFML. (Redrawn from Jensen et al. 2009)

To promote the homogeneous distribution of the resin within the composite, holes are drilled into the metal foils core, although this step requires a particular care, since an important influence of the hole features on the mechanical properties of the composite has been reported, with particular regard to fatigue life. Porous aluminum foils have been considered as a possible alternative approach (Fig. 3.44). In the process, named VARTM-infused *plasma coated laminates* (VARTMPCL), the fiber fabric is coated with a porous metal layer, obtained by depositing the Al-alloy via plasma-spraying (see Sect. 7.2.1). In Fig. 3.45 the main steps of the deposition process are illustrated. The fabric, fixed on a rotating drum, is coated with the metallic layer by repeated scans of the torch.
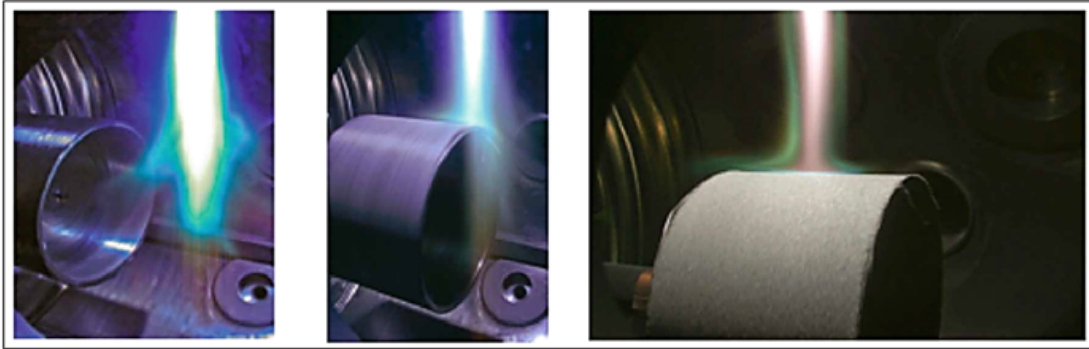
Fig. 3.45 Deposition of porous Al-alloy layer onto the fabric to produce FML via the VARTMPCL processing (Jensen et al. 2009, reproduced with permission of the Publisher)
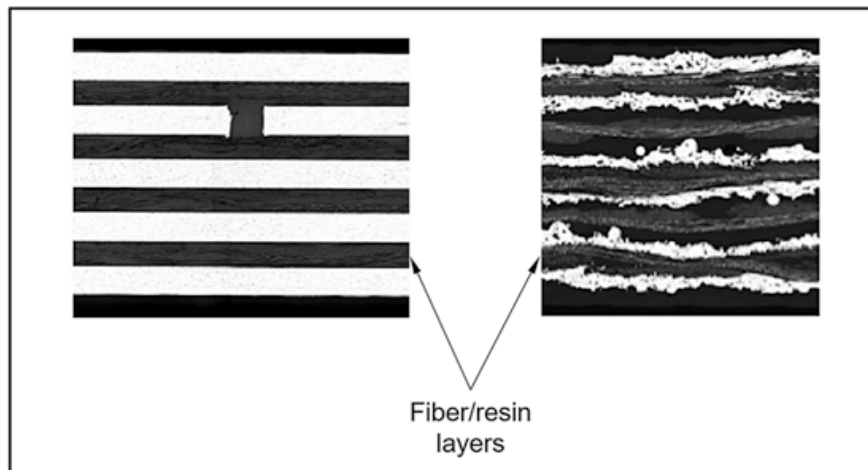

Fig. 3.46 Comparison of the microstructure of the VARTMFLM (left) and VARTMPCL (right) – 0.38 mm thick foils (Jensen et al. 2009, reproduced with permission of the Publisher)

The thickness and the other coating features can be tuned by selecting the torch deposition parameters and the rotating and translational speed of the drum. It is also possible to coat the fabric on both sides by just turning it over and replacing it back onto the drum and then going ahead with the deposition. The alternate layers of fiber felts and porous alloy layers are subjected to the VARTM process in the same way as the "hole-drilled" VARTMFML systems.

Figure 3.46 shows the microstructure of FML with the same stratigraphy and composition but with a difference consisting in the VARTM technique used for their production. Considering the rather different microstructures and, thereby, properties of the two materials, they may have different applications: the VARTMFML typically exhibits good mechanical properties, whereas the VARTMPCL products are preferable for their functional properties, like enhancing electrical and thermal conductivity, interesting, for instance, to improve the resistance of the composite to lightning strikes. From the structural point of view, the VARTMPCL materials suffer from the extreme irregularity of the aluminum layers, generally resulting in

an early crack initiation. Although the intrinsic damage tolerance of these materials renders them capable to withstand also relatively high defect concentrations, still, safety criteria may suggest more conservative choices.

For a complete exploitation of FMLs, several post-production treatments have been developed to manufacture composite components with the right geometry required by any specific application. Joining techniques are very important to produce components with complex shapes and geometries. An alternative approach, largely used even in the preparation of the GLARE fuselage panels of the A380, is the *stretch forming*. The only precaution that has to be taken when stretch forming FML components is the delamination that may occur when excessive bending and straining are imparted to the component, favored by the elastic modulus mismatch between the metal and prepreg layers. Notwithstanding the possibility of forming FMLs using different approaches, joining still remains a fundamental aspect for obtaining complex piece geometries. Adhesives are used to join different parts, but in doing this, a continuity of the fiber felts should be preserved, in order to avoid an excessive weakening of the final pieces. Riveting is also used, exploiting the good deformability of the FML, and still sticking to the recalled precautions. The complexity and critical dependence of the FML properties, namely, the mechanical properties, which will be discussed in Sect. 3.4.4, on their actual microstructure, renders all production steps extremely critical.

3.4.4 *Mechanical Properties*

With reference to the values in Table 3.28, the generally anisotropic character of the mechanical properties of FMLs can be clearly seen, depending on the direction of the applied load with respect to the composite symmetry. The tensile and compression behavior of FMLs is influenced by the plasticity of the metallic component, displaying a nonelastic trend, depending on the load application direction: either longitudinal (L) or transverse (T). Although the metallic component behaves as a monolith and its properties cannot be modulated and adapted that much, the orientation of the fibers can be optimized, to avoid a too heterogeneous and anisotropic material to be obtained and to maximize the performances along the most demanding directions in terms of mechanical stress field.

The composite design requires a thorough analysis of its complex mechanical behavior. For this purpose the Stress-Strain Calculation Program (SSCP) provides excellent indications, at least in static loading conditions (Hagenbeek et al. 2003). The key factor for a good fatigue resistance of FMLs can be identified in the relatively thin layers building up the composite. This condition determines, within each layer, a biaxial plane stress, to be regarded as a beneficial factor for a slow crack propagation (Dieter 1988). In addition to this mechanism, crack bridging, i.e., the transfer of the load from the cracked metallic foil to the still undamaged fibers,

Table 3.28 Tensile and compressive mechanical properties of ARALL and GLARE materials along longitudinal (L) and transverse (T) directions (Laliberte et al. 2000)

Parameter	Direction	Material					
		A-2	A-3	G-2	G-3	G-4	G-5
Ultimate tensile strength [MPa]	L	717	821	1213	745	1027	683
	LT	317	780	317	745	607	683
Yield strength [MPa]	L	366	607	393	303	352	–
	LT	228	331	228	303	25	–
Young's modulus [GPa]	L	66	66	66	58	57	70
	LT	53	49	50	58	50	70
Ultimate strain [%]	L	2.5	2.2	4.7	4.7	4.7	–
	LT	12.7	8.6	10.8	4.7	4.7	–
Compressive yield strength [MPa]	L	255	345	413	310	365	283
	LT	234	360	236	310	285	283
Compressive elastic modulus [GPa]	L	65	64	67	59	60	–
	LT	53	50	52	59	54	–

A ARALL, *G* GLARE, *L* longitudinal, *T* transverse

contributes to enhance the fatigue resistance of the composite. An appropriate adhesion strength between fibers and metal foil completes the picture and determines the right balance among different mechanisms, all of them very much dependent on the layered structure of the FML. This aspect, i.e., the central role of the layered structure in determining the mechanical properties and in particular the fatigue behavior of FMLs, is clearly demonstrated by the curves in Fig. 3.47. In the case of FMLs, the crack propagation rate tends to decrease with increasing crack length, whereas in a bulk Al-alloy, the opposite situation is usually observed.

This behavior, exhibited by the laminate composites, is most interesting for aerospace applications, since the integrity of the component is preserved all through its useful lifetime. This can be achieved thanks to the effective action of the mentioned toughening mechanisms, capable to actively counteract the fatigue damages introduced into the material structure by service conditions. The damage tolerance of FMLs is proved by the fatigue data in Fig. 3.48. The behavior of ARALL is compared to that of bulk aluminum alloys. Interestingly, the number of cycles for the appearance of first fatigue crack (N_i) in the case of the ARALL material is lower or, at most, comparable with N_i of the bulk alloys. The maximum number of cycles (N_f), i.e., the fatigue life, of the FML is order of magnitudes larger than the fatigue life of all the reference Al-alloys (Lanciotti and Lazzeri 2009). The damage tolerance of FMLs has been also confirmed with reference to notched samples: the data for the FMLs are comparatively better than those for aluminum alloys (Wu and Yang 2005). This situation is particularly important for materials to be used for those parts more directly exposed to impacts, like the leading edges of the wings, the engine entrance ducts, etc., in which notch-like defects can be produced
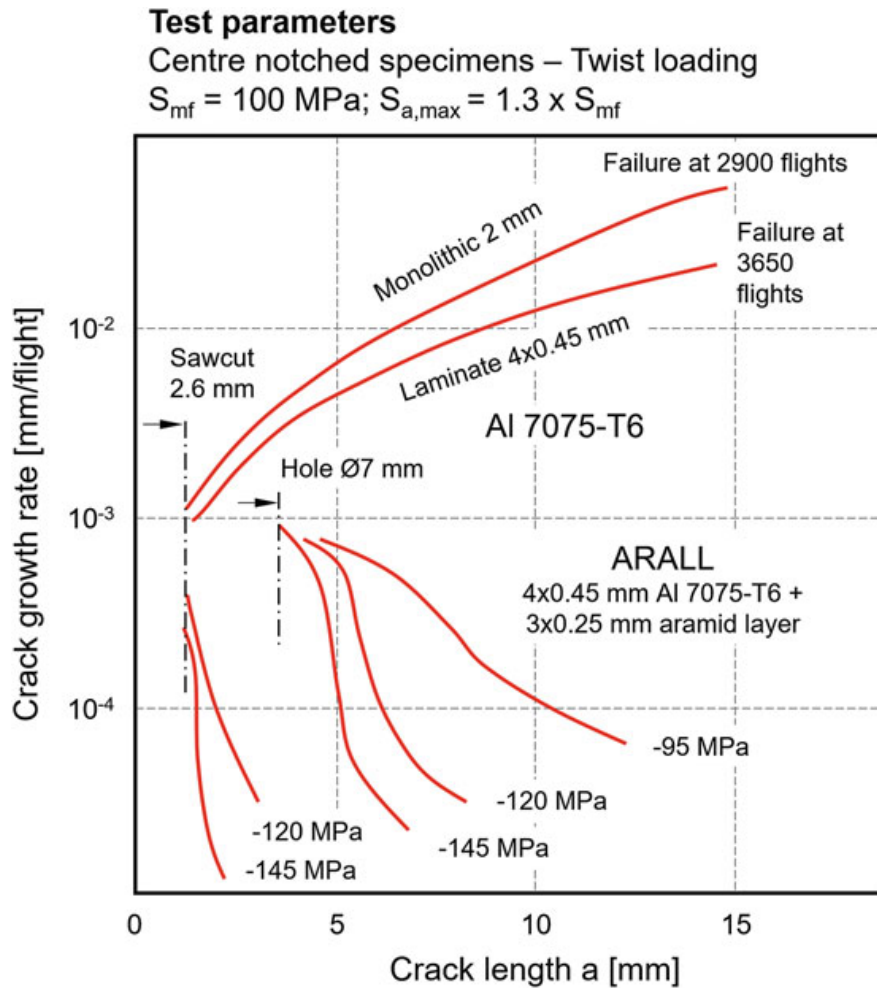
Fig. 3.47 Crack growth rate vs crack length for a bulk aluminum alloy (7075 – T6) and an ARALL composite. The maximum applied loading spectrum twist was truncated at 1.3 times the S_{mf}. Three different compression residual stress levels in the Al sheets are shown: −95 MPa, −120 MPa, and −145 MPa. (Redrawn from Buhl 1992)

by the bird strikes, hailstorms, etc. Other kinds of defects can be rather ascribed to structural features, like riveting, joint edges, and screws. Not always, the impact damages are immediately visible, and radiographic investigations are recommended, to prevent possible severe consequences, particularly as concerns the strength and stiffness of the structure. In addition to mechanical damages, changes in the FML properties may derive from environmental interactions, in the form of corrosion phenomena and water absorption. Water may enter the composite as air humidity, which may permeate the fibrous part of the composite.

Moreover, condensation on the cold metallic surfaces may result in liquid water infiltration, although the presence of outer aluminum foils and epoxy-sealed layers reduce significantly these phenomena with respect to the standard structural composites. Water absorption may produce the delamination of the prepreg layers and their detachment from the metallic foils with a consequent reduction in strength, stiffness, and fatigue life (Botelho et al. 2007, 2009). Surface corrosion may be
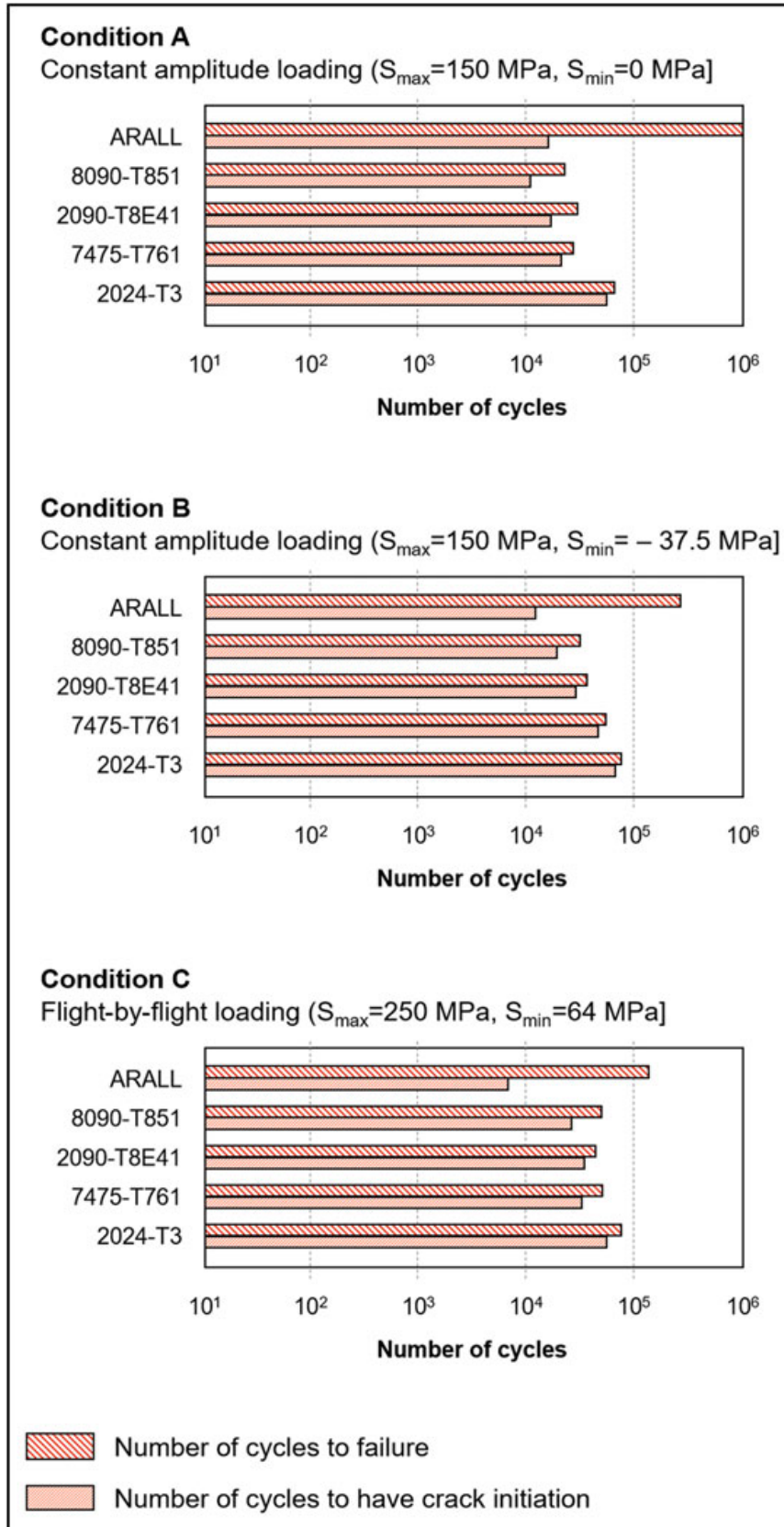
Fig. 3.48 Comparative fatigue data for bulk Al-alloys and an ARALL composite. For each graph the relevant fatigue test conditions (**a–c**) are indicated. (Redrawn from Buhl 1992)

avoided by anodizing the aluminum foils and by protecting the surface with a primer layer containing inhibitor substances (Wu and Yang 2005).

3.4.5 Applications

The initial focus, as concerns the application of FMLs was to use ARALL in the wing structures, with particular regard for a panel with a tank inspection hatch of the Fokker F-27 aircraft (Vermeeren 2003). This aircraft was selected for this study, since at the time, i.e., the early 1980s, a complete background information was available. The idea was discussed by the involved research parties, i.e., Fokker, Delft University, and ALCOA. The outcome of the study was a full-size panel $(2.0 \times 1.5 \text{ m}^2)$, which achieved the target of 25% weight reduction with respect to the same part made in aluminum alloy. A series of products followed the early panel in ARALL 1, using different alloys:

- ARALL 1: with 7075 alloy layers, stretched after curing;
- ARALL 2: with 2024 alloy layers, in the as-cured condition.

  In the following years, other products were made available:

- ARALL 3: same as ARALL 1 but with 7475 alloy in the place of 7075 alloy layers;
- ARALL 4: produced using a high-temperature adhesive, interesting for military applications.

An important indication emerging from the qualification tests carried out on these early products was the sensitivity of ARALL to the presence of drilled holes, that reduced significantly the strength of the material. Moreover, notwithstanding general excellent material properties as concerns fatigue crack growth, specific piece geometries displayed premature fatigue cracks. This is the case of the areas close to doublers bonded on the structure to increase its strength. However, these cracks regarded the outer aluminum layer only, and the residual strength of the component was still within the safety levels, thanks to the still integer fibers. Interestingly, similar cracks would have certainly resulted in a premature failure of an aluminum component, and in the end, the wing panel was very successful. In addition to wing panels, ARALL provided an effective solution to the excessive weight problems of the C-17 military transport aircraft that limited the loading capacity. For this reason, ARALL was chosen for the cargo door $(5.6 \times 9.7 \text{ m}^2)$ with a relevant weight reduction of 26%. However, the complex production steps and joining necessary to obtain a complete door resulted too demanding, so that in the end, only 30 of these doors were actually produced. Furthermore, the cost-effective, highly performing aluminum alloys initially hindered the use of the FMLs in the fuselage. However, when GLARE 3 and 4 were made available, most of the limitations, which were there in ARALL materials and in GLARE 1 and 2, mainly because of the unidirectionality of the fibers, were overcome. The cross-ply structure of the fibers and the asymmetry in the properties, associated with the peculiar fiber distribution,
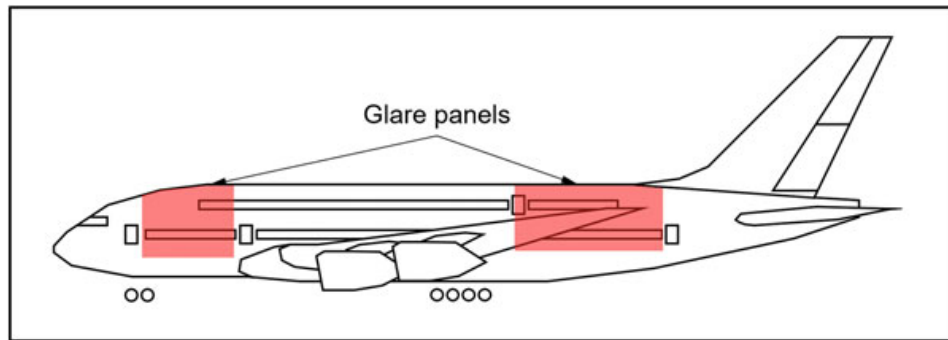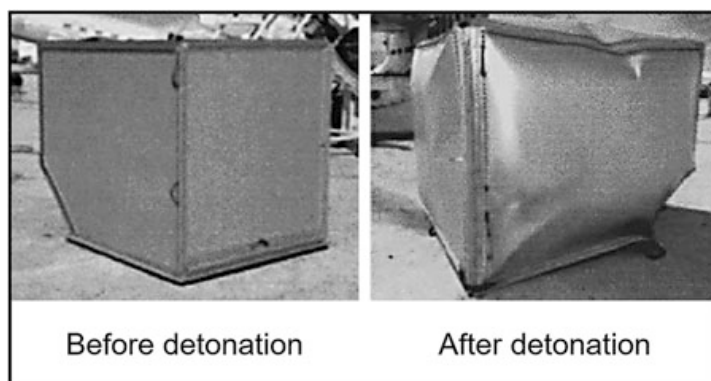
Fig. 3.49 The position of GLARE panels in the fuselage of the A380. (Redrawn from Wu and Yang 2005)

Fig. 3.50 The ECOS³™ container before and after a blast test (Vlot and Gunnink 2001, reproduced with permission of the Publisher)

could be exploited for the fabrication of large fuselage parts. In this fundamental development for FMLs in aerospace applications, the studies and tests conducted by Airbus for several years, in some cases on full size components, have been fundamental. Figure 3.49 gives the distribution of GLARE panels used for the fuselage of the Airbus A380. This laminate composite is employed in association with other structural composites, namely, graphite-fiber reinforced polymer, with a significant overall weight reduction.

The combination of aluminum and glass fibers in GLARE induces in the composite an extremely high fire resistance. In fact, although fire resistance of aluminum is rather poor, when an aluminum alloy is coupled with the glass fiber felt, the situation is completely different. A GLARE sample, exposed to a fire source, might still exhibit the melting of the aluminum outer layer. However, the glass fibers felt remains in place, thus preventing the heat to propagate toward the inner layers of the composite, that in this way are preserved. Fire resistance, coupled with the excellent impact resistance of FMLs in general and particularly of GLARE, has fostered the use of these materials for cargo and luggage containers capable to resist possible explosions. Figure 3.50 shows the effect of a blast test on the ECOS³™ container made of GLARE 3.

As a final example of application of FMLs, these materials are also used as patches for repairing cracks in polymer matrix composites. In this regard, the smaller

thermal mismatch between aluminum and GLARE, as compared to aluminum with respect to polymer matrix composites, is exploited. An example of this application is the use of a GLARE patch to repair a crack in the fuselage of a C-5A Galaxy transport aircraft (Vermeeren 2003).

New systems are continuously investigated, as concerns both the metallic part and the prepreg felt, in order to improve the already excellent properties achieved so far. Processing is also paramount to make these materials really attractive also for large-scale, low-cost productions. One of the latest aspects that is under consideration is the use of thermoplastics rather than thermosetting polymers as binder materials. In the future, renovated and growing interest can be foreseen for FMLs featuring natural reinforcing fibers, like the mentioned BRALL and RAFAL with bamboo and ramie natural reinforcement, respectively.

References

Aleris Corporation (2015) Aerospace Aluminum A5028 AlMgSc – The Strong Lightweight. Available via DIALOG. https://www.aleris.com/wp-content/uploads/2016/02/AL-2342_012-Aktualisierung-BR-AlMgSc-2015-06-03-WEB.pdf. Accessed 04 January 2018.

APWORKS (2017) Material Data Sheet – Scalmalloy®. Available via DIALOG. http://www.apworks.de/en/scalmalloy/. Accessed 04 January 2018

APWORKS (2017) Scalmalloy ®. Available via DIALOG. http://www.apworks.de/en/scalmalloy/. Accessed 04 January 2018

ASM International (1991) ASM Handbook Vol. 2 – Properties and selection: Nonferrous Alloys and Special-Purpose Materials. ASM International, Materials Park, Ohio

ASM International (1992) ASM Handbook Vol. 3 – Alloy phase diagrams. ASM International, Materials Park, Ohio

ASM International (2003) ASM Handbook Vol. 13A – Corrosion: Fundamentals, Testing and Protection. ASM International, Materials Park, Ohio

ASM International (2015) ASM Subject Guide – Aluminum and Aluminum Alloys. ASM International, Materials Park, Ohio

Atrens A et al (2015) Review of Recent Developments in the Field of Magnesium Corrosion. Advanced Engineering Materials 17(4): 400–453

Belov et al (2002) Iron in Aluminium Alloys: Impurity and Alloying Element. CRC Press

Benedyk J C (2010) International Temper Designation Systems for Wrought Aluminum Alloys: Part II – Thermally Treated (T Temper) Aluminum Alloys. Light Metal Age: 16–22

Blawert C et al (2006) Anodizing Treatments for Magnesium Alloys and Their Effect on Corrosion Resistance in Various Environments. Advanced Engineering Materials 8 (6): 511–533

Boeing (2008) AERO Magazine 06. Available via DIALOG. http://www.boeing.com/commercial/aeromagazine/articles/qtr_4_06/index.html. Accessed 8 October 2017.

Botelho E C et al (2006) A Review on the Development and Properties of Continuous fiber/epoxy/aluminum Hybrid Composites for Aircraft Structures. Materials Research 9 (3): 247–256

Botelho E C et al (2007) Influence of Hygrothermal Conditioning on the Elastic Properties of Carall Laminates. Applied Composite Materials 14: 209–222

Botelho E C, Da Silva D A, Rexende M C (2009) Hygrothermal Aging Effect on Fatigue Behavior of GLARE. Journal of Reinforced Plastics and Composite Materials 28: 2487–2499

Buhl H (1992) Advanced Aerospace Materials. Springer Verlag, Berlin

Cahn R et al (2005) Structure and Properties of Nonferrous Alloys. Materials Science and Technology 8–9. Wiley & sons

Cardarelli F (2008) Materials Handbook 2nd edn. Springer Verlag, London

Carter C, Norton M (2007) Ceramic Materials – Science and Engineering. Springer

Czerwinski F (2011) Magnesium Alloys – Design, Processing and Properties. InTech

Davis J R (2001) Aluminum and Aluminum Alloys. ASM International

Davy H (1808) Electro-Chemical Researches, on the Decomposition of the Earths: With Observations on the Metals Obtained from the Alkaline Earths, and on the Amalgam Procured from Ammonia. Philosophical Transactions of the Royal Society of London 98: 333–370.

Dieter G E (1988) Mechanical Metallurgy. McGraw Hill

Djukanovic G (2017) Are Aluminium-Scandium Alloys the Future? http://aluminiuminsider.com/aluminium-scandium-alloys-future/. Accessed 1 January 2018

Donachie M J (2000) Titanium – A Technical Guide. ASM International, Materials Park, Ohio

Dziubinska A, Gontarz A (2015) A new method for producing magnesium alloy twin-rib aircraft brackets. Aircraft Engineering and Aerospace Technology: An International Journal 87(2): 180–188

Dziubinska A, Gontarz A (2016) A new technology for producing AZ31 magnesium alloy aircraft brackets with a triangular outline. Aircraft Engineering and Aerospace Technology: An International Journal 88(3): 452–457

Esmaily M et al (2017) Fundamentals and advances in magnesium alloy corrosion. Progress in Materials Science 89: 92–193

Federal Aviation Administration (2012) Aviation Maintenance Technician Handbook-Airframe Volume 1. Federal Aviation Administration

Filatov Y A et al (2000) New Al-Mg-Sc alloys. Materials Science and Engineering A 280: 97–101

Gasik M (2013) Handbook of Ferroalloys: Theory and Technology. Butterworth Heinemann

Gupta M, Gupta N (2017) The Promise of Magnesium Based Materials in Aerospace Sector. International Journal of Aeronautical Science & Aerospace Research 4 (1):141–149

Gupta M, Gupta N (2017) Utilizing Magnesium based Materials to Reduce Green House Gas Emissions in Aerospace Sector. Aeronautics and Aerospace Open Access Journal 1 (1): 1–6

Gutowski T G (1997) Advanced Composites Manufacturing 1st edn. John Wiley & Sons, New York

Hagenbeek M, Van Hengel C, Bosker O J, Vermeeren C A J R (2003) Static Properties of Fiber Metal Laminates. Applied Composite Materials 10: 207–222

Heinz A et al. (2000) Recent developments in aluminum alloys for aerospace applications. Mat Sci Eng A 280: 102–107

Horst F, Mordike B (2006) Magnesium Technology-Metallurgy, Design Data, Applications. Springer Verlag Berlin-Heidelberg

Hosford W F (2010) Mechanical Behavior of Materials. Cambridge University Press

Hull D (1981) An Introduction to Composites Materials. Cambridge University Press

Hull D, Bacon J (2011) Introduction to Dislocations. Elsevier

Jensen B J et al (2009) Fiber Metal Laminates made by the VARTM process. In: 17th International Conference on Composite Materials, British Composite Society, Edinburgh, 27–31 July 2009

Kaufmann G (2000) Introduction to Aluminum Alloys and Tempers. ASM International

Kettner M et al (2007) The InnMag Project – Processing Mg for Civil Aircraft Application. Advanced Engineering Materials 9(9): 813–819

Laliberte J F, Poon C, Straznicky P V(2000) Applications of fiber-metal laminates. Polymer Composites 21: 558–567

Lanciotti A, Lazzeri L (2009) Fatigue resistance and residual strength of riveted joints in FML. Fatigue & Fracture of Engineering Materials & Structures 32: 837–846

Lequeu P, Lassince P, Warner T (2007) Aluminum alloy development for the Airbus A380-Part 1 & 2. Adv Materials & Processes July: 33–35 & 41–44

Lequeu P, Smith K P, Daniélou A (2010) Aluminium-Copper-Lithium Alloy 20150 Developed for Medium to Thick Plate. Journal of Materials Engineering and Performance 19: 841–847

Lumely R (2011) Fundamentals of Aluminium Metallurgy. Woodhead Publishing Ltd

Lyon P, Syed I, Heaney S (2007) Elektron 21 – An Aerospace Magnesium Alloy for Sand Cast and Investment Cast Applications. Advanced Engineering Materials 9(9): 793–798

Magnesium Elektron (2012) Magnesium Alloy Welding Rod Datasheet. Available via DIALOG. https://www.magnesium-elektron.com/wp-content/uploads/2016/10/Magnesium-Alloy-Weld-Rod_0.pdf. Accessed 31 December 2017.

Magnesium Elektron (2014) Elektron ® 675 Datasheet. Available via DIALOG. https://www.magnesium-elektron.com/wp-content/uploads/2016/10/Elektron-675_0.pdf.   Accessed 28 November 2017.

Magnesium Elektron (2014) Elektron ® ZREI Datasheet. Available via DIALOG. https://www.magnesium-elektron.com/wp-content/uploads/2016/10/Elektron-ZRE1_0.pdf.   Accessed 31 December 2017)

Magnesium Elektron (2015) Elektron ® QE22 Datasheet. Available via DIALOG. https://www.magnesium-elektron.com/wp-content/uploads/2016/10/Elektron-QE22_2.pdf.   Accessed 28 November 2017.

Magnesium Elektron (2016) Elektron ® 21 Datasheet. Available via DIALOG. https://www.magnesium-elektron.com/wp-content/uploads/2016/10/Elektron-21_1.pdf.   Accessed 28 November 2017.

Marker T R (2013) Evaluating the flammability of various magnesium alloys during laboratory and full-scale aircraft fire tests. US Department of Transportation

McCafferty E (2010) Introduction to Corrosion Science. Springer Verlag, New York

Meyer G (2001) Die (ungleichen) Dydimium-Zwillinge. Chemie in unserer Zeit 35(2):116–123

Nature Materials (2016) No Easy Solutions for Aerospace (editorial). Nature Materials 15 (8): 803

Ostrovsky I, Henn Y (2007) Present state and future of magnesium application in aerospace industry. In: International Conference "New Challenges in Aeronautics" ASTEC'2007, Moscow, 19–22 August 2007

Parker R L (1967) Data of Geochemistry – Composition of the Earth's crust. US Government Printing Office

Pekguleryuz M O, Celikin M (2010) Creep resistance in magnesium alloys. International Materials Science Reviews 55: 197–217

Pepperhoff W, Acet M (2001) Constitution and Magnetism of Iron and its Alloys. Springer, Berlin Heidelberg

Perkguleryuz M O, Kainer K U, Arslan Kaya A (2013) Fundamentals of Magnesium Alloy Metallurgy. Woodhead Publishing

Polmear I J (2006) Light Alloys – From Traditional Alloys to Nanocrystals, 4th end. Butterworth-Heinemann

Polmear I J et al. (2017) Light Alloys – Metallurgy of the Light Metals. Butterworth-Heinemann

Porter D, Easterling K E, Sherif M Y (2009) Phase Transformations in Metals and Alloys, 3rd end. CRC Press

Prasad E N, Gokhale R, Wanhill R (2014) Aluminum – Lithium Alloys. Elsevier

Prasad E N, Wanhill R (2017) Aerospace Materials and Material Technologies. Springer

Rendigs K H (1994) Metallic structures used in aerospace during 25 years and prospects. In: 50 years of Advanced Materials or Back to the Future, Proceedings of the 15th International European Chapter Conference of the Society for the Advance of Material and Process Engineering, Toulouse, 1994

Röyset J, Ryum N (2005) Scandium in Aluminium Alloys. International Materials Reviews 50 (1): 19–44

Scandium International Mining Corp (2017) The Aluminum-Scandium Alloy Advantage. Available via DIALOG. http://www.scandiummining.com/i/pdf/Scandium-Alloy-Fact-Sheet.pdf. Accessed 01 January 2018

Sinmazçelik T et al (2011) A review: Fibre metal laminates, background, bonding types and applied test methods. Materials and Design 32: 3671–3685

Staley J T, Lege D J (1993) Advances in aluminum alloy products for structural applications in transportation. Journal of Physics IV, Colloque C7, 3: 179–190

Starke Jr E A, Sanders Jr T H, Palmer I G (1981) New Approaches to Alloy Development in the Al-Li System. Journal of Materials Aug 1981: 24–33

Starke Jr E A, Staley J T (1996) Application of modern aluminum alloys to aircraft. Progr Aerospace Sci 32: 131–172

The Aluminum Association (2015) International Alloy Designation and Chemical Composition Limits for Wrought Aluminum and Wrought Aluminum Alloys. The Aluminum Association Inc, Arlington

The CM Group (2012) The Global Mg Industry in 2011 – The Impact of Chinese Production, Costs and Shipments. IMA Annual Conference, San Francisco, 21 May 2012

Thompson G E et al (1999) Anodizing of Aluminium Alloys. Aircraft Engineering and Aerospace Technology 71: 228–238

Totten E G, MacKenzie S, Scott D (2003) Handbook of Aluminum Volume 1 – Physical Metallurgy and Processes. Marcel Dekker Inc.

Vermeeren C A J R (2003) An Historic Overview of the Development of Fiber Metal Laminates. Applied Composite Materials 10: 189–205

Vlot A, Gunnink J W (2001) Fibre Metal Laminates. Springer–Science+Business Media

Williams J C, Starke Jr E A (2003) Progress in structural materials for aerospace systems. Acta Materialia 51: 5775–5799

Wu G, Yang J M (2005) The Mechanical Behavior of GLARE Laminates for Aircraft Structures. Journal of Materials 57(1): 72–79

Wu R et al (2015) Recent progress in magnesium-lithium alloys. International Materials Review 60 (2):65–100

Wulandari W et al (2010) Magnesium: current and alternative production routes. Chemeca: Australasian Conference on Chemical Engineering. Available via DIALOG. http://ro.uow.edu.au/engpapers/1254. Accessed 07 Nov 2017

Xu W et al (2015) A high-specific-strength and corrosion-resistant magnesium alloy. Nature Materials 14: 1229–1237

Zhang J et al. (2013) Experimental study on strengthening of Mg-Li alloy by introducing long-period stacking ordered structure. Scripta Materialia 68: 675–678

Zhu Y M, Morton A J, Nie J F (2010) The 18R and 14H long-period stacking ordered structures in Mg-Y-Zn alloys. Acta Materialia 58(8): 2936–2947

Further Reading

ASM International (1999) ASM Specialty Handbook: Magnesium and Magnesium Alloys. ASM International, Materials Park, Ohio

ASM International (2008) ASM Handbook Vol. 15 – Casting. ASM International, Materials Park Ohio

Baker et al (2004) Composite Materials for Aircraft Structures 2nd edn. American Institute of Aeronautics and Astronautics Inc.

Davis J R (2001) ASM Specialty Handbook: Aluminum and Aluminum Alloys. ASM International, p 351–416

Rana S, Fangueiro R (2016) Advanced Composite Materials for Aerospace Engineering: Processing, Properties and Applications. Woodhead Publishing Limited

Zhang S, Zhao D (2012) Aerospace Materials Handbook. CRC Press